

UTC FINAL REPORT

Bridge Monitoring

PI: Jacobo Bielak

Research Team: George Lederman, Siheng Chen, Zihao Wang, Fernando Cerda, Piervincenzo Rizzo, James Garrett, Haeyoung Noh, Jelena Kovacevic, and Jacobo Bielak.

Executive Summary

Already in the present but even more so in the near future there will be computing power, communication devices (cell, WiFi, DSRC) and many sensors (speed, acceleration, GPS, cameras, radar, sonar, etc.) on standard vehicles. Their primary purpose is for safety and comfort, but with small additions these can be used to observe the condition of the infrastructure around the vehicle and report it to state agencies. By continuously collecting this data from many vehicles throughout the road network the agency acquires a timely and comprehensive view of the status of its infrastructure at a low cost and can plan the maintenance of it accordingly.

In this project, we have explored using such vehicle based sensors (in this case accelerometers) to assess the condition of bridges.

The majority of the work we have done in this project is develop new algorithms to analyze data collected from 10m long laboratory scale model. In addition, however, we have begun to collect data from operational settings to see if our algorithms are more widely applicable.

We can break down the work we achieved in duration of this project into three main tasks.

Task 1: demonstrate our ability to identify the condition of a laboratory scale model from sensors placed on a model vehicle crossing over the bridge. This task looked at basic changes in the bridge included the addition of extra mass, the addition of dampers or the modification of the boundary conditions.

Next we wanted to expand on these promising results to consider additional scenarios.

Task 2 was to consider changes in mass, damping and rotational restraint while the bridge is subject to different temperature conditions. We addressed these issues by collecting additional data from our laboratory scale model, while experimenting with new algorithms for data analysis.

Task 3 was (1) to quantify and localize damage on the bridge, and (2) to consider uncertainty about the condition of the bridge. While previous work focused on classification of the state of the bridge between discrete groups, to address (1) we work built a regression to consider an infinite number of classes with the output describing magnitude and position of the damage. To address part (2), we considered the same data sets as before but only labeled a small portion of the data. Here “labeling” refers to identification of the state of the bridge so the algorithm can learn. In real scenarios the condition of the bridge is often not know, or worse could be incorrectly labeled, so we found algorithms that could handle this uncertainly. We show that even with only 10% of the data labeled, our algorithms could learn how to label the unlabeled portions (label propagation) and still achieve high accuracy.

Lastly, we wanted to move beyond the limitations of the laboratory scale model. **Task 4** was to collect data from operational structures, including a multistory parking garage on Carnegie Mellon’s Pittsburgh Campus, and the bridges along Pittsburgh’s Light Rail Line. This task forced us to employ new data collection techniques for handling uncontrolled environments and new data management techniques for storing much larger data sets.

The impact of this project has been two-fold. First we have advanced the state of the art for indirect bridge health monitoring, and made such a low cost technology more likely. In the last two years, 1 journal paper has been accepted for publication, 1 has been submitted and is under review, and 4 peer reviewed conference papers have been accepted. Second this grant has helped train civil engineering students to learn more about signal processing, while encouraging signal processing students, to examine applications in infrastructure.

Contents

Executive Summary	2
List of Figures	5
Background	7
Problem statement.....	7
Proposed solution to the problem: an indirect approach.....	8
Task 1: Validation of the Indirect Approach with the Laboratory Scale Model	11
Experimental Setup and Protocol.....	12
Details of the Bridge and Vehicle Models	13
Motion Control and Data Acquisition Equipment	14
Protocol.....	14
Signal Analysis and Classification.....	16
Preprocessing	17
Feature extraction.....	17
Classification.....	20
Classification Results.....	21
Discussion	25
Task 2: Effect of temperature and boundary condition on the indirect health monitoring of a bridge model	27
Introduction.....	27
Experimental setup and protocol	28
Classification Experiments and Results.....	36
Effect on Classification Accuracy of Variations of Vehicles, Bridges, Vehicle Speeds and Severity of Change.....	36
Effect of Roughness and Damage Location.....	41
The Effect of Different Locations of Damage	44
Effect of Temperature gradient scenarios	52
Discussion.....	53
Task 3: Damage Localization, Quantification and Bridge Condition Uncertainty.....	56
Data Analysis for SHM.....	56
Classification System.....	56
Progress.....	56
Feature Extractor.....	57
Classifier	57
Multiresolution Framework	58

Summary	58
Comparison	59
Conclusions	60
Task 4: Garage Experiments and Light Rail Data Collection.....	61
Garage Field Experiments.....	61
Laboratory Experiments.....	64
DATA SELECTION.....	64
EXPERIMENTAL RESULTS.....	67
Port Authority Project	72
Conclusions.....	77
Bibliography	78

List of Figures

Figure 1: Direct and indirect SHM different in terms of sensor location.	8
Figure 2: Experimental setup.	13
Figure 3: Experimental vehicle CAD drawings.	14
Figure 4: Roller support - Rotational restraint	15
Figure 5: General classification system.	17
Figure 6: Time-domain signals	17
Figure 7: Discrete Fourier transform of the signal.	18
Figure 8: Mean energy distribution (normalized to unit energy).	18
Figure 9: Discriminant power (normalized to unit discriminant power).	19
Figure 10: Summary of feature extraction process.	20
Figure 11: Clustering of two scenarios.	20
Figure 12: Classification accuracy results (a) Average by damage type and (b) by speed.	22
Figure 13: Classification results for rotational restraint scenarios.	23
Figure 14: Classification results for damping increase scenarios.	24
Figure 15: Classification results for concentrated mass scenarios.	25
Figure 16: Experimental setup. General photo and Vehicle picture.	28
Figure 17: Introduced modifications to the bridge structure.	29
Figure 18: Bridge longitudinal view; normal and Infrared images.	34
Figure 19: B1: Damage detection for different vehicles, speeds, and severity scenarios	37
Figure 20: B2: Damage detection for different vehicles, speeds, and severity scenarios.	38
Figure 21: B1: Damage severity classification accuracy for different vehicles	39
Figure 22: B2: Damage severity classification accuracy for different vehicles	40
Figure 23: Rotational restraints scenarios cluster analysis.	40
Figure 24: Damage detection comparison among bridges with different roughness profiles.	43
Figure 25: Damage detection comparison among scenarios.	47
Figure 26: Location classification comparison among scenarios	52
Figure 27: Classification accuracy of damage scenarios for specific temperature scenario.	53
Figure 28: Classification accuracy of damage scenarios regardless temperature scenario	53
Figure 29 – Comparison of three methods, Fourier Discriminant Features, Local Discriminant Features and Sparse Representation for 18 scenarios	59
Figure 30 – Comparison of Fourier Discriminant Features and Multiresolution Classification ..	59
Figure 31 – Discriminant Accuracy at Various Labeling Ratios	60
Figure 32 – Experimental Setup for Field Tests	62
Figure 33 – Illustration Of Garage Experiments.	62
Figure 34 – Detail of the Robot	63
Figure 35 – Slight Gap between Track and Bridge Allowing for Data Selection	64
Figure 36 – Data Selection Lab Data	65
Figure 37 – Detail of Broom Handle	65

Figure 38 – Garage Experiment Data Selection	66
Figure 39 – Waterfall Plot, Data from Back Wheel, Laboratory Experiments.....	67
Figure 40 – Waterfall Plot, Data from Back Chassis.....	68
Figure 41 – Waterfall Plot, Data from Bridge Sensor, Laboratory Experiments	68
Figure 42 – Waterfall Plot, Signals from the Robot	69
Figure 43 – Frequency Domain Waterfall Plot Deck Sensor	70
Figure 44 – Frequency Domain Waterfall plot.	70
Figure 45 – Frequency Domain Waterfall Plot Robot.....	71
Figure 46 – Detail of Lower Frequencies from Robot.....	71
Figure 47 – Installed Equipment on the Train	72
Figure 48 –Schematic of the Sensors Placed on the light rail car.....	73
Figure 49 – GPS Plots.....	73
Figure 50 – Raw Train Signal.....	74
Figure 51 - Example Signals over a bridge at Differnt Temperatures	75

Background¹

Bridge structural health monitoring (SHM) has been an active research field for over 30 years. It is a multidisciplinary problem that involves: sensors, data acquisition systems, data analysis and data interpretation. In general terms, the objective of bridge SHM is the early detection and characterization of damage conditions before they pose a threat to the structural integrity of a bridge and the public it serves. An analogy can be made with the medical field where the early detection of pathology allows for several treatment options to be undertaken to restore health. A late diagnosis might lead to chronic illness or death. If diagnosed properly, prognosis and treatment follow diagnosis.

Problem statement

The current state of the aging bridge infrastructure in the USA and around the world requires more accurate diagnostic tools for a large stock of bridges. There has been an increase in public, as well as political, awareness of the current state of the bridge infrastructure. Old and new bridges are now under public scrutiny after catastrophic collapses. The collapse of the I-35 bridge over the Mississippi River on Aug. 1, 2007 is a noticeable example, as well as the collapse of other bridges around the globe (e.g., Shershan Bridge, Pakistan, Sep. 1 2007; Harp Road Bridge, USA, Aug 15 2007; Loncomilla Bridge, Chile, Nov 18, 2004.).

The research community has been developing structural health monitoring (SHM) techniques to aid in the ongoing bridge management efforts of local bridge authorities. The current standard bridge inspection practice is based on biannual visual inspections, which are subjective by nature. Sensor-based SHM is perceived as the technology that could improve the current visual inspection process (FHWA-2001). Monitoring bridge structural systems helps in planning different bridge intervention strategies, such as maintenance actions, repair or replacement (Frangopol et al. 2008). Moreover, the life-span of the bridge structure can be extended (even if the bridge shows deterioration) if the data shows it to be healthy.

Traditional bridge SHM techniques entail the placement of sensors on the structure for measuring physical parameters that are then used as indicators of the structural behavior. SHM and damage assessment have been very active research areas, and have motivated several excellent review and overview papers, which highlight some of the most relevant approaches (e.g., Van der Auweraer and Peeters 2003; Farrar and Worden 2007). Brownjohn (2006) describes some general and fundamental objectives for monitoring civil infrastructure and points out some historical applications. More specific review topics include wireless, structural health monitoring, design of devices, and the trend for localized processing (Lynch, 2007); vibration-based condition monitoring (Doebling et al. 1998, Carden and Fanning 2004); damage identification using inverse methods (Friswell 2006); unsupervised learning (Fulgate et al. 2000, Worden and Dulieu-Barton 2004, Worden and Manson 2007); and vibration-based condition monitoring methods (Carden and Fanning 2004).

Two main approaches of this type have been pursued in recent years. One is a global vibrational approach and the other is the local approach (Mal et al 2005). The first looks at the vibration of the whole structure, while the latter focuses on the wave propagation along structural elements. We refer to these two approaches based on sensors placed on the structure as *direct* approaches. The direct approaches are especially useful when monitoring progression of damage of a particular known damage condition, or monitoring a critical member of a bridge structure.

¹ This background section is based around from Cerda's PhD dissertation.

However, the transition of the traditional SHM techniques from the research community to the practical field implementation still needs to overcome difficult challenges due mainly to technical and economic considerations (Farhey 2005, 2007). One such real world application of a monitoring program is on the Lehigh River Bridge, SR-33. It was reported that during the three year monitoring program, the direct cost of the equipment made up 40% of the total monitoring cost. For a long term monitoring program, this direct cost must be addressed several times during the lifetime of the structure, due to software or equipment obsolescence. The other 60% of the cost is related to labor and other related items (Frangopol et al. 2008). Some of the challenges of the *direct* approach include: labor intensive sensor deployment and maintenance, sensor system cost, powering the sensors system, data transmission and data interpretation.

Some of these challenges are currently being addressed by the research community. With respect to the power supply of the sensor systems, a popular approach for direct monitoring is energy harvesting to make the system self-reliant. Among the power options, one can consider solar energy (Alippi and Galperti 2008) and vibration-based approaches (Beeby et al. 2006). However, other challenges, such as the lifespan of the sensor systems with respect to the lifespan of the sensed structure and deployment and maintenance costs, are unlikely to be solved with the same approach. Electrical systems and electronics are far more vulnerable to ambient conditions than structural elements and therefore less reliable than the system they are sensing. The threat of atmospheric conditions can also be extended to involuntary damage and vandalism. Depending on the socio-economic condition of a particular country, leaving electronic equipment unsupervised has to be carefully planned for and designed to prevent theft of the equipment.

The direct approach remains impractical to this day as a first diagnostic scan, especially when one considers the large bridge population of buildings that needs to be inspected (e.g. 600,000 bridges over 20 ft.) in the US bridge inventory.

Proposed solution to the problem: an indirect approach

The need for more efficient techniques for the SHM of bridges has led to the development of additional approaches to the direct method. One such approach is the *indirect SHM*, so-called because it makes use of vibration data collected from sensors installed on vehicles crossing the bridge, rather than from sensors installed on the bridge itself (Lin and Yang 2005).

Figure 1 depicts the direct and the indirect SHM approaches. In principle, the vehicle-bridge interaction data captured by the moving vehicle provides information about the bridge, which can be used for diagnostic purposes. In other words, the indirect approach uses vehicle vibration data $q_{vi}(t)$ for diagnosing a bridge's condition rather than data $q_b(t)$ collected directly from the bridge. The use of signal processing techniques and machine learning algorithms allow one to explore the feature space of the signals collected from the vehicle and extracting vehicle-response patterns for bridge SHM. The indirect SHM approach was conceived only in the last decade, and is currently being actively researched.

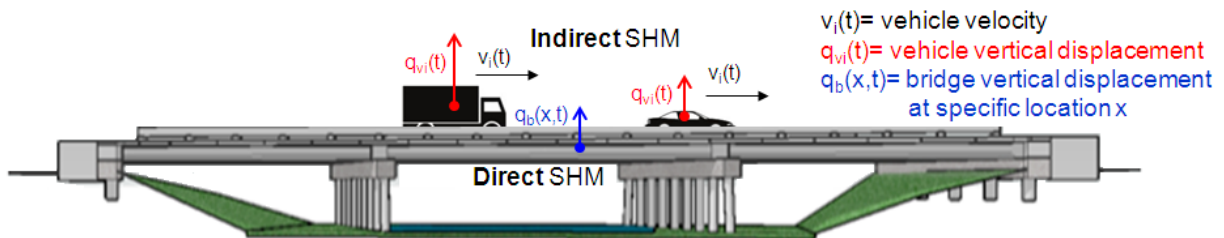


Figure 1: Direct and indirect SHM different in terms of sensor location.

The indirect approach can be viewed as being complementary to the *direct approach*. However, it has several conceptual advantages over the direct approach. The *indirect approach* allows the interrogation of a large bridge stock; it can be powered by the vehicle electrical system; it has no need to stop traffic for initial instrumentation of the structure or on-site maintenance actions; it can leverage the fleets of smart vehicles that communicate among themselves for other purposes such as: collision avoidance, traffic optimization, emergency localization or autonomous driving. The indirect approach is a data-based approach that can capture patterns of complex phenomena from large amounts of data. It takes advantage of advances in signal processing and pattern recognition algorithms.

Considering the practical future implementation of this approach, two possible scenarios might be feasible to obtain instrumented vehicle data. The first scenario that could be implemented over the medium-term considers the instrumentation of a specific fleet of vehicles that interrogate bridge structures as they go about their daily business. In this scenario, possible candidate fleets would be utility trucks or other type of public vehicles, such as transportation buses or mail trucks. They would be equipped with accelerometers, GPS, data acquisition systems and data transmission systems in order to determine their precise location and to collect their dynamic interaction data. The second scenario can be considered as a long-term vision. In the future, commercial vehicles will be readily equipped with a great number of sensors for different purposes. Some of the instrumentation that vehicles already have today are tire pressure sensors, accelerometers for adaptive suspension systems, GPS, front and rear cameras, internet connection and onboard computers. Akinci et al. envisioned taking full advantage of the opportunities that arise from having on-line vehicles making their data accessible for public interest (Akinci et al. 2003).

In the following paragraphs, we briefly review recent research efforts related to indirect SHM.

The indirect SHM approach was introduced by Yang et al. (2004), to extract the fundamental frequencies of a bridge. Yang and his colleagues derived a closed-form solution for a single-degree-of-freedom oscillator moving over a single-span, simply supported beam by assuming that the beam vibrates only in its fundamental mode. The obtained solution allowed for the identification of the two main dimensionless parameters that affected the bridge response. These parameters were S and μ , $S = \pi v / L \omega_b$, a normalized vehicle velocity, where v = vehicle velocity, L = length of beam, and ω_b = bridge's natural fundamental frequency; and $\mu = \omega_b / \omega_v$, where ω_v is the vehicle (oscillator) vertical natural frequency. Yang et al. (2005) then expanded the closed-form solution presented in 2004, to include several mode shapes as the basis for the dynamic response of the beam.

An experimental validation of the vehicle-based approach for extracting the natural frequencies of a bridge was conducted using an instrumented two-wheeled cart attached to a vehicle traveling over a simply-supported girder bridge; a heavy load truck was used to act as oncoming traffic (Lin and Yang 2005). The authors were able to identify the fundamental frequency of the bridge from the cart data, even with the simulated oncoming traffic. Toshinami et al (2010) also aimed at extracting bridge frequencies from vehicle response.

McGetrick et al. (2009) developed a numerical 1D model and studied the variations of dynamic parameters using the data derived from the numerical model. The authors report high sensitivity in the peak magnitude frequencies of the acceleration power spectral density to slight changes in the bridge structural damping. The same authors used laboratory model data (McGetrick et al. 2010) to identify the predominant frequencies of bridges and found good

agreement between the signals acquired directly from the bridge and those from the vehicle as the vehicle travels over the bridge.

Kim and Kawatani (2008) presented an approach for accurately identifying damage on a bridge structure. This approach requires data from both the vehicle and the bridge. It was first explored with numerically simulated data and later through experiments (Kim et al. 2010). A hypothesis-testing scheme that looks for patterns in the bridge response from a laboratory experiment identified successfully only severe damage conditions on the bridge structure (Isemoto et al 2010).

Based on these studies, it is reasonable to conclude that vehicle responses collected from a vehicle while travelling over a bridge contain useful information of the structural condition of the bridge. However, past studies of the indirect approach concentrated mainly on identifying certain interaction properties and indexes, such as the fundamental frequency of the bridge, power spectral density magnitude variations from vehicle data, the agreement between vehicle and bridge data predominant frequencies or the identification of severe structural changes. Thus, there is a need to complement the ongoing efforts with more robust signal processing and machine learning techniques that will allow one to detect small variations in the vehicle signature response and, therefore, allow exploration of the use of the indirect approach for diagnostic purposes.

The main objective of this work is to explore the use of the indirect method for developing a practical bridge SHM approach enhanced by signal processing and pattern recognition.

Task 1: Validation of the Indirect Approach with the Laboratory Scale Model²

We hypothesize that an array of sensors, mounted on moving vehicles that travel across the bridge of interest, can be helpful in identifying structural damage and thus serve as an indicator for more detailed analysis using a physical model. This approach is referred to as *indirect health monitoring*.

Yang and Chang (2009) reported results associated with field experiments where the first two natural frequencies of a bridge were extracted from the vehicle response by using empirical mode decomposition. Bu et al. (2006) measured the dynamic response of a vehicle moving on top of a simply supported Euler–Bernoulli beam. The vehicle served as a sensor and force transducer to detect damage defined in terms of the reduction of flexural stiffness. The model incorporated noise measurements, road surface roughness, and model errors such as underestimating vehicle parameters or bridge flexural stiffness.

Kim and Kawatani (2008) developed a pseudo-static damage detection method that makes use of the coupled vibration of a vehicle-bridge system. It requires data collected from both the bridge and the vehicle to characterize the damage. A numerical model that included the roadway roughness effect was used to test the approach. It was subsequently validated experimentally for different vehicle speeds and different amounts of reduction of the moment of inertia of the girders. McGetrick et al. (2009) modeled a simplified quarter car-bridge interaction to extract the fundamental natural frequency and corresponding damping of the bridge from the spectra of the vehicle accelerations. They found that better accuracy was achieved at lower speeds and smoother road profiles. Moreover, the magnitude of the acceleration power spectral density's peaks decreased with increasing bridge damping and this decrease was easier to detect with a smoother road profile. This work was validated experimentally by observing the effects of a vehicle moving across a steel girder that included a road surface profile. The effects of varying vehicle model mass and speed were investigated as well (McGetrick et al. 2010).

Isemoto et al. (2010) developed a hypothesis-testing scheme for damage detection based on the bridge vertical acceleration data induced by a passing vehicle. An experimental vehicle-bridge model, including roadway roughness, was used and only severe damage scenarios were identified. Miyamoto and Yabe (2011) exploited the vibration induced by a public bus for the indirect health monitoring of existing short- and medium-span reinforced/prestressed concrete bridges. The tests demonstrated a correlation between the vehicle vertical acceleration and the bridge vibration at midspan. By means of a numerical 3D finite element model, the distribution of characteristic deflection values was found for a particular driving speed and two severe damage scenarios.

Yin and Tang (2011) proposed a finite-element method to simulate the interaction of a vehicle and a cable-stayed bridge. The vertical displacement from the vehicle was used to identify tension loss and deck damage. The relative displacement of a passing vehicle of a bridge with known damaged conditions is used to generate a vector basis. The proper orthogonal decomposition on the relative displacement of a vehicle passing a bridge with an unknown damage condition is optimized with the known basis, and parameters of the unknown damaged bridges are reconstructed. Finally, Sirigoringo and Fujino (2012) proposed an indirect approach to estimate the fundamental natural frequency of a bridge using the response of a passing instrumented vehicle. The method was validated experimentally on a full-scale simply supported

² Task 1 section is based on Cerda's PhD dissertation.

short span bridge by using a light commercial vehicle instrumented with accelerometers. The spectra of the vehicle's dynamic responses while crossing the bridge were analyzed to reveal the first natural frequency of the bridge when the vehicle moved with constant velocity. The experimental study considered traveling speed ranging from 10 to 30 m/s.

All of the above indirect monitoring studies aimed at identifying the dynamic parameters of a bridge by either observing a single damage-sensitive feature or by optimizing model-based damaged sensitive vectors. The authors of these studies, however, did not report on detecting various types of damage conditions, the confidence with which the detection was ascertained, or the effects of different boundary conditions, weather patterns, traffic loads, or different vehicle speeds on the structural diagnosis.

Results are presented from a study that aims at bridging this gap. The long-term objective is to create a decentralized monitoring approach using fleets of vehicles that can continuously store or send data about the bridges over which they travel. In the laboratory, a bridge model is subjected to different vehicle speeds, damage scenarios, and structural boundary conditions. In addition to the indirect measurement of the bridge motion obtained through the vehicle vibration, other three sensors were placed directly on the bridge. In contrast to previous studies, the indirect and the direct data were used independently. This allows comparing the indirect and the direct strategies and to evaluate the effectiveness of our indirect damage detection algorithm.

Experimental Setup and Protocol

A laboratory experimental setup was built to collect data from a vehicle, which could be used to detect changes in the condition of the bridge. Using this model, acceleration data from a bridge structure and a vehicle passing over it can be collected and later analyzed for characterizing vehicle-bridge interaction patterns. The complete experimental setup consists of mechanical components that make up the bridge and vehicle system, a vehicle motion control system, and data acquisition equipment. The different mechanical components resemble a simply supported bridge structure and a four-wheeled vehicle with an independent suspension system at each wheel. The motion control equipment is able to move the vehicle over an acceleration ramp, a bridge and a deceleration ramp, causing the vehicle to reach a target speed before the end of the acceleration ramp, then maintain that velocity over the bridge, followed by a deceleration of the vehicle so that it stops at the end of the deceleration ramp. The data acquisition system records accelerations at different locations on the vehicle and the bridge, as well as the position of the vehicle. This experimental setup was inspired by the work of Kim et al. (2010).

An overview of the setup is shown in Figure 2. The vehicle, approximately in the middle of the figure, is pulled by a belt system. The vehicle was instrumented with Vibra-metrics accelerometers (Model 5102) powered by cables supported by a cable delivery system that moves parallel to the vehicle. The cables and the vehicle are propelled by a motor at the leftmost part of the experimental setup.

The travelling path of the vehicle corresponds to the acceleration/deceleration ramps and the bridge as labeled in Figure 2a. The simply supported bridge structure is in the middle of the travelling path. Below the simply supported bridge there are two reaction beams that are used to support the bridge reactions and the added dampers.

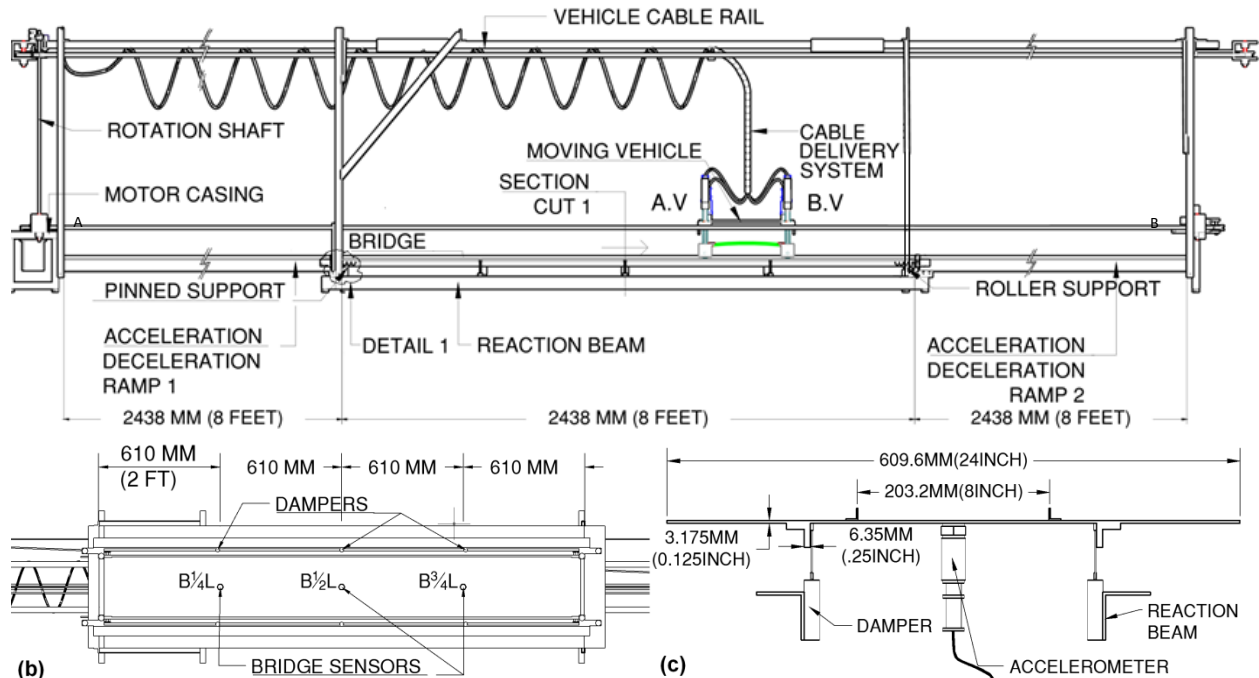


Figure 2: Experimental setup.
 a) General lateral view. b) Bridge bottom view. c) Bridge cross section.

Details of the Bridge and Vehicle Models

The bridge is simply supported by a roller support at the left and a pinned support at the right. The vehicle enters the bridge from the left. The whole system is constructed to act as a closed force loop system. The longitudinal forces generated by the motor to move the vehicle are transmitted between the two supports by two connecting beams labeled as “reaction beams” in Figure 2a. The bridge structure is instrumented with three 5102 Vibra-metrics accelerometers as in Figure 2b. The sensors are equally spaced along the longitudinal direction of the bridge and named accordingly as $B\frac{1}{4}L$, $B\frac{1}{2}L$ and $B\frac{3}{4}L$ where $L=2438$ mm. The reaction beams act as a support for localized dampers that connect to the bridge structure as in Figure c. The bridge deck consists of an aluminum plate, and two angle beams act as the bridge girders. On top of the plate two angle beams serve as rails for the travel path of the vehicle. Detailed dimensions of the bridge section are shown in Figure 2c.

The bridge has a total mass of 18.3 kg, a fundamental natural frequency of 7.23 Hz, a fraction of critical damping of 3.6 percent. These are the properties of the bridge in the pristine condition, later referred to as Scenario 1.

Figure 3a shows a 3D view of the vehicle constructed for the experimental setup with the main components labeled. The vehicle was instrumented with two accelerometers connected to the suspension shafts in order to record the acceleration at the wheel level and with two accelerometers placed on the suspension to acquire data filtered by the suspension system. To keep the symmetry of the vehicle, two calibrated weights were placed on top of the un-sensed wheel shafts. Similarly to the bridge structure, the vehicle was built mainly with aluminum parts.

Two reference points are labeled on the longitudinal direction of the vehicle as points A Vehicle (A.V) and B Vehicle (B.V). A top view of the vehicle is shown in Figure 3b. The length and width of the vehicle as well as the labels assigned to the four sensors are also indicated. The

sensor labels are defined by their position and location to the reference point. Suspension A.V and Suspension B.V are labeled S.A.V and S.B.V, respectively, and the two wheel level sensor locations are labeled W.A.V and W.B.V. A picture of the model vehicle is shown in Figure 3c.

The frequency of the A.V and B.V axles of the vehicle were determined through free vibration experiments on the suspension. These experiments were performed on the vehicle when separated from the belt of the vehicle motion control system. The frequencies were obtained by averaging the power spectra of five free vibration experiments; the results are summarized in Table 2.

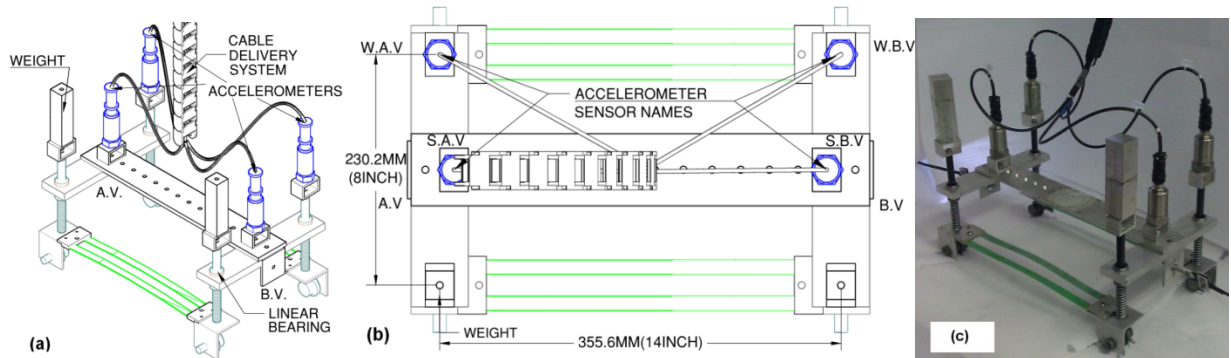


Figure 3: Experimental vehicle CAD drawings. (a) Parametric view. (b) Top view. (c) Vehicle picture.

Table 1: Vehicle properties.

Vehicle weight [kg]	4.8
A.V axle frequency[Hz]	5.0
B.V axle frequency[Hz]	5.5

Motion Control and Data Acquisition Equipment

A National Instruments[®] PXI system running in LabView[®] was assembled to operate the instrumented vehicle and to allow for data acquisition and storage. The system consisted of a PXI Chassis (NI PXI 1031) with a motion control card (NI PXI 7342), a motion interface (UMI 7772), a stepper drive (P70360) and a dual shaft stepper motor (NEMA 34). A feedback loop for position was achieved with an encoder. The acceleration data were digitized and stored for post-processing using two digitizers (NI 9234).

Protocol

Three different types of “damage” scenarios were designed: 1) variations on the support condition by imposing rotational restraints, 2) increase of damping at different locations, and 3) a mass increase at the midspan. For each kind, four levels of severity were devised in order to obtain a total of 12 different damage scenarios. Table 2 shows the twelve conditions of damage (thirteen in total). For each case the resonance frequency and the critical damping are reported and compared to the baseline, i.e. Scenario 1. For all cases, the fundamental natural frequency of vibration and the damping coefficient are determined by means of conventional free-vibration experiments.

The rotational restraint mechanism was built into each of the four beam supports of the bridge model. As shown in Figure 4a, an aluminum bar (12x1x1/8 inch) was attached to the main

girder of the bridge at one extreme and connected to the support at the other extreme to provide vertical restraint. The plate was drilled down to 6.35 mm [1/4 in] with 12.7 mm radius [1/2 in] to provide only a partial restraint.

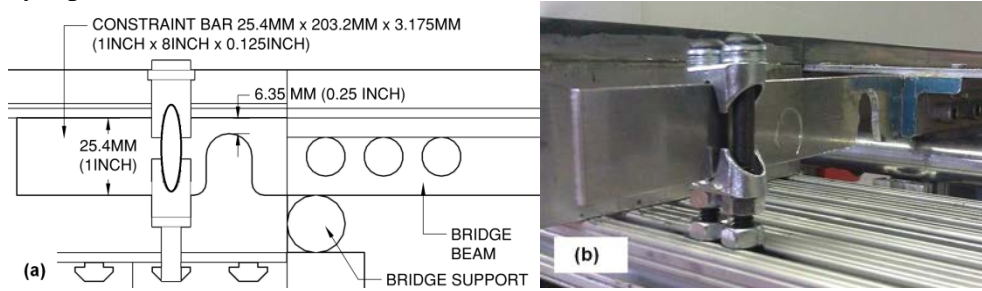
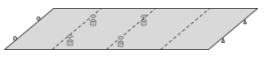


Figure 4: Detail 1 – Roller support - Rotational restraint (a) technical drawing and (b) picture.

Variation of the rotational restraints simulates the case of rubber bearings becoming stiffer in time or steel corrosion occurring on rocker supports. This condition is denoted as frozen bearings and it is a common cause of undesired stress in the structure, and, therefore, a reduction in the load capacity. In Table 2, the variations of the rotational restraints are described as scenarios 2 to SC5. In Scenarios 2-5, one, two, three and all four supports are restrained, respectively. As expected, the greater the number of rotational restraints, the higher the fundamental frequency, which provides an indicator of change to the bridge structure. The variation of localized damping is achieved by adding dampers to the bridge at locations schematized in Table 2 (Scenarios 6 to 9). A set of AIRPOT adjustable dampers were used. They were calibrated to provide the same damping coefficient. In Scenarios 6-9, one, two, four and six dampers, respectively were attached to the bridge structure as depicted in the schematics of Table 2.

Table 2: Damage scenarios.

Schematics	SC	f [Hz]	% f shift	% ζ_{crit}	% ζ shift
	1	7.23	-	3.63	-
	2	7.46	3.17	6.34	74.9
	3	7.66	6.00	6.45	77.8
	4	8.11	12.2	7.97	119
	5	8.56	18.4	9.43	158
	6	7.24	0.17	8.52	134
	7	7.25	0.28	11.3	211
	8	7.28	0.73	26.4	629
	9	7.30	0.98	31.4	766
	10	7.19	0.56	4.44	22.4
	11	7.18	0.66	4.34	19.5
	12	7.14	1.29	4.07	12.2
	13	7.09	1.85	4.37	20.5

Finally, the concentrated mass at the midspan of the structure consisted of weights equal to 50 g, 100 g, 200g and 300 g. As expected, the presence of the mass decreased the fundamental frequency of vibration of the structure.

Eight different vehicle speeds, varying from 1 m/s to 2.75 m/s, were considered for each damage scenario.

Signal Analysis and Classification

In general terms, the task of distinguishing various bridge conditions is a signal-processing task of classification. The classification task is first described in general, and then we explain how it was used in our setting. Assume a real signal x of length N , i.e., $x \in R^N$ (see Original signal in Figure 5). The problem, then, can be formulated as that of designing a map from the signal space of vibrational signals $X \subset R^N$ to a response space of class labels $Y \subset \{1, 2, \dots, C\}$ (in Figure 4 these are Damaged and Pristine labels). That is, the decision $d : X \rightarrow Y$ is the map that associates an input signal with a class label.

A general classification system consists of a feature extractor and a classifier (see Figure 5). Since the dimensionality of the input space is typically large, the feature extractor is introduced to reduce this dimensionality by setting up a feature space $F \subset R^k$ where $k \leq N$ between the

input space and the response space. The feature extractor is the map defined as $f : X \rightarrow F$ and the classifier as a map $g : F \rightarrow Y$.

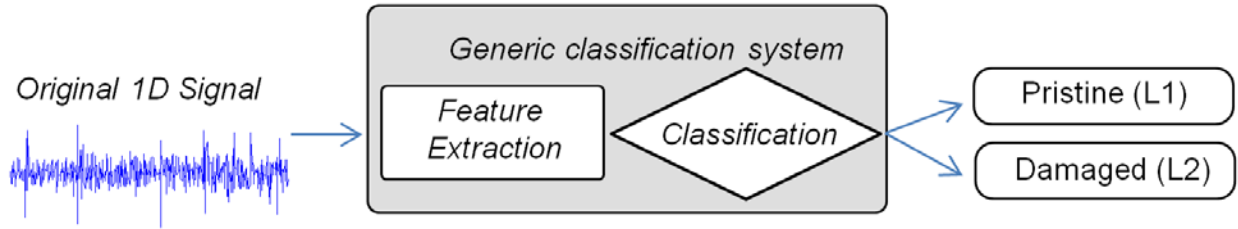


Figure 5: General classification system.

Preprocessing

Figure 6 shows the signal obtained from the vibration of the vehicle, from the time when it starts moving, through its motion across the bridge, until it is brought to a stop. The only relevant information for the bridge characterization, however, is that of the vehicle moving across the bridge. The reference start time was chosen as the moment when the rear wheels enter the bridge and as the end time the instant when the front wheels exit the bridge. That portion of the signal is highlighted in Figure 6a-d by the two vertical lines. The extracted portions of the signals are then normalized to have zero mean and unit variance.

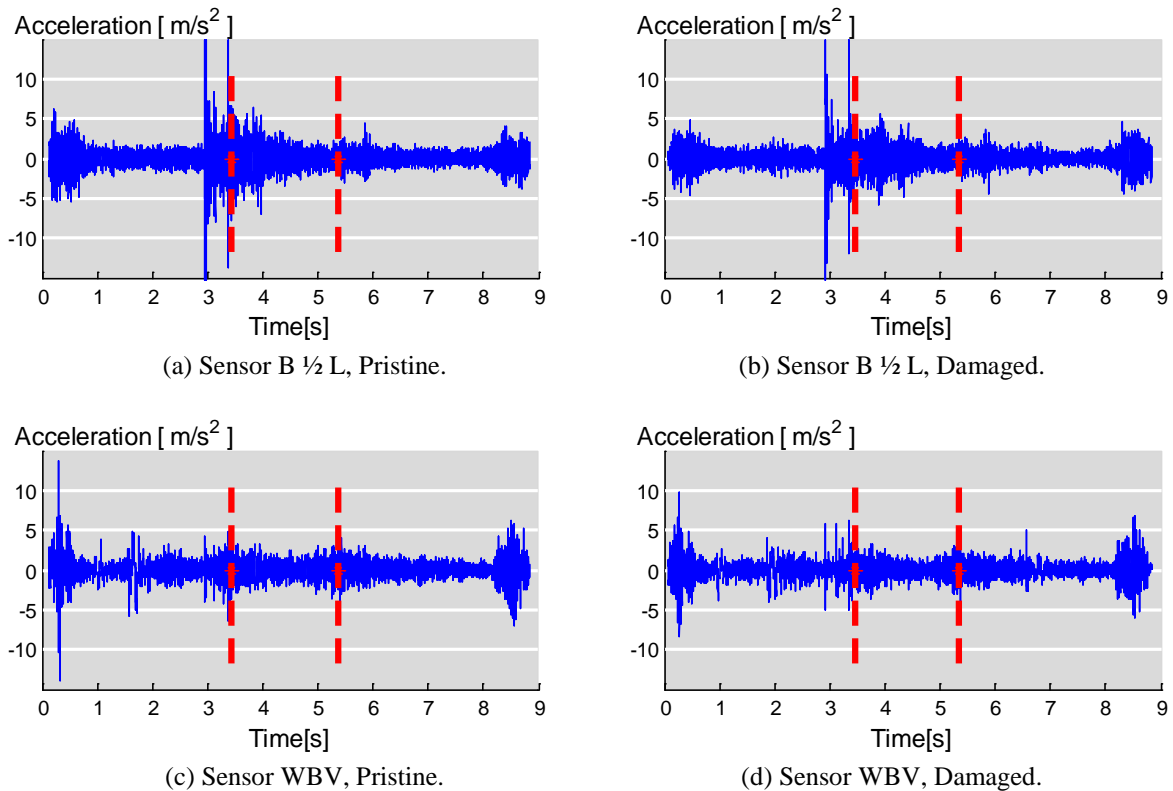


Figure 6: Time-domain signals.

Feature extraction

A linear structural system can be characterized in the frequency domain by its predominant natural frequencies, and their corresponding mode shapes and damping values. We explore therefore the use of frequency spectra characteristics for damage detection.

Considering the fundamental natural frequencies of the damage scenarios and the vehicle main bouncing frequency, we limited the analysis frequency spectrum to up to 33 Hz. For example, looking at the spectrum of the signal in Figure 7 for signals from two different scenarios, a pristine and a damaged one, we see that potentially we could tell responses apart from separate sensors by looking at magnitudes at certain characteristic frequencies. We thus decided to use frequencies as features, hoping to distinguish among different scenarios. Our task is then to find a set of features to maximize differentiation between classes.

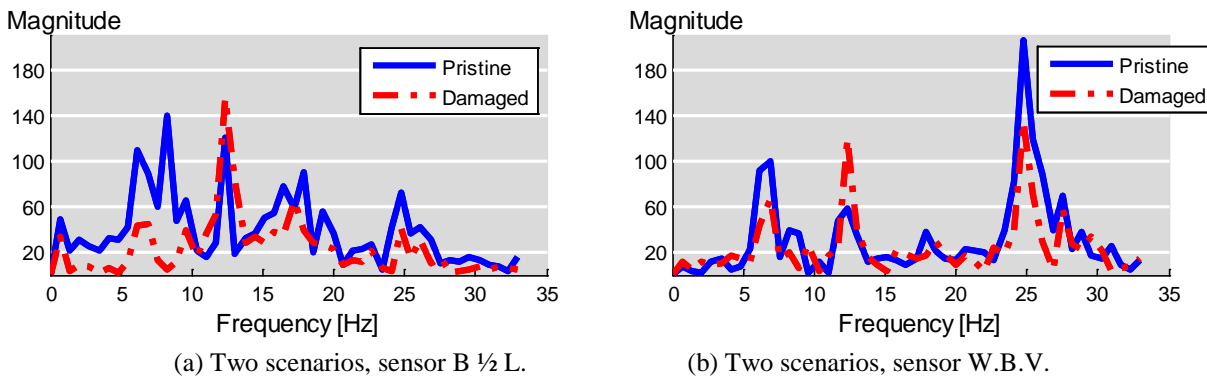


Figure 7: Discrete Fourier transform of the signal.

Since the acceleration signal contains a large number of spikes and other transient signals, the spectra are noisy with little consistency between runs. To reduce noise and keep non-transient frequencies of interest, a typical approach is to average the spectra across frequency. Averaging the frequency spectra is a well-known technique used in noisy signal processing. For example, on radar signal analysis, a redundant number of antennas capture noisy signals from the same source and average them to increase the signal to noise ratio.

After averaging, we calculate the frequency-domain energy distribution for each scenario. This technique relies on the assumption that each scenario has its unique energy distribution in the frequency domain. Since we wish to tell classes apart and not individual runs, we average all the energy distributions from the same class and use the mean energy distribution as the representative member of that class (see Figure 8).

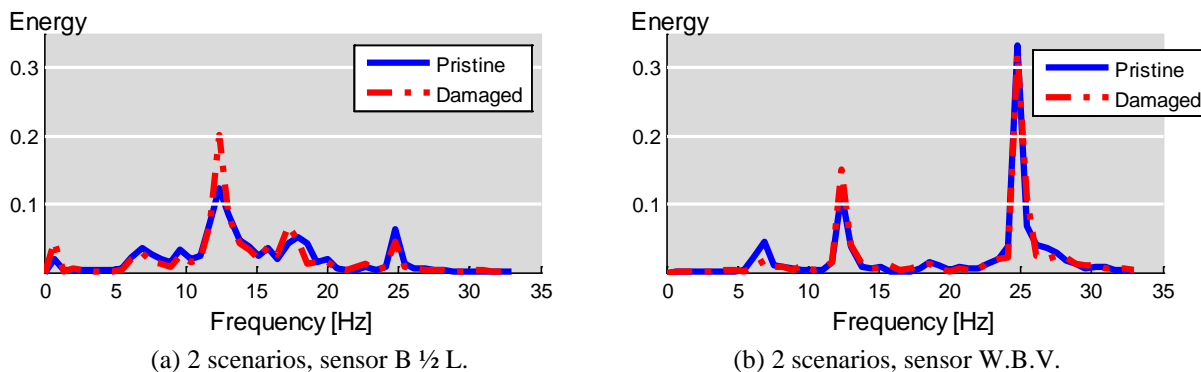


Figure 8: Mean energy distribution (normalized to unit energy).

Let $\{x_i^{(c)}\}_{i=1}^{N_c}$ be a set of signals with N_c samples belonging to Class c . The Fourier energy map is

$$\Gamma_c(j) = \frac{\sum_{i=1}^{N_c} \|w_j^T x_i^{(c)}\|^2}{\sum_{i=1}^{N_c} \|x_i^{(c)}\|^2} \quad (1)$$

where w denotes Fourier basis vector and j denotes the frequency band. To evaluate the power of discrimination of every Fourier basis vector, we need a discriminant measure D to evaluate the power of discrimination. We will assume that higher discriminant power provides higher discrimination between classes.

For the j th Fourier basis vector, the power of discrimination Δ is denoted by

$$\Delta_j = D(\{\Gamma_c(j)\}_{c=1}^C). \quad (2)$$

There exist numerous choices for the discriminant measure; we use J-divergence (Kullback and Leibler 1951). Let $p = \{p_i\}_{i=1}^n$, $q = \{q_i\}_{i=1}^n$ be two nonnegative sequences with $\sum p_i = \sum q_i = 1$, J-divergence between p and q ,

$$J(p, q) = \sum_{i=1}^n p_i \log \frac{p_i}{q_i} + \sum_{i=1}^n q_i \log \frac{q_i}{p_i} \quad (3)$$

Figure 9 shows a graph of the discriminant power between the frequency signals previously depicted in Figure 8.

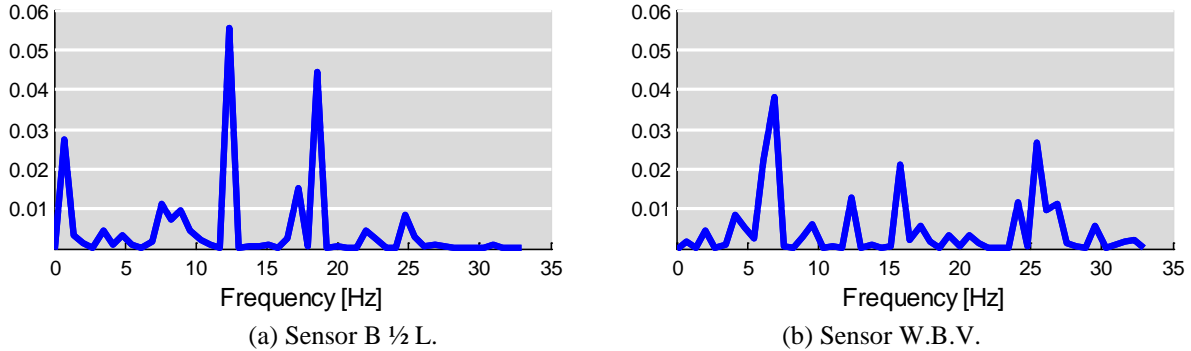


Figure 9: Discriminant power (normalized to unit discriminant power).

To help understand the feature selection method, we summarize our assumptions and conclusions thus far: 1) to differentiate signals from different scenarios, we use frequencies as features. 2) if the discriminant power is higher, it is easier to discriminate between classes. The discriminant power will thus predict how well a feature will perform during classification; 3) a small number of frequencies provide most of the discriminative power; in other words, the frequency feature set is sparse. Only those frequencies that have large discriminative power are selected (this is called nonlinear approximation); see Figure 10.

Algorithm (Fourier Discriminant Basis Vectors Selection)
Task: Find $k(\leq n)$ most discriminant Fourier basis vectors
Given a dataset consisting of C classes of signals $\{\{x_i^{(c)}\}_{i=1}^{N_c}\}_{c=1}^C$
Step 1: Take the DFT of x .
Step 2: Construct Fourier energy map Γ_c for $c = 1, \dots, C$
Step 3: Determine the power of discrimination $\Delta_j = D(\{\Gamma_c(j)\}_{c=1}^C)$ for every Fourier basis vector w_j
Step 4: Order Fourier basis vectors by their power of discrimination.
Step 5: Use $k(\leq n)$ most discriminant Fourier basis vectors for constructing classifier

Figure 10: Summary of feature extraction process.

This selection method performs nonlinear approximation in the Fourier domain and is data adaptive. Different data may give different frequency information and different discriminant powers. Since this method learns from the data and always chooses the frequencies with large discriminant power, it is more robust than traditional linear approximation.

Figure 11 shows the first 3D feature space. Blue circles denote the pristine scenario and red asterisks the damaged scenario. We see that with just three Fourier discriminant basis vectors, it is easy to separate the two classes.

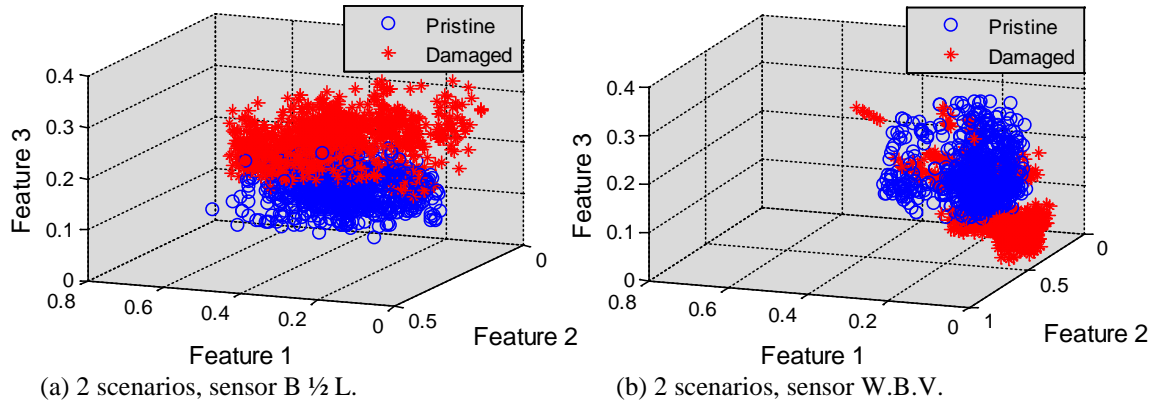


Figure 11: Clustering of two scenarios.

Classification

The second part of a classification system is the classifier itself. In this process we take as input a feature vector and output a class label. The classification problem here is called supervised learning, as a labeled training set is given. Different classifiers are available, such as naïve Bayes, neural networks and many others (Duda et al 2000). In this work the support vector machine (SVM) was selected, which is described next.

When looking for the best boundary between classes, it is desirable to achieve two things: 1) find the boundary that gives high classification accuracy; 2) avoid overfitting. To satisfy these two requirements, SVM maximizes the margin, which means the distance between a decision boundary and a data point, and expresses it as a function of the weight vector and bias of the separating hyperplane, which is used to separate the space into two half spaces. In addition, there is low risk of overfitting because SVM produces a linear boundary.

In each scenario, data for 32 runs was collected, out of which 3 were averaged, yielding $C_{32}^3=4960$ available samples for each scenario. As our dataset, 1000 out of 4960 samples were

chosen for each scenario. 20-fold cross validation was performed. Each time, 2000 data samples, consisting of 1900 training samples and 100 testing samples, were used to create and test the SVM-based classifier. A Fourier discriminant basis search algorithm was used and the top 5 frequencies that provide the largest discriminant power were selected as features. Then a kernel SVM was used as the classifier.

Classification Results

The results of the classification experiments are presented and discussed in terms of the classification accuracy, which is defined as the number of test samples correctly classified divided by the total number of test samples.

For the two classes defined, pristine and damaged, scenarios 2-13 belonged to the latter class. The data collected from all seven accelerometers were used.

Figure 12 shows the variation of the average classification accuracy for different variables. Figure 12a shows the average across the different severities, speeds and sensor locations for each damage type. The three bridge sensors, B1/4L, B1/2L and B3/4L, are averaged and referred to as “Bridge”, the two sensors at the wheel level, (W.A.V and W.B.V) are averaged and referred to as “Wheel” and the two sensors at the suspension level, (S.A.V and S.B.V) are averaged and referred to as “Suspension”. The standard deviation across the averaged variables is shown at the top of each bar. An average classification accuracy for all the sensors for each damage type is depicted with a black line and corresponding percentage. The baseline in Figure 12a and b is 50%, which is the expected probability of randomly choosing between two labels (pristine or damaged). Classification accuracy values of over 90% are obtained despite the subtle changes introduced in the bridge structure. The amount of change inflicted was deliberately small to test the detection capability of the combined indirect approach using the signal processing techniques described in Section 0. The signals from the sensors located at the wheel level were classified consistently across the different damage types, and more accurately than those from the sensors located on the bridge or on the vehicle at the suspension level.

The classification results in Figure 12b show how the average classification accuracy for all damage scenarios varies for different vehicle speeds. Similarly to Figure 12a, each bar represents the mean accuracy classification across the different damage scenarios. At the top of each bar, the corresponding standard deviation is shown. Looking at Figure 12b, one can see that there is a jump between the first four speeds, between 1 and 1.75 m/s and the four higher speeds from 2 to 2.75 m/s. The average across the two groups of speeds is shown by a black line and corresponding percentage. There is about a 7% difference in classification accuracy between these two speed ranges. This classification accuracy difference is consistent for the average classification accuracy of the sensors at the different locations (i.e., Bridge, Wheel and Suspension).

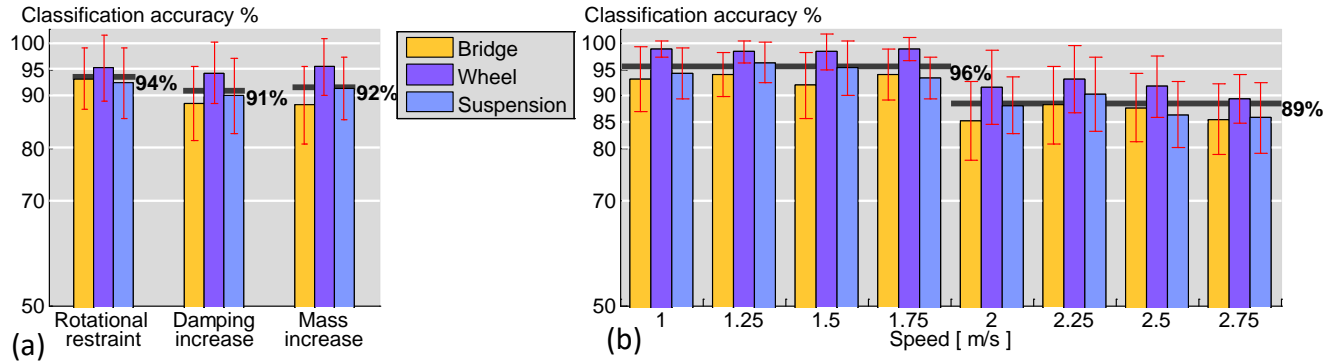


Figure 12: Classification accuracy results (a) Average by damage types. (b) Average by speeds.

Figure 13 illustrates the sensitivity of the classification method to different severity levels of damage for each scenarios. Figure 13a, b and c shows the average classification for the different damage severity levels for the rotational restraint damage type for different vehicle speeds. For all of these graphs, the thickness of the line depicts the level of damage, with the thinnest line indicating the least amount of damage inflicted (e.g., only one of four rotational restraints invoked in SC2) and the thickest line indicating the maximum amount of damage inflicted (e.g., all four rotational restraints invoked in SC5).

Figure 13a, b and c shows the average classification accuracy for each rotational restraint damage severity level for the signals from all the sensors on the bridge, all the sensors on the suspension, and all the sensors on the wheel, respectively. Figure 13d, e, and f break the results down for each sensor and show the average classification accuracy for each rotational restraint damage severity level for each signal from the three sensors on the bridge, B1/4L, B1/2L and B3/4L, from the two sensors on the suspension, S.A.V and S.B.V, and from the two sensors on the wheel, W.A.V and W.B.V, respectively.

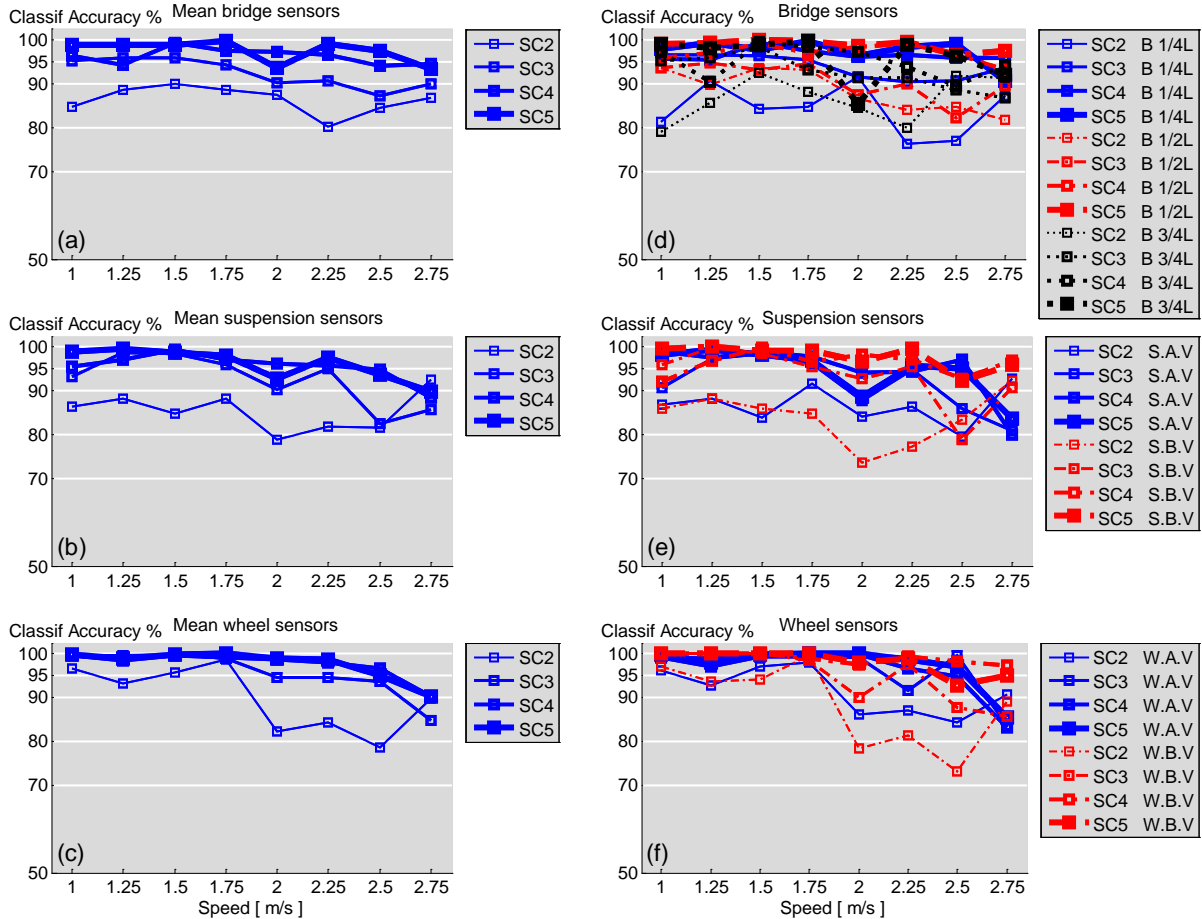


Figure 13: Classification results for rotational restraint scenarios (a,d) Bridge sensors, (b,e) Suspension sensors (c,f) Wheel sensors.

As can be seen from the graphs in Figure 13, the classification accuracy for SC2 is lower than for the other rotational restraint scenarios (SC3, SC4 and SC5), and increases as the severity of damage increases. For SC2, there is a variation in the classification accuracy with respect to the speed. However, the more severe rotational restraint scenarios seem to be more independent of the speed with high classification accuracy for low speeds and a slight parabolic decrease for higher speeds. No significant difference in the classification accuracy is apparent in Figure 13 regarding the sensor location. This shows that in terms of classification accuracy, the signal processing approach performs as well with sensor data from the vehicle (sensor or wheel) as with sensor data directly measured on the bridge. In other words, the results would indicate that in this particular set of experiments, the indirect approach has a classification accuracy that is as good as that of the direct approach.

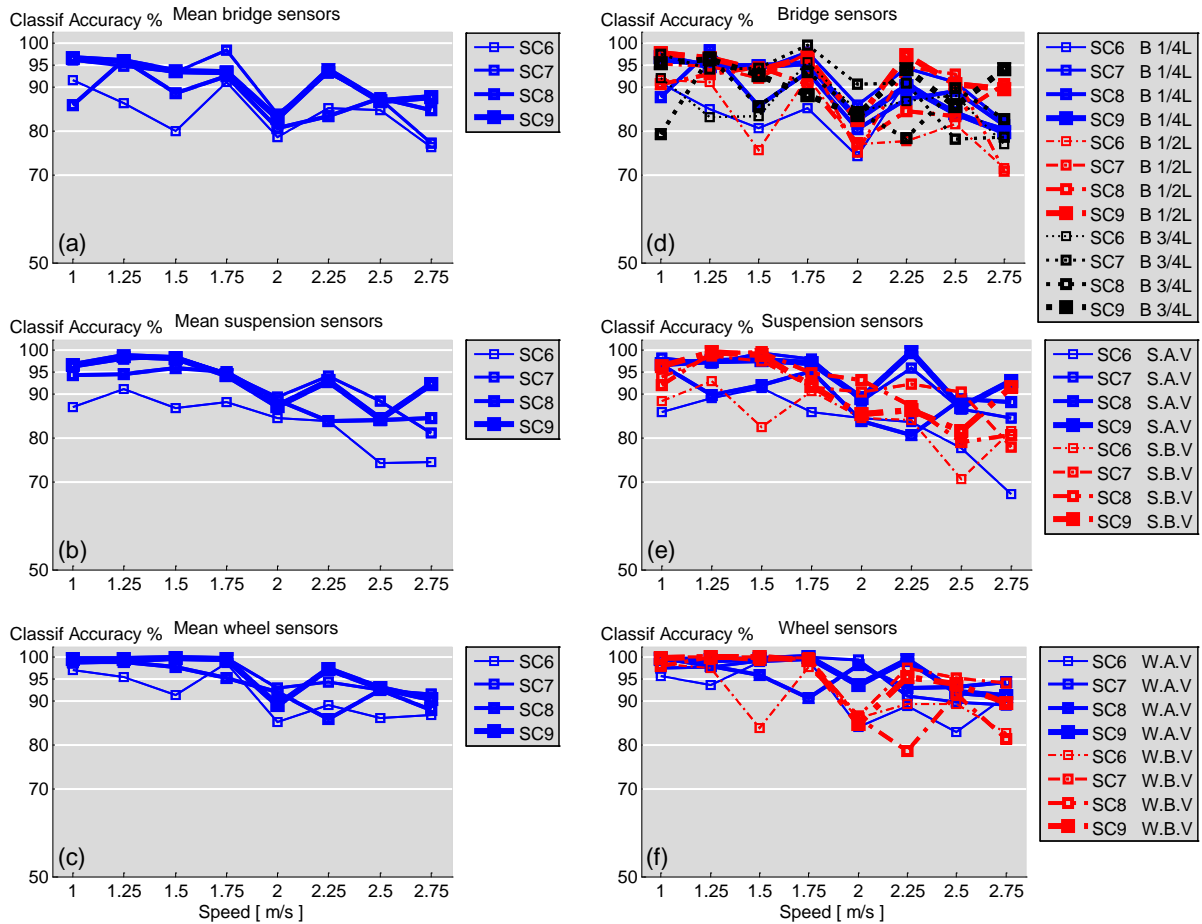


Figure 14: Classification results for damping increase scenarios. (a,d) Bridge sensors, (b,e) Suspension sensors (c,f) Wheel sensors.

Figure 14 and Figure 15 are similar in nature to Figure 13, but display the classification accuracies for the two other damage types explored: the scenarios with increasing amounts of damping and with increasing amounts of mass. Figure 14a b and c shows Scenario 6, the scenario with the single damper, as the one with the least classification accuracy across all speeds. In terms of effects due to changes of vehicle speed, a decrease in the classification accuracy appears to occur when the vehicle velocity is 2 m/s as shown in Figure 14a. In general terms, the same observations from Figure 13 apply to Figure 14. There is a slight decrease of the classification accuracy with higher speeds, and the classification accuracy seems to be independent of the sensor location; that is, there is little difference in the classification capability between the direct and the indirect approaches. Figure 15 shows the classification results for the scenarios with a mass increase at the midspan. Even though the inflicted change in the bridge structure is quite subtle, the classification accuracy is high, especially for the lower speeds. The same observations made for Figure 14 can be made for Figure 15 regarding the variation of classification accuracies with respect to the vehicle speed and the sensor locations.

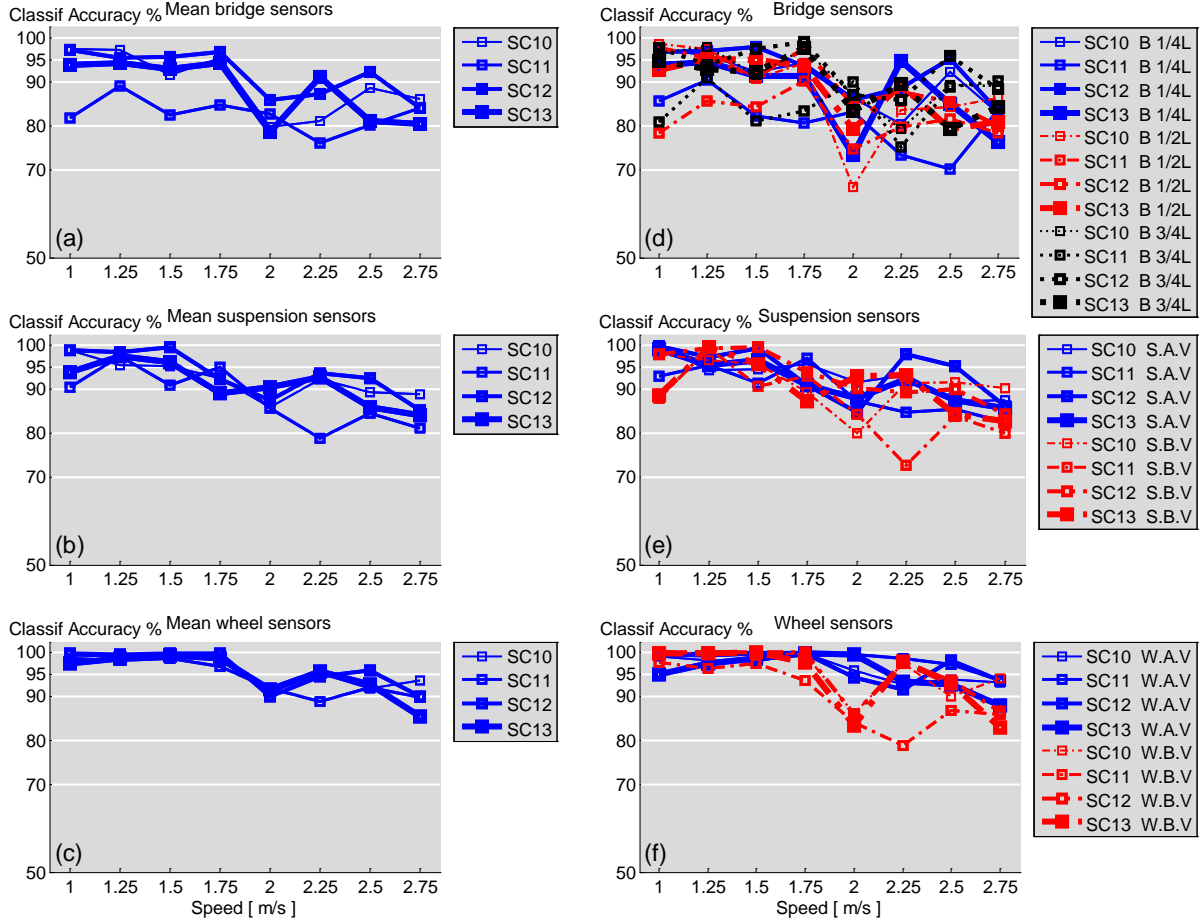


Figure 15: Classification results for concentrated mass scenarios. (a,d) Bridge sensors, (b,e) Suspension sensors (c,f) Wheel sensors.

Discussion

The damage detection capability of an indirect monitoring approach based on data collected from moving vehicles was proposed and evaluated for bridge monitoring by applying classification to experimental data taken from a laboratory vehicle-bridge physical model.

To perform numerous test repetitions, a fully automatic vehicle-bridge model needed to be built. In this study, the amount of experimental data samples is significantly greater than that from previous experiments. Each scenario was run 32 times at eight different velocities. Three different damage types were built into the experimental setting, and each damage type had four different severity scenarios.

The synchronized acceleration data from the bridge and the vehicle, and the vehicle position data, allowed for the comparison of the *direct* and *indirect* approaches in terms of the accuracy with which each could classify the existence of damage for different extents of damage.

A feature extraction technique based on averaging the power spectrum from a set of data was used to achieve very high noise reduction. Then, features extracted from the Fourier domain were automatically chosen from the denoised data samples based on their significance and classified using an SVM classifier.

High classification accuracy was achieved across three *distinct types of changes* inflicted into the bridge structure: 1) a change in the support conditions obtained by introducing rotational restraints at the supports; 2) an increase in the damping of the bridge structure; and 3) a localized mass increase at the midspan of the bridge.

The *severity* of the changes inflicted in the bridge structure was consistent with higher classification accuracy. For example, SC3, SC4 and SC5 imposed more significant changes into the bridge structure than SC2, and consistently higher classification accuracy was obtained. Nonetheless, the classification accuracy achieved for the subtle change inflicted on SC2 is on average above 85%.

The detection of the various changes in the bridge structure was quite insensitive to the vehicle *speed*. This effect can be important for practical applications where vehicle speeds cannot be readily controlled. However, a small jump was observed between the lower and higher speeds, where the classification accuracy decreases by about 7 percent at the higher speeds.

Independent of the sensor *location*, high classification accuracy was achieved across all the sensors. The *indirect* and *direct* approaches seem to be equally effective for damage detection when applying the proposed signal processing techniques. Of the two sensor locations considered in the *indirect* approach, the wheel level and the suspension level, the sensors at the wheel level performed better than the sensors at the suspension level.

Given the simplicity of the model considered, the results presented are strictly applicable only to the particular experimental setup and cannot be generalized for full-scale structures at this time. On the other hand, we observed a high degree of consistency in the classification accuracies across the very different types and severity of damage and for different vehicle speeds. This gives us hope that our approach might be applicable to more general systems. In the next task we attempt to validate the robustness of these results for more realistic systems and conditions. These scenarios include different roadway roughness profiles, atmospheric conditions and other bridge interaction variables such as different vehicle/bridge mass ratios, the effect of ongoing traffic and torsional effects on the bridge by non-symmetric loading from the vehicle path.

Task 2: Effect of temperature and boundary condition on the indirect health monitoring of a bridge model

Introduction

The indirect approach to the health monitoring of bridge structures uses a smaller number of sensors, mounted on moving vehicles that travel across the bridge of interest, to collect data that may help in identifying structural damage and thus serve as an indicator for more detailed analysis.

In the previous task we presented the initial results of a study that proposes to employ fleets of vehicles to routinely acquire and send data about the bridges over which they travel. A laboratory-scaled (i.e., 8 ft. (2438 mm) long) bridge model was subjected to different vehicle speeds, damage scenarios, and structural boundary conditions. In addition to the indirect measurement of the bridge motion obtained through the vehicle vibration, sensors were installed on the bridge to compare the effectiveness of the proposed indirect approach to a conventional direct SHM paradigm. The indirect and direct approaches seem to be at least equally effective for damage detection when applying the proposed signal processing techniques. The average damage detection accuracy obtained was over 90% for three different types of damage scenarios and four different severities of damage. Of the two sensor locations considered in the indirect approach, the wheel level and the suspension level, the sensors at the wheel level performed better than the sensors at the suspension level. In both cases, the indirect sensors outperformed the direct sensors. However, the previous results were constrained to one vehicle and one bridge.

This task (2) builds upon work in the previous task (1) and presents a study where the effect of three instrumented moving vehicles was evaluated on two Bridges; the effect of temperature; and simulated road roughness were also considered. With respect to the previous work in the area of indirect bridge health monitoring, this presents four new evaluations of the effectiveness of this indirect SHM approach: 1) the effect of temperature and roughness on the accuracy of the damage classification; 2) the generality of the approach when three different vehicles instead of one are used to collect data; 3) the generality of the approach when two slightly different bridge models are tested; and 4) how well classification of damage scenarios can be performed for different locations and severities.

Although the environmental and operating conditions have been addressed in the literature for direct SHM approaches (Farrar et al. 1998; Peeters and Roeck 2001; Cornwell et al. 1999; Sohn 2007; Meruane and Heylen 2011; Yan et al. 2005a-2005b, Deraemaeker et al. 2008, Serker Kamrujjaman et al 2010, Zhu and Rizzo 2011), this project presents new insights concerning the effect of certain environmental conditions on the indirect SHM approach using vehicle accelerations.

This task is organized into 4 sections, with the first being the introduction. The second section presents a description of the experimental setup and protocol used for the experiments described in this paper. The third section presents the experimental results in four subsections: a discussion of the effects of vehicle and bridge variations; a discussion of the effects of roadway roughness; a discussion of the effect of varying the location of damage and the effects of temperature gradients. The fourth section presents a brief discussion.

Experimental setup and protocol

The indirect SHM proposed in this study was tested on two bridge models. A picture of the bridge setup, hereafter designated as B1, is presented in Figure 16a. A picture of the vehicle is presented in Figure 16b. Details and technical drawings of the experimental setup were presented in Section 3.2 and shown in Figure 13. The model consisted of three segments of 8ft. (2438 mm) long each: an acceleration ramp made of 2 in. x 1 in. x 1/8 in. (50.8 mm. x 25.4 mm. x 3.175 mm.) 6063-T52 Aluminum Arch. Channel section, a bridge deck consisting of a simply supported aluminum plate with angle sections as girders as previously shown in Figure 13c, and a deceleration ramp identical to the first segment. The deck was a 8 ft.x 2 ft. (2438 x 610 mm) aluminum plate with thickness equal to 1/8 in. (3.175 mm). The second bridge herein indicated as B2, differed from B1 by having smaller (3.175 mm instead of 6.35 mm) angle sections as longitudinal girders.



Figure 16: Experimental setup. a) General angle photo of experimental setup, b) Vehicle picture. W.A.V. is the wheel level on the A axle, and S.A.V. is the suspension level on the A axle. W.B.V. and S.B.V. are the corresponding wheel and suspension levels on the B axle.

To create three different vehicles for testing the generality of our concept for different vehicles, three different masses were placed at the midspan of the bar connecting the front and rear axle of the vehicle. As such three vehicles with different dynamic properties were able to be used in testing the indirect SHM approach. The fundamental frequencies of the three vehicles are summarized in Table 3.

Table 3: Vehicle properties.

	V1	V2	V3
Vehicle weight [kg]	4.8	5.2	5.7
A.V axle frequency[Hz]	5.0	4.6	4.5
B.V axle frequency [Hz]	5.3	4.8	4.7

In this study, the effect of damage scenarios, temperature variation, and surface roughness on the response of the sensors was evaluated. To simulate different damage scenarios, the following boundary conditions were varied: (a) rotational restraints, (b) damping and (c) mass. Rotational restraints were added to the bridge at the each of the four supports of the bridge girders as detailed in Figure 17a. Six dash-pot dampers (Figure 17b) were progressively connected to the deck to change the bridge damping characteristics. An additional mass (from 50g up to 300g) was positioned at different locations on the deck in order to simulate a change in

the natural frequencies and mode shapes of the structure. Two roughness conditions, hereafter indicated as R1 and R2, were simulated when testing the indirect SHM approach for classifying each of the damage scenarios. R1 represents the case of accidental imperfections of nominally smooth guide rail over which the vehicle travels. R2 represents the case of a built-in roughness profile for a particular bridge. R2 was achieved by modifying the rail that guides the moving vehicle with an angle section that had been randomly filed down to generate a roughness profile as shown in Figure 17c. The roughness profile measured for B1R2 and B2R2 is shown in Figure 17d, where track 1 is the right rail on the A-B motion direction and track 2 the left rail on the A-B motion direction. Finally, six electric heat sheets were attached underneath the deck in order to model the effect of changes in temperature. The heat sheets location is shown in Figure 17e. A circuit was built to discretely turn on and off the heat sheets and produce different temperature distribution. An infrared camera was used to record and report the bridge temperature scenarios.

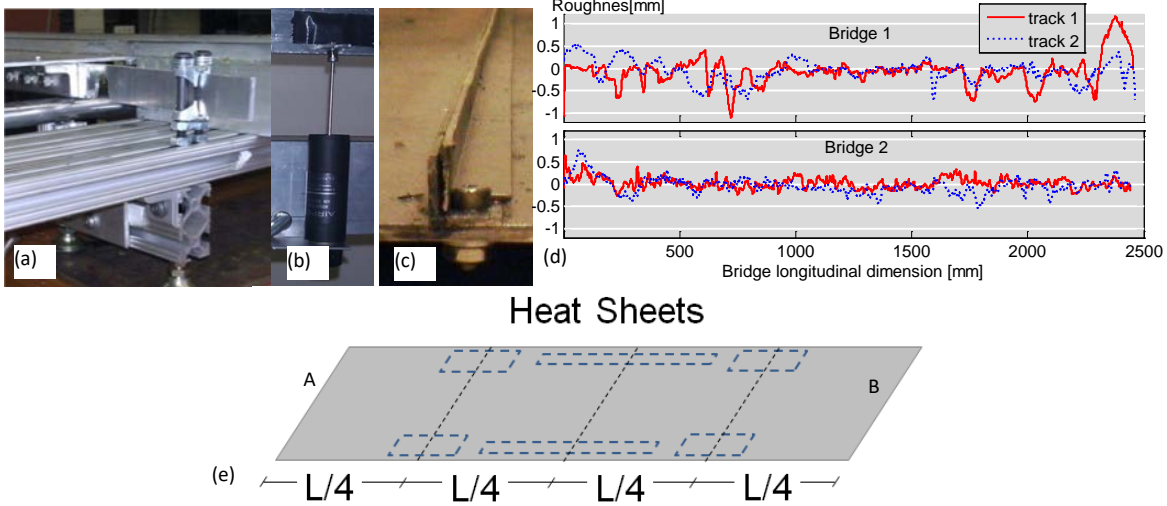
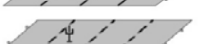
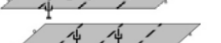
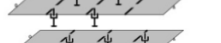
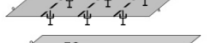
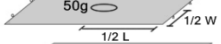


Figure 17: Introduced modifications to the bridge structure. (a) Rotational restraints (b) Additional damping and (c) Roadway roughness profile built on top of guide rail (d) Measured additional roughness (e) Scheme for Heat Sheet locations. A and B are reference points for the forward travelling direction.

Three sets of experiments were conducted. In the first set, 13 different boundary conditions were created and the three vehicles were used to monitor both bridges B1 and B2. Table summarizes the location of the rotational restraints (scenarios SC020BiR1-SC050 BiR1), dashpots (SC060 BiR1-SC090 BiR1), and masses (SC100BiR1-SC130BiR1), where $i=1$ for Bridge 1 and $i=2$ for Bridge 2. The table also presents the corresponding fundamental frequency (f [Hz]) and % critical damping ($\% \zeta_{crit}$) for both bridges. We used conventional free vibration testing to determine these dynamic parameters. The variation with respect to the baseline condition (SC010BiR1, the *undamaged* scenario) is presented as well in terms of % f shift and % ζ_{crit} shift in Table 4. These dynamic parameters in Table 4 are shown to illustrate the magnitude of the change imposed to the bridge structure for the different damage scenarios. Then, classification analysis was performed with data collected from vehicle-bridge interaction experiments. Each of the three vehicles crossed the bridge at 8 different speeds ranging from 1 to 2.75m/s at 0.25 m/s increments. To assess repeatability, 32 iterations were performed for each combination of vehicle, damage scenario and vehicle speed. Data was recorded when the vehicle was moving in both the forward (A-B) direction and backward (B-A) direction. As such, a total of 13 (scenarios) \times 2 (bridges) \times 3 (vehicles) \times 8 (speeds) \times 32 (iterations) \times 2 (motion directions) = 39936 individual experiments were conducted. However, in this paper only the forward motion

is considered from this point forward, which means that 19968 experiments composed the first set of interaction experiment data set.

Table 4: Damage scenarios: types and severity.

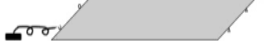
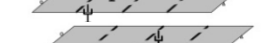
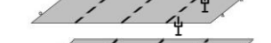
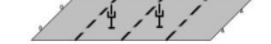
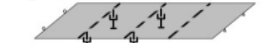
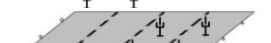
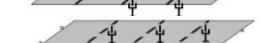
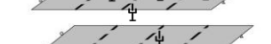
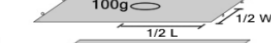
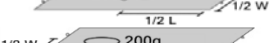
Schematics	B1 R1					B2 R1				
	SC	f [Hz]	% f shift	% \mathfrak{z}_{crit}	% \mathfrak{z}_{crit} shift	SC	f [Hz]	% f shift	% \mathfrak{z}_{crit}	% \mathfrak{z}_{crit} shift
	010B1R1	7.23	0.00	3.63	0.0	010B2R1	5.75	0.000	7.70	0.00
	020B1R1	7.46	3.17	6.34	74.9	020B2R1	6.07	5.56	8.59	11.6
	030B1R1	7.66	6.00	6.45	77.8	030B2R1	6.36	10.5	11.3	46.0
	040B1R1	8.11	12.2	7.97	120	040B2R1	6.72	16.8	13.9	79.9
	050B1R1	8.56	18.4	9.37	158	050B2R1	7.11	23.7	14.4	86.7
	060B1R1	7.24	0.17	8.52	135	060B2R1	5.80	0.87	14.3	86.3
	070B1R1	7.25	0.28	11.3	212	070B2R1	5.81	1.04	15.8	105
	080B1R1	7.28	0.73	26.4	629	080B2R1	5.96	3.66	30.2	293
	090B1R1	7.30	0.98	31.4	767	090B2R1	5.94	3.22	46.7	507
	100B1R1	7.19	-0.56	4.44	22.5	100B2R1	5.73	-0.43	6.97	-9.52
	110B1R1	7.18	-0.66	4.34	19.5	110B2R1	5.71	-0.72	6.60	-14.2
	120B1R1	7.14	-1.29	4.07	12.3	120B2R1	5.69	-1.02	6.42	-16.6
	130B1R1	7.09	-1.85	4.37	20.5	130B2R1	5.66	-1.60	6.41	-16.8

In the second set of experiments, the effect of roughness and location of damage was studied. The roughness condition R2 was compared to the smooth rail condition R1 for some scenarios and after only the roughness condition is used as it is a more realistic condition.

Table 5 summarizes the configurations and dynamic characteristics of both bridges under roughness scenarios R2. The scenarios in

Table 5 allowed comparing the effect of roughness on scenarios SC020BiR2, SC030BiR2, SC070BiR2, SC080BiR2, SC110BiR2 and SC120BiR2, with their corresponding SC020BiR1, SC030BiR1, SC070BiR1, SC080BiR1, SC110BiR1 and SC120BiR1, where $i=1$ for Bridge 1 and $i=2$ for Bridge 2.

Table 5: Damage scenarios: locations and roadway roughness

Schematics	B1 R2					B2 R2				
	SC	f [Hz]	% f shift	% z_{crit}	% z_{crit} shift	SC	f [Hz]	% f shift	% z_{crit}	% z_{crit} shift
	010B1R2	7.77	0.00	13.04	0.00	010B2R2	5.80	0.00	5.81	0.00
	020B1R2	7.86	1.06	15.63	0.20	020B2R2	5.95	2.62	9.85	0.69
	021B1R2	7.87	1.30	19.64	0.51	021B2R2	5.95	6.10	8.53	0.47
	022B1R2	8.00	2.99	13.46	-0.03	022B2R2	6.15	6.90	13.55	1.33
	023B1R2	8.17	5.20	24.85	0.91	023B2R2	6.20	12.07	9.23	0.59
	030B1R2	8.10	4.27	16.17	-0.24	030B2R2	6.50	13.79	8.46	0.46
	031B1R2	8.30	4.27	21.05	0.61	031B2R2	6.60	8.62	11.61	1.00
	032B1R2	8.40	8.14	19.53	-0.5	032B2R2	6.30	6.90	9.32	0.60
	033B1R2	8.10	6.85	9.98	-0.23	033B2R2	6.20	-0.86	13.14	1.26
	070B1R2	7.77	0.00	18.93	0.45	070B2R2	5.75	-0.86	19.00	2.27
	071B1R2	7.77	0.00	27.06	1.08	071B2R2	5.75	-0.86	33.13	4.70
	072B1R2	7.77	0.00	18.54	-0.42	072B2R2	5.75	-0.86	18.82	2.24
	073B1R2	7.77	0.00	23.40	0.79	073B2R2	5.75	-0.86	23.42	3.03
	080B1R2	7.67	-1.30	34.52	1.65	080B2R2	5.75	-0.86	40.47	5.97
	081B1R2	7.67	-1.30	33.80	1.59	081B2R2	5.75	-0.86	37.91	5.52
	082B1R2	7.67	-1.30	35.51	1.72	082B2R2	5.75	-0.86	39.85	5.86
	083B1R2	7.70	-0.88	37.03	1.84	083B2R2	5.75	-0.86	40.36	5.95
	110B1R2	7.67	-1.30	11.82	-0.09	110B2R2	5.65	-2.59	10.16	0.75
	111B1R2	7.67	-1.30	12.28	-0.06	111B2R2	5.65	-2.59	10.87	0.87
	112B1R2	7.67	-1.30	11.70	-0.10	112B2R2	5.65	-2.59	9.64	0.66
	113B1R2	7.67	-1.30	13.81	0.06	113B2R2	5.65	-2.59	8.99	0.55
	120B1R2	7.60	-2.16	11.25	-0.14	120B2R2	5.60	-3.45	9.04	0.56
	121B1R2	7.70	-0.88	12.55	-0.04	121B2R2	5.65	-2.59	9.41	0.62
	122B1R2	7.77	0.00	12.62	-0.03	122B2R2	5.65	-2.59	8.86	0.52
	123B1R2	7.60	-2.16	11.28	-0.14	123B2R2	5.60	-3.45	8.17	0.41

To conduct experiments related to the effect of damage location, four cases for each damage scenario were conducted. For example, in the damage scenario where a single rotational restraint is applied (SC020BiR2), it is applied at four different locations; for these four locations, the labels SC020BiR2, SC021BiR2, SC022BiR2 and SC023BiR2 were used. The same was done for scenarios SC030 BiR2, SC070 BiR2, SC080 BiR2, SC110 BiR2 and SC120 BiR2 with corresponding scenarios where the location of damage was changed. Vehicle 1 (V1 from Table 3), operated at four speeds ranging from 1.5 to 2.25m/s in 0.25 m/s increments in the second experiment set. As such, 25 (scenarios) x 2 (bridges) x 1(vehicle) x 4 (speeds) x 32 (iterations) = 6400 experiments composed the second set of experiments.

In the third set of experiments, the effect of a temperature gradient on the bridge was investigated. The bridge B1 with roughness R2 was subjected to eleven different temperature patterns, as summarized in the leftmost column of Table 6. For illustrative purposes, Figure 18 shows one of these patterns. In order to make the infrared measurements accurate, the surface of the deck was painted using a standard gray paint. For each pattern four different damage scenarios were devised. One is the pristine condition and the other three represent one of each of the three damage types. Vehicle V1 was used at speeds ranging from 1.5 to 2.25m/s at 0.25 m/s increments. A total of 11 (temperature gradients) x 4 (bridge scenarios) x 4 (speeds) x 1 (vehicle) x 1 (bridge) x 32 (iterations) = 5632 experiments composed the third set of experiments.

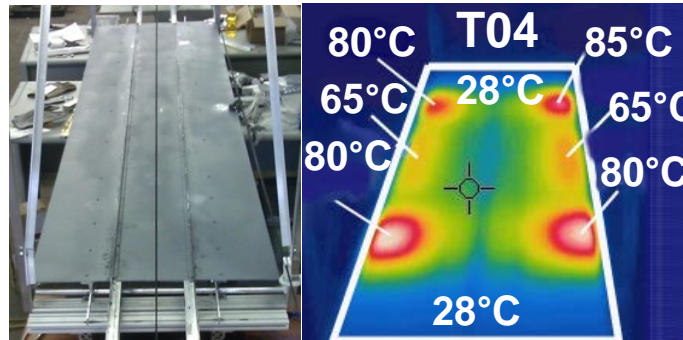


Figure 18: Bridge longitudinal view; normal and Infrared images.

The different scenarios described in this section were processed for feature extraction and classified using the same methodology as described in Task 1. The Following describes the classification experiments performed results obtained.

Table 6: Damage scenarios: temperature B1 R2

Infrared Images	Schematics	SC	f [Hz]	% f shift wrt T00	% f shift wrt SC010	ξ	% ξ_{crit} wrt T00	% ξ_{crit} wrt SC010
		010B1R2	7.26	0.00	0.00	9.30	0.00	0.00
		020B1R2	7.40	0.00	1.92	6.32	0.00	-32.06
		070B1R2	7.16	0.00	-1.39	13.45	0.00	44.67
		110B1R2	7.16	0.00	-1.39	5.78	0.00	-37.85
		010B1R2	7.63	4.98	0.00	13.06	40.48	0.00
		020B1R2	7.71	4.08	1.05	12.15	92.35	-6.98
		070B1R2	7.68	7.28	0.77	14.43	7.32	10.52
		110B1R2	7.61	6.22	-0.22	9.03	56.27	-30.86
		010B1R2	7.46	2.66	0.00	14.49	55.90	0.00
		020B1R2	7.55	2.04	1.30	12.33	95.28	-14.90
		070B1R2	7.47	4.23	0.11	17.75	31.98	22.47
		110B1R2	7.44	3.87	-0.23	12.87	122.72	-11.21
		010B1R2	7.59	4.51	0.00	9.54	2.66	0.00
		020B1R2	7.91	6.79	4.14	14.79	134.25	55.02
		070B1R2	7.67	7.04	1.00	17.17	27.67	79.92
		110B1R2	7.59	5.99	0.00	11.77	103.65	23.29
		010B1R2	7.32	0.81	0.00	15.58	67.60	0.00
		020B1R2	7.50	1.35	2.46	19.0	200.86	21.95
		070B1R2	7.47	4.23	1.95	16.63	23.63	6.72
		110B1R2	7.38	3.05	0.80	12.39	114.49	-20.46
		010B1R2	7.52	3.47	0.00	15.58	68.71	0.00
		020B1R2	7.60	2.72	1.17	11.45	81.25	-27.01
		070B1R2	7.57	5.63	0.67	16.26	20.91	3.68
		110B1R2	7.53	5.16	0.22	10.01	73.33	-36.15
		010B1R2	7.67	5.56	0.00	13.35	43.60	0.00
		020B1R2	7.66	3.40	-0.16	13.46	113.15	0.84
		070B1R2	7.47	4.23	-2.63	22.23	65.33	66.57
		110B1R2	7.42	3.52	-3.29	17.0	194.25	27.35
		010B1R2	7.71	6.13	0.00	12.84	38.10	0.00
		020B1R2	7.86	6.12	1.90	10.2	61.55	-20.53
		070B1R2	7.67	7.04	-0.55	16.19	20.41	26.14
		110B1R2	7.67	7.04	-0.55	11.11	92.28	-13.47
		010B1R2	7.39	1.74	0.00	10.98	18.10	0.00
		020B1R2	7.66	3.40	3.59	11.35	79.78	3.41
		070B1R2	7.47	4.23	1.02	16.57	23.24	50.96
		110B1R2	7.46	4.11	0.91	11.34	96.35	3.33
		010B1R2	7.53	3.70	0.00	10.65	14.54	0.00
		020B1R2	7.66	3.40	1.62	10.51	66.50	-1.25
		070B1R2	7.48	4.46	-0.67	15.40	14.48	44.59
		110B1R2	7.48	4.46	-0.67	12.87	122.75	20.86
		010B1R2	7.73	6.37	0.00	9.80	5.44	0.00
		020B1R2	7.91	6.79	2.33	10.0	58.31	2.00
		070B1R2	7.73	7.98	0.11	17.16	27.57	75.04
		110B1R2	7.67	7.04	-0.76	11.39	97.17	16.22

Classification Experiments and Results

Effect on Classification Accuracy of Variations of Vehicles, Bridges, Vehicle Speeds and Severity of Change

The signal processing described in Task 1 was used for damage detection and severity identification. The damage detection is a two class experiment (i.e., damaged or undamaged) while the severity classification in this task (Task 2) is a four class experiment (i.e., 020BiR1-050BiR1).

Damage detection. The first class in this two label experiment, *undamaged*, is associated with pristine condition represented by any scenario labeled as SC010BiR1 in Table 4. Scenarios labeled SC020BiR1-SC0130BiR1 were associated with the second class, *damaged*. We thus obtained, 7 (sensors) x 12 (scenarios) x 8 (speeds) x 3 (Vehicles) x 2 (Bridges) = 4032 separate assessments of classification accuracy. The classification accuracy is the proportion of true estimated results (both true positives and true negatives) in the population and is a very good indicator of the effectiveness of correctly classifying new incoming data. The results are presented for each bridge separately in Figure 19 - Figure 22.

Figure 19 show the results associated with Bridge 1. Three separate bars are used to associate the sensors to their respective location (Bridge, Wheel or Suspension). The separation of the results by location of bridge sensor allows for a comparison between the *direct* and *indirect* approach. The vertical bars represent the standard deviation associated with of the averaged results of 288 experiments for the bridge sensors 3 (sensors) x 12 (scenarios) x 8 (speeds) = 288 (detection experiments), and 192 detection experiments for the wheel and suspension sensors 2 (sensors) x 12 (scenarios) x 8 (speeds) = 192 detection experiments). At the top of each bar the standard deviation is shown. The average accuracy obtained for all the sensors is shown with a black line behind the bar graphs with numeric value of average included. Figure 19a shows the classification accuracy relative to the rotational restraints as determined using each of the three vehicles. In the framework of the binary classification performed here, an accuracy of 50% represents the probability of randomly assigning a label to one of the two classes. Overall the performance of the sensors mounted on the wheel is comparable to the direct monitoring, and superior to the accelerometers mounted on the suspensions. There is not a significant difference between Vehicle 1 and Vehicle 3 in Figure 19a. Similarly Figure 19b and 6c show the results associated with the damping and the mass increases, respectively. In Figure 19b and 19c there is a 5% to 6% decrease in accuracy between Vehicle 1 and Vehicles 2 and 3. The rotational restraints scenarios are less sensitive to vehicle changes than the damping increase or the mass increase scenarios. The consistent results of the rotational restraint can be attributed to % change in the natural frequency of the rotational restraint scenarios being more significant than the damping or mass increase scenarios (see Table 5). The fundamental frequency of the rotational restraint scenarios vary up to 18% for Bridge 1 and 23.7% for Bridge 2 while the mass and damping increase scenarios vary less than 4%. Figure 19a - c suggest that: 1) the increase of the vehicle mass has a detrimental impact on the classification accuracy that is more significant for slight changes in the bridge; and 2) the sensors at the wheel level outperform all other sensors.

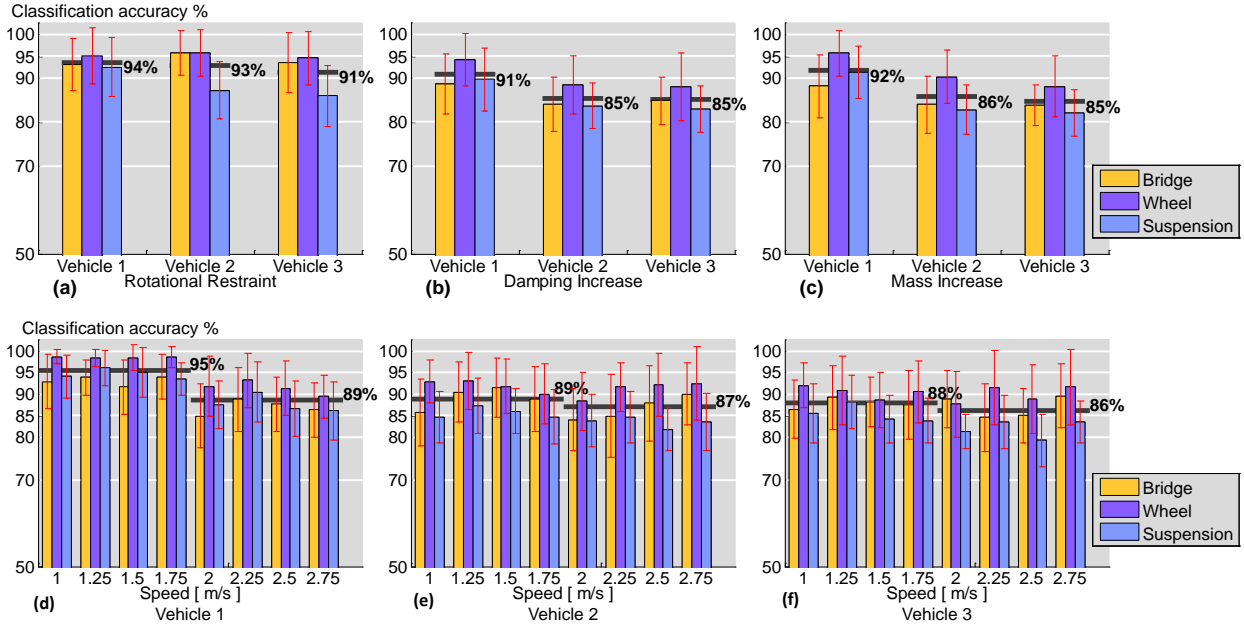


Figure 19: Bridge 1: (a-c) Damage detection accuracy for different vehicles averaged across different speeds and severity scenarios of the same damage type: (a) Rotational Restraint; (b) Damping Increase and (c) Mass Increase. (d-f) Damage detection accuracy for different speeds averaged across the different damage scenarios of the same vehicle: (d) Vehicle 1; (e) Vehicle 2 and (f) Vehicle 3.

The effect of the vehicle speed on the classification accuracy is shown in Figure 19d-f. An average of the first four speeds and the last four for all the sensors is depicted with a black line behind the bar graphs with an associated numeric value. Figure 19a shows a decrease among the first four and the last four speeds. The other two vehicles, Figure 19b and c are more stable with respect to speed variation.

Similar to Figure 19, Figure 20 reports on the results associated with Bridge 2. Figure 20a-c shows a small change in the average classification results for the different vehicles and better classification accuracy with respect to the results for Bridge 1. Figure 20a shows an average 96% classification accuracy for the Rotational Restraints scenarios. Figure 20b shows an average 93% classification accuracy for the Damping increase scenarios. Figure 20c shows an average 90% classification accuracy for Mass Increase scenarios. Figure 20d-f shows the classification accuracy across the different speeds for Bridge 2. Figure 20d-f shows a steadier trend across the different speeds for all the vehicles for Bridge 2 when compared to Bridge 1 in Figure 19d-f. The overall average classification accuracy for the three vehicles and different speeds is about 93% for Bridge 2.

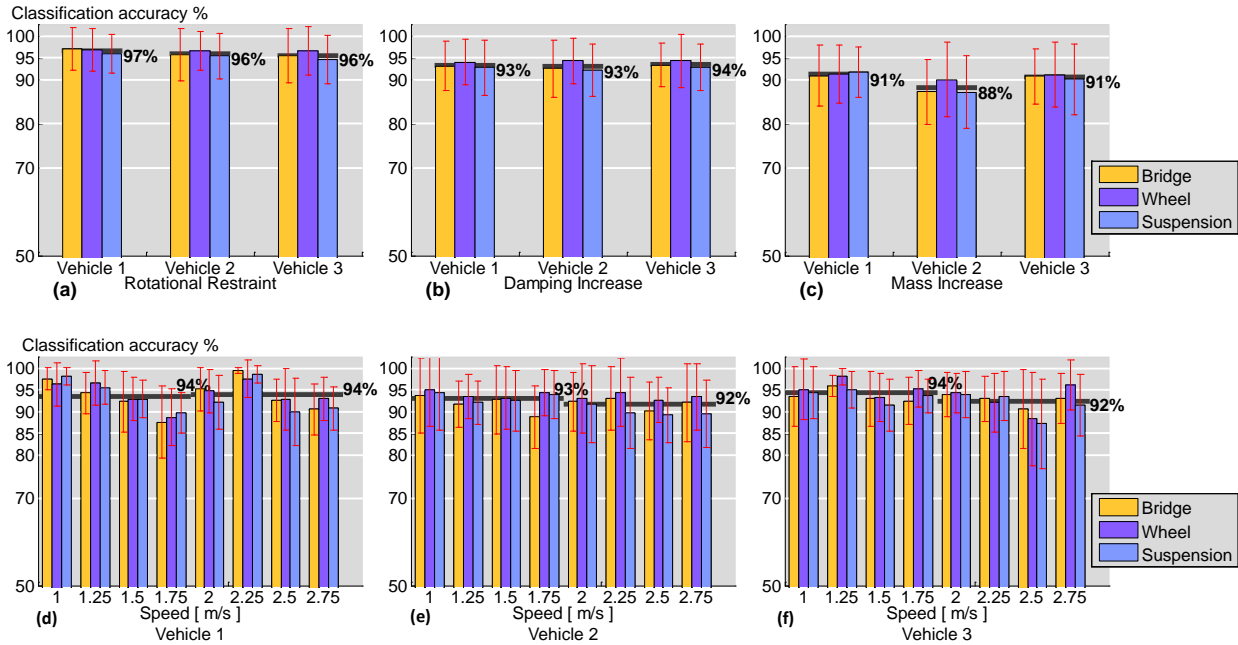


Figure 20: Bridge 2: (a-c) Damage detection accuracy for different vehicles averaged across different speeds and severity scenario of the same type: (a) Rotational Restraint; (b) Damping Increase; and (c) Mass Increase. (d-f) Damage detection accuracy for different speeds averaged across the different damage scenarios: (a) Vehicle 1; (b) Vehicle 2; and (c) Vehicle 3.

Severity classification. The severity classification experiments were defined as four label classification experiments for each damage type: Rotational Restraints, Damping Increase and Mass Increase. SC020BiR1, SC030BiR1, SC040BiR1 and SC050BiR1 are the four scenarios for the Rotational Restraint damage type as shown in Table 2. The four Damping Increase severity levels were defined by the scenarios: SC060BiR1, SC070BiR1, SC080BiR1 and SC090BiR1. Finally, the four mass Increase severity levels were defined by the four scenarios: SC100BiR1, SC110BiR1, SC120BiR1 and SC130BiR1. Each of the severity classification experiments considered was run with the corresponding data of the 4 labels, from a particular sensor and for a particular damage type (one of three), vehicle (one of three), vehicle speed (one of eight) and bridge (one of two). We ran, therefore, 1008 total classification experiments 7 (sensors) \times 3 (damage types) \times 8 (speeds) \times 3 (vehicles) \times 2 (bridges) = 1008. Just as in the case of the damage detection experiments, the results are shown for each bridge separately. Results for Bridge 1 are shown in Figure 21 and for Bridge 2 in Figure 22. The three sensor locations (Bridge, Wheel and Suspension) were represented by separate bars in the bar graphs. In Figure 21, the baseline for this case was set at 25%, which is the probability of randomly assigning a label among the four labels, $P=1/4$.

Figure 21a-c show the average classification accuracy results for Bridge 1 for each of the three damage types for each of the three different vehicles used (similar to Figure 19a-c and Figure 20a-c). Consistent trends as the ones observed in the two-label detection experiments can be seen in the four-label severity classification experiments. The Rotational Restraint scenarios

are on average higher in classification accuracy than the other two damage types because of a more significant shift in the natural frequency of the bridge cause by rotational restraint. The classification results for the four-label experiments across the different speeds for Bridge 1 are shown in Figure 21d-f. A significant decrease in the average classification accuracy for Bridge 1 occurs for the last four speeds in comparison to the first four speeds for vehicle 1. The classification accuracies for the other two vehicles are less sensitive to a change in speed.

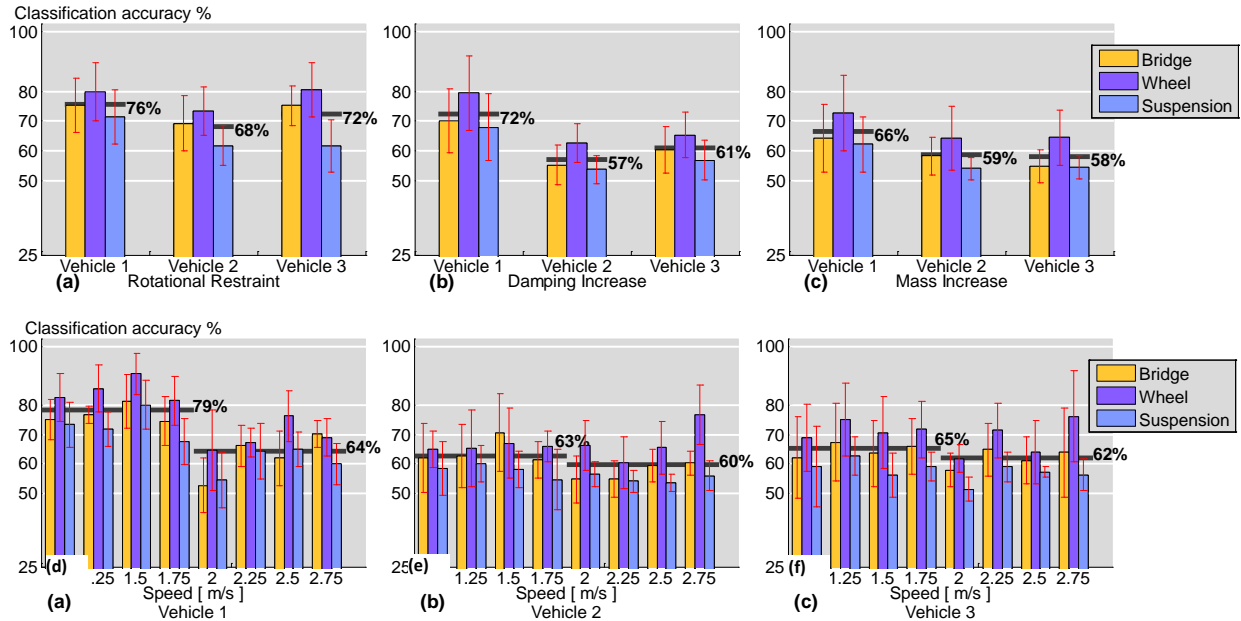


Figure 21 Bridge 1: (a-c) Damage severity classification accuracy for different vehicles averaged across different speeds and severity scenario of the same damage type: (a) Rotational Restraint; (b) Damping Increase; and (c) Mass Increase. (d-f) Damage severity classification accuracy for different speeds averaged across the different damage scenarios of the same vehicle: (d) Vehicle 1; (e) Vehicle 2; and (f) Vehicle 3.

Similarly, Figure 22 presents the classification accuracies for Bridge 2 in the same manner that Figure 21 does for Bridge 1. Figure 22a-c shows better classification accuracy with respect to the results for Bridge 1 shown in Figure 21a-c. An 80% classification accuracy was obtained for the Rotational Restraints scenarios as shown in Figure 22a, a 73% classification accuracy for the Damping increase scenarios is shown in Figure 22b, and a 67% classification accuracy for Mass Increase scenarios is shown in Figure 22c.

Figure 22d-f show the classification accuracy for damage types on Bridge 2 for different vehicle speeds. It shows a steadier trend across the different speeds for all the vehicles for the damage scenarios on Bridge 2 when compared to Bridge 1 in Figure 21d-f. The overall average classification accuracy for the three vehicles and different speeds is about 73% for Bridge 2. Overall the classification results obtained for Bridge 2 were higher than those for Bridge 1 and more stable with respect to the different speeds.

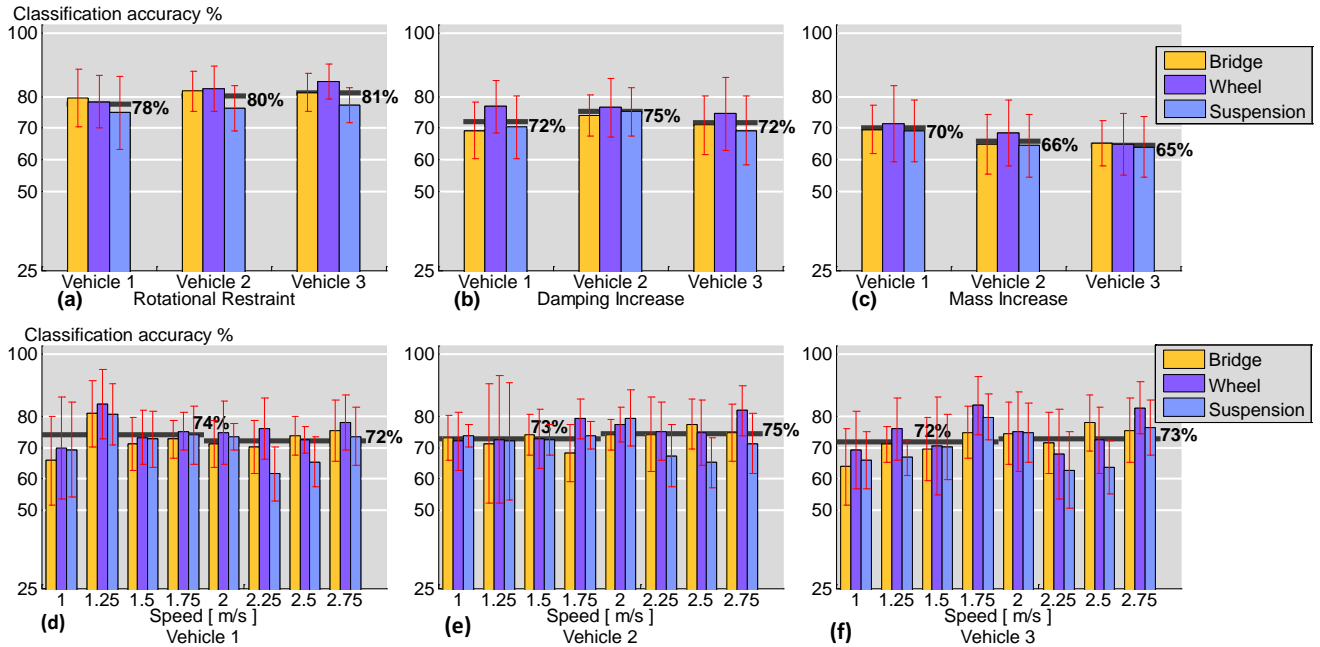


Figure 22: Bridge 2: (a-c) Damage severity classification accuracy for different vehicles averaged across different speeds and severity scenario of the same damage type: (a) Rotational Restraint; (b) Damping Increase; and (c) Mass Increase. (d-f) Damage severity classification accuracy for different speeds averaged across the different damage scenarios of the same vehicle: (d) Vehicle 1; (e) Vehicle 2; and (f) Vehicle 3.

The classification results obtained were further inspected by creating cluster plots of the four Rotational Restraint scenarios: SC020B1R1, SC030B1R1, SC040B1R1 and SC050B1R1. Figure 23 shows the cluster plot generated using the first three frequency features for the samples defined for Bridge 1, Vehicle 1, Speed 1 and without additional built-in roughness. The most significant frequencies are used as features for the different scenarios as described in Section 3.3.2. One can see that the high classification accuracy obtained for the rotational restraint scenarios can be well justified when looking at the cluster plots. The four different severity scenarios for the rotational restraints generated distinct clusters that can be distinguished by the naked eye.

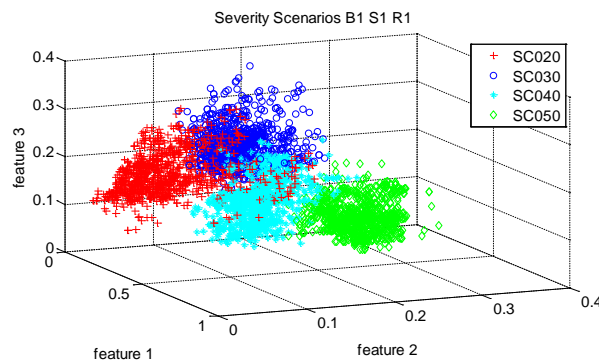


Figure 23: Rotational restraints scenarios cluster analysis. Vehicle 1, Bridge 1, Speed 1 m/s, R1 (Roughness from accidental imperfections).

Effect of Roughness and Damage Location

Tables 4 and 5 showed the second set of scenarios run for determining the effects of roadway roughness on classification accuracy. For this set of experiments, both bridges were modified to include a roadway profile as described in Section 4.2. We compared the damage detection accuracy for two different roughness conditions, R1 and R2.

Damage detection accuracy for different roughness. In a second set of experiments, we explored the accuracy of damage detection when a roadway roughness profile exists. The average classification accuracies obtained with and without roughness were plotted in Figure 24. Figure 24 a – d show the cases of the two rotational restraint scenarios Bridges 1 and 2. The caption and the scheme below in each plot in Figure 24 identifies the corresponding scenario of one or two rotational restraints. Similarly, schemes and captions identify the corresponding scenario for each plot in Figure 24. Figure 24 e – h show the cases of the two damping increase scenarios in Bridges 1 and 2, and Figure 24i – l show the mass increase scenarios in Bridges 1 and 2. Each graph in Figure 24 shows the average classification accuracy for Vehicle 1 and a specific Bridge (Bridge 1 in Figure 24a,b,e,f,i,j or Bridge 2 in Figure 24b,c,g,h,k,l), using four different vehicle speeds (1.5, 1.75, 2 and 2.25m/s), the different sensor location and the two different roughness profiles (that of the purchased angle referred to as R1 and that of the manufactured roughness referred to as R2, both were discussed in Section 4.2). The baseline was set to 50% and each bar represents the average results obtained for a particular sensor location as in the previous damage detection graphs.

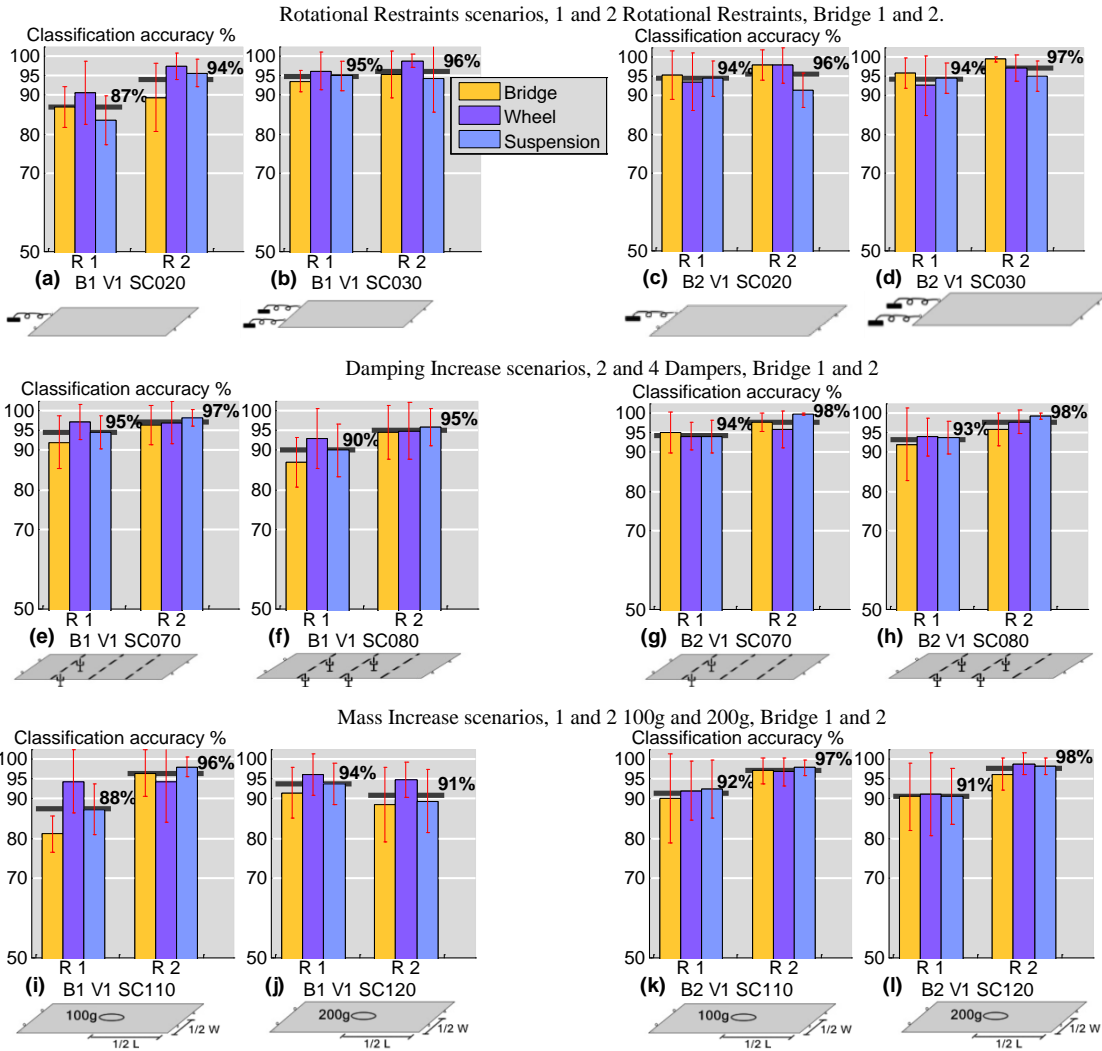


Figure 24: Damage detection comparison among bridges with two different roughness profiles. (a-d) two Rotational Restraints scenarios: (a-b) Bridge 1 and(c-d) Bridge 2; (e-h) two Additional Damping scenarios: (e-f) Bridge 1 and (g-h) Bridge 2; (i-l) two Additional Mass scenarios: (i-j) Bridge 1 and (k-l) Bridge 2.

The comparison presented in Figure 24 shows an increase in the damage detection capability when the bridge had more significant roadway roughness (case R2). These results indicate that roadway roughness may actually contribute to more accurate classification for the indirect approach, which is admittedly counter to what one might have expected when adding this variable to the problem. Intuitively, however, we can possibly explain this increase in classification accuracy as a result of the roadway roughness increasing the vibration of the bridge allowing the vehicle to better capture the dynamic characteristics of the bridge structure. However, including the roadway roughness in the manner we did in this experiment (adding an additional portion of the rail) also increased the natural frequency of the undamaged bridge (See

Table 2), and the increase in classification accuracy also could be attributed to a different vehicle/bridge frequency ratio. More investigation is necessary on this issue, but the experiment does begin to dispel concerns that adding roadway roughness would make the classification accuracy worse.

The Effect of Different Locations of Damage

Using the second set of scenarios shown in

Table 4, we setup two types of classification experiments. The first was a set of damage detection experiments for the same amount of damage at different locations, and the second was a set of four label classification experiments where the location was made to be different between scenarios with the same amounts and type of damage. These two sets of classification experiments are further described in the following two sub-sections.

Detection accuracy for damage at different locations. We explored the accuracy of damage detection for scenarios with the same amount of damage of a certain type at different locations on the bridge structure (see

Table 5). In these two-label experiments, we explore the dependence of the accuracy for detecting different types of damage on the location of that damage. As in previous sections, each of the detection experiments considered data from a particular sensor, different damage scenarios, a particular speed, a particular vehicle and a particular bridge. We obtained therefore 7 (sensors) \times 24 (damage scenarios) \times 4 (speeds) \times 1 (Vehicle) \times 2 (Bridges) = 1344 separate assessments of classification accuracy. The corresponding average results shown in Figure 25 are grouped by scenarios of the same damage type and severity level but for different locations. For example, in Figure 25a, SC020 is the scenario of a single rotational restraint at a particular location and SC021, SC022 and SC023 are also single rotational restraints but at different locations as defined in

Table 5.

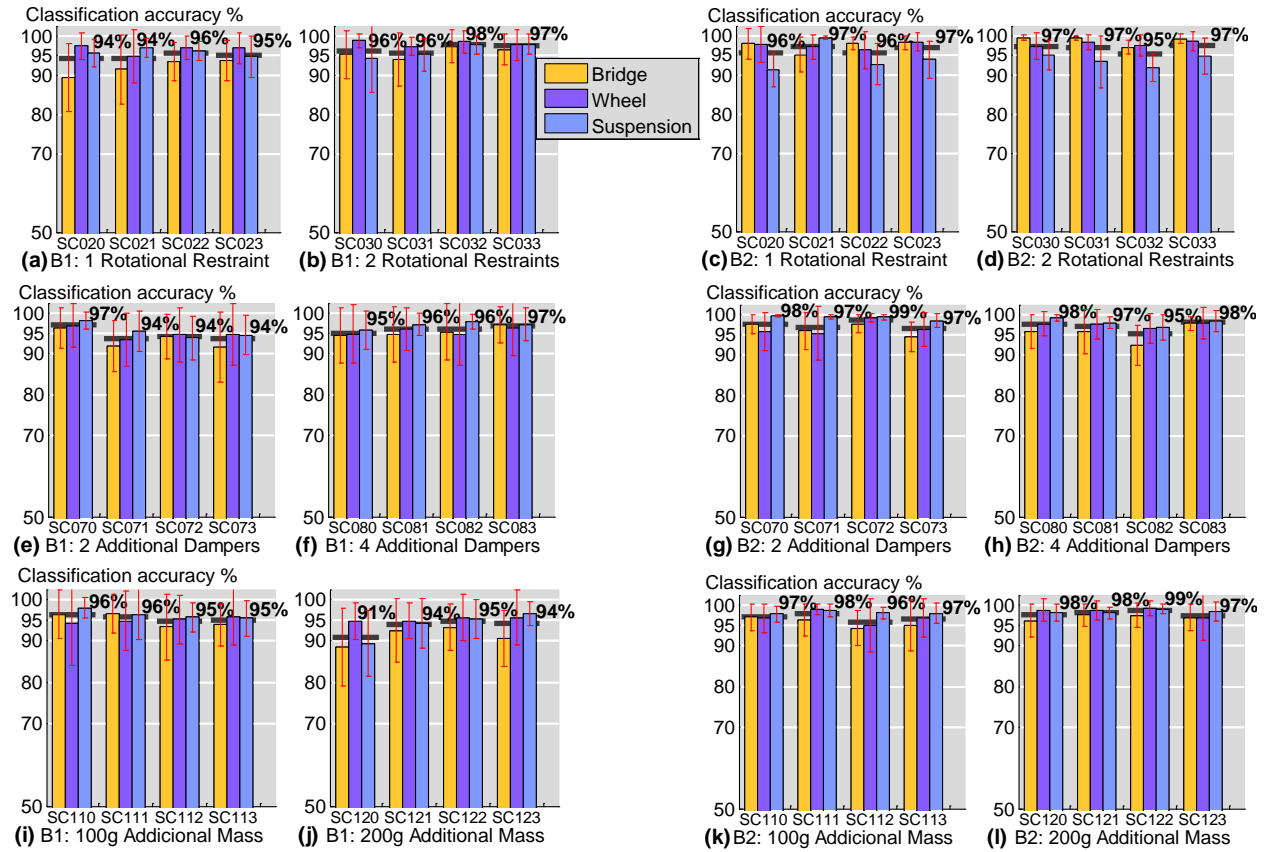


Figure 25: Damage detection comparison among scenarios with different damage locations: Bridge 1 (a,b,e,f,i,j), Bridge 2 (c,d,g,h,k,l).

Figure 25a shows the detection results for different locations of a single rotational restraint for Bridge 1, and Figure 25b shows the average detection results for two rotational restraints at different locations for Bridge 1. Among the scenarios shown in Figure 25b, SC030 and SC031 have both rotational restraints on one side of Bridge 1. The other two scenarios in Figure 25b, SC032 and SC033 had two rotational restraints, one on each side of Bridge 1. Similarly, Figure 25c shows the same scenario for Bridge 2 as that shown for Bridge 1 in Figure 25a. In both bridges, the damage detection accuracy obtained was above 95%. These results suggest that for the damage scenarios modeled, they can be detected with a very high accuracy regardless the location of the applied damage. The same is true for the other scenarios plotted in Figure 25.

Location classification. We also performed a four-label classification experiments on the data from the same set of experiments described in

Table 5. The four labels were defined as the four possible locations of damage of a particular damage type and severity applied to the bridge. In the caption of Figure 26, we named SC02- the four-label location classification experiment for classifying among the four scenarios in which a single Rotational Restraint is applied (SC020, SC021, SC022 and SC023 for Bridge 1 or 2 and Roughness 2). Similarly, we used SC03-, SC07-, SC08-, SC11- and SC12- in Figure 26 for naming the four-label location classification experiments corresponding to scenarios that vary the locations of scenarios SC030, SC070, SC080, SC110 and SC120, respectively as defined in

Table 5. Each four-label location classification experiment was run for a specific sensor, scenario type and severity, speed and bridge. We ran therefore 7 (sensors) x 6 (scenario types and severity) x 4 (speeds) x 1 (vehicle) x 2 (bridges) = 336 four-label location classification experiments. As in previous figures, we plot the different bridge results separately; Figure 26a plots the results for Bridge 1 and Figure 26b plots the results for Bridge 2. The baseline of Figure 26 was set at 25%, $P=1/4$ (P =direct probability).

In Figure 26a, the lowest classification accuracy obtained was 67% for SC08-, which suggests a small difference between the scenarios with four dampers. We can confirm this small variation by looking at

Table 5. SC080 through SC083 in

Table 5 share the same two middle dampers and show small variation in the fundamental frequencies. They would be therefore hard to classify by using the simple frequency-based features that we have used in this study. SC11- and SC12-, which group the location variation for a 100g and a 200g increase as defined in

Table 5, also show small or no variation of the natural frequency. However, even for this challenging case an average classification of over 70% was achieved. In Figure 26b, corresponding to Bridge 2, the lowest classification accuracies obtained were for scenarios SC08- and SC11- (four dampers and a 100g increase at different locations accordingly) there the classification accuracies for both scenarios was over 60%.

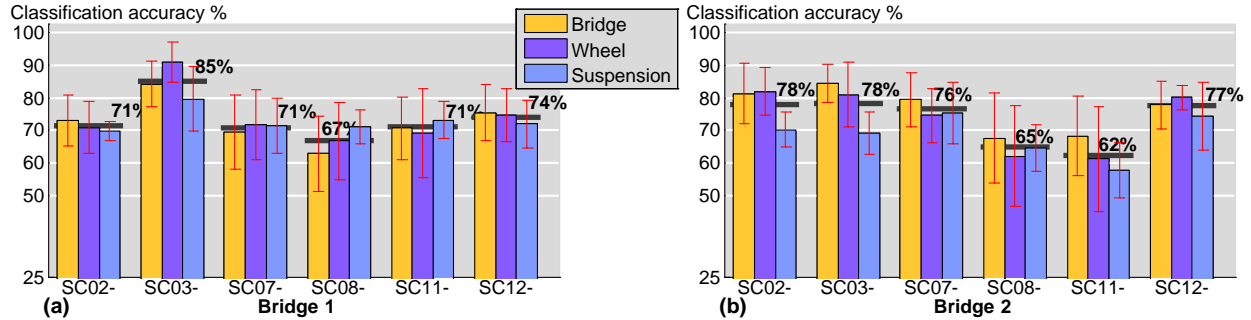


Figure 26: Location classification comparison among scenarios with different damage location: (a) Bridge 1, (b) Bridge 2.

Effect of Temperature gradient scenarios.

We now consider the third data set obtained when the thermal conditions were varied, which was described in Table 6. We ran two different classification experiments using the same signal processing and classifications approach as presented in Section 3.3. The first classification experiment was a damage detection experiment assuming the temperature scenario to be known, and the second classification experiment was a damage detection experiment assuming the temperature scenarios to be unknown. In this second classification experiment, the data from the 11 different temperature gradients for a particular bridge damage scenario is used to define a label. The next two subsections describe the obtained results.

Damage detection within same temperature scenario. As shown in Table 6, four different bridge scenarios: SC010B1R2 (Undamaged), SC020B1R2, SC070B1R2 and SC110B1R2, were run under each specific temperature gradient scenario. We performed damage detection experiments (two labels: Undamaged vs Damaged) for each of the three damage scenarios: SC020B1R2, SC070B1R2 and SC110B1R2 at a particular temperature scenario. In other words, each damage scenario is defined by the corresponding experimental iterations that were conducted for the given temperature scenario that consist of 1 (temperature gradient scenario) x 1 (bridge damage scenario) x 1(speed) x 1 (vehicle)x 1 (bridge) x 32(runs) = 32 iterations to define a particular damage scenario. Figure 27 shows the average and standard deviation of the classification accuracy obtained for the damage detection experiment for each the three damage scenarios under a specific temperature gradient conditions. That is the average of 3(damage scenarios) x 4 (speeds) = 12 classification accuracy experiments. In all these experiments Vehicle 1 was used and the speeds ranged from 1.5 to 2.25m/s at 0.25 m/s increments. The baseline of the graph was set to 50% as in all the previous two-label damage detection graphs. The obtained results show that the average classification accuracy might vary by as much as 15% for the different temperature scenarios (see the results for T02 and T03). This variation suggests that some temperature scenarios might be more favorable for damage detection than others. The results obtained from the bridge sensors and from the vehicle sensors achieved roughly the same classification accuracy.

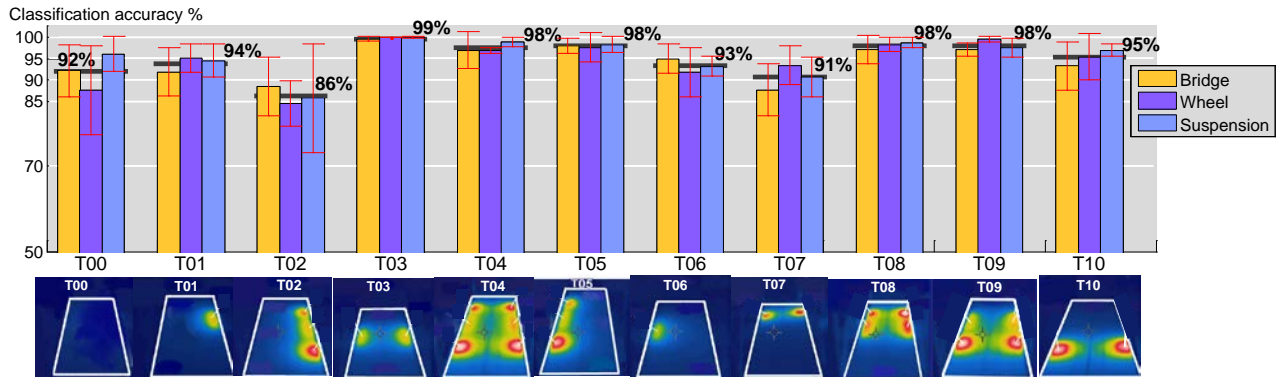


Figure 27: Classification accuracy of damage scenarios for specific temperature gradient scenario.

Damage detection without considering temperature information. The second classification experiment considered a particular bridge condition to define a particular bridge damaged label with all the temperature variations. That is, SC010 is now defined by the 32 runs at each of the 11 different temperature conditions. The other three scenarios in Table 6: SC020, SC070 and SC110 are also defined for this condition. In this case we are treating the temperature condition as an embedded variable in the data. Figure 28 shows the average classification results obtained for the detection experiments. The overall results show an interesting average classification accuracy among the three damage scenarios. The average classification results decrease with respect to the previous experiments shown in Figure 27, where the temperature was considered a known variable. This decrease was expected as this is a more challenging experiment where the embedded variable can mask the damage changes made to the bridge structure. In general terms, it can be seen that the Wheel and Suspension sensors achieved classification accuracies similar to or better than those using the sensor located on the bridge structure.

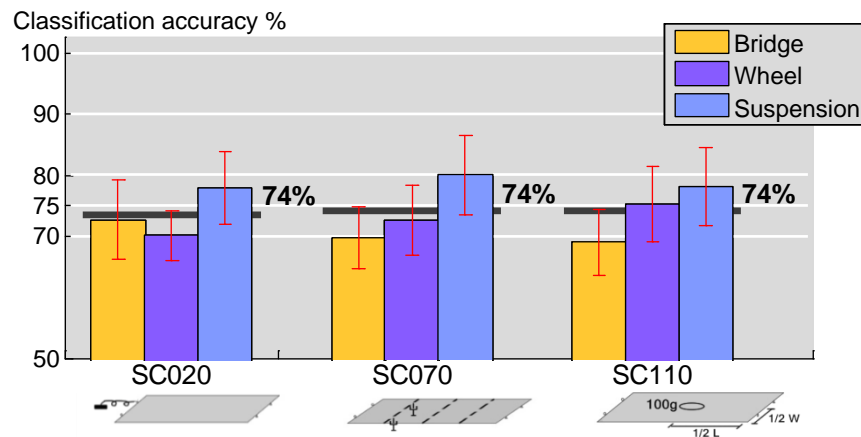


Figure 28: Classification accuracy of damage scenarios regardless temperature scenario for training and testing.

Discussion

In summary, we further validated an *indirect* bridge SHM approach for different temperatures based on vibration data collected from a vehicle as it traverses the bridge structure, and compared the results with the traditional *direct* monitoring approach that uses sensors placed

on the bridge structure. We built an automated laboratory scale experimental setup that allowed for data acquisition and accurate control of the speed of the vehicle, accurately known modifications to the bridge, and multiple repetitions. We used a simple feature extraction and classification approach to perform several classification experiments on the collected data. We explored the space of possible variations to the vehicle-bridge interaction system to test the robustness of the indirect monitoring approach versus the direct monitoring approach. The variations considered two different bridges, eight different vehicle speeds, three different masses of vehicle, two roughness scenarios, 11 different temperature gradients, and three different types of damage made to the bridge (rotational restraints, additional damping and an additional mass). The different types of damage were explored in terms of detecting the existence of the damage and also classifying among scenarios with different damage locations and different levels of damage severity.

For the vehicle variation, the introduction of a higher mass to the vehicle chassis decreased the average classification accuracy for the mass increase and damping increase scenarios in Bridge 1 by about 6%, and showed no significant difference for Bridge 2. The detection classification results for the sensors located at the wheel level and at the suspension system of the moving vehicle (*indirect monitoring*) were comparable with the results obtained with sensors located on the bridge structure (*direct monitoring*).

For the different vehicle speeds, the Bridge 1-Vehicle 1 combination showed a 6% decrease in the damage detection classification accuracy between speeds of 1.75 m/s and 2m/s; however, all other Bridge-Vehicle combinations showed low dependence on speed. The detection results obtained using the indirect and direct monitoring approaches were similar. The severity classification results show similar trends to the damage detection classification accuracy for Bridges 1 and 2, but about 20% lower than those for damage detection. The decrease is attributed to the increase of the number of labels from two labels in the detection experiments to four labels in the severity classification experiments.

The inclusion of roadway roughness increased the detection rate for almost all the damage scenarios compared. The indirect and direct monitoring approaches showed comparable results for all cases.

Different locations of the same magnitude of damage showed similar average damage detection classification accuracy for both bridge structures. The location classification accuracy, a four label classification task, showed variations from 85% to 67% for Bridge 1 and from 78% to 62% for Bridge 2. This variation can be attributed to the choice of scenarios implemented. Some scenarios were very similar to others they were being classified against. The indirect and direct monitoring approaches showed comparable results for all location classification cases.

Two types of damage detection experiments were conducted regarding various temperature gradient conditions. The first damage detection experiment compared damage scenarios within the same temperature gradient conditions. The variation of the detection accuracy of about 15% suggests that there are temperature gradient conditions more favorable than others for detecting damage scenarios. The second damage detection experiments assumed that there was no information about the temperature gradients and treated it as an embedded variable in the data. The classification results for the three scenarios explored on this case showed remarkable consistency for the three scenarios explored of about 74%. Once again the sensors considered as indirect performed just as well as those sensors located on the bridge structure.

The results showed in this section, match, in most cases, the intuition about the behavior of the vehicle-bridge interaction systems with the obtained trends in terms of the classification

accuracies. That is, scenarios that had a greater variation of the dynamic characteristics identified by free-vibration experiments had also higher detection accuracy.

The signal processing methodology used in this work was based on frequency based features and a standard classification algorithm. The numerical classification results could be greatly improved by exploring other feature space representations and other classification algorithms.

From this work, it is clear further research was needed to validate the indirect versus the direct approach for bridge SHM. The results presented thus far are constrained to the corresponding experimental setup. Task 4 in this report will explore other systems and scales where indirect monitoring could be employed.

Task 3: Damage Localization, Quantification and Bridge Condition Uncertainty

In this section we investigate questions which will be of great interest to agencies who own bridges. Assuming there is damage, they will want to know where the damaged has occurred and the severity of the damage. We conducted experiments to answer these questions. In particular our goal was to see how changes in the severity of the damage and location of the damage would change the dynamic response of the bridge so that we could create a general framework for looking at these changes. In these experiments we defined “damage” as the placement of an additional mass on the bridge which would change the frequencies of the bridge in a similar manner to the way that frequencies of the bridge might change as the stiffness of the bridge decreased.

A full write-up of this work is presented in Lederman et al. 2014, which has been included in the Appendix.

The second part of this task was to consider cases where the condition of the bridge is not known. Our approach to structural health monitoring is model free—we do not build a finite element model of the bridge because this can be expensive and inaccurate. Instead we have the algorithms learn about the nature of the bridge. For this learning process to occur the data must be “labeled”—for example, the bridge could be labeled as healthy and then the initial signals would become the baseline. Later changes in the bridge would then be compared to this baseline.

However, in practice we will have to begin monitoring bridges at different stages in their life cycle. When the bridge inspectors give a condition assessment, signals collected during that time period can be labeled by their assessment. However this assessment might change, or worse, the inspectors could have misclassified the condition of the bridge. To accomplish this task we looked at a different approach for selecting features and for classifying the data. A full write up of this work can be found in Chen et al 2013, which can be found in the Appendix. However a brief overview of the work is given below.

Data Analysis for SHM

The goal of data analysis is to analyze patterns of various damage types and label each observation into a predefined class. In data analysis for SHM, we can detect presence or absence of damage, or go one step further and detect the severity, location and type of damage. These tasks are signal-processing problems known as classification.

Classification System

A classification system often has two core components, a feature extractor and a classifier. The feature extractor extracts numerical features from the data with the aim of discriminating classes based on those features. The task of the classifier is to label each observation into a predefined class based on those features.

Progress

So far, we have tried several different feature extractors and classifiers to (1) study the potential power of each algorithm, (2) find the suitable situations in which to use each algorithm, (3) study the difficulty of classification problem, and (4) upgrade our classification system to achieve better results.

Feature Extractor

A feature extractor often includes two approaches: representation and discrimination. Generally speaking, representation approach is robust to noise and does not need training data, while the discrimination approach is sensitive to noise and needs training data, but often achieves better classification results. In bridge SHM project, data is noisy and we have access to few labeled samples (it is expensive to physically inspect the bridge and label it as damaged/undamaged, etc). Up to this point, we have used Fourier discriminant features, principal component analysis, sparse representations, and local Fisher discriminant analysis. We are constantly studying the effectiveness of various feature extractors for use in this project as well as how to combine the advantages of both representation and discrimination approaches.

(1) Fourier discriminant features

Fourier discriminant features choose the most discriminative frequencies as features. It consists of two steps: 1. the data is represented in a Fourier basis; 2. J-divergence is used as the discriminant measurement to evaluate the discriminative power of each frequency and then sort frequencies by their discriminative power. Step 1 provides representation by a fixed basis and Step 2 adaptively discriminates data.

(2) Principal component analysis (PCA) (Abdi et al 2010.)

PCA is a standard representation algorithm. It learns an orthogonal linear transformation from the given data that transforms the data into a new coordinate system such that the first coordinates captures the greatest variance, the second coordinate captures the second greatest variance, and so on.

(3) Sparse representations (Wright 2009, Aharon 2006).

Sparse representations represent signals with a linear combination of a small number of elementary signals called atoms that account for most or all information of a signal. Often, the atoms are chosen from a so called over-complete dictionary. The aim of a sparse representation is often to reveal certain structures of a signal and to represent these structures in a compact and sparse representation. The representation dictionary is learned from data, so it is data adaptive.

(4) Local Fisher discriminant analysis (LFDA) (Sugiyama 2007)

LFDA is an advanced discrimination algorithm that improves on the popular linear discriminant analysis. It provides a linear supervised dimensionality reduction mechanism and is particularly useful when some classes consist of separate clusters. LFDA has an analytic form of the embedding matrix and the solution can be easily computed by solving a generalized eigenvalue problem. Compared to linear discriminant analysis, it considers local information and provides more than $(c-1)$ nontrivial eigenfunctions, where c is the number of classes.

Classifier

We have used two types of classifiers. Supervised classifiers are trained on the labeled data and tested on unlabeled data. Semi-supervised classifiers are trained on both labeled and unlabeled data and tested on unlabeled and unseen data. We have used support vector machine (SVM) and graph-based semi-supervised learning.

(1) Supervised learning (Bishop 2006)

Supervised learning is the machine-learning task of inferring a function from labeled training data. Some popular supervised learning algorithms include naïve Bayes (Domingos 1997),

logistic regression (Hilbe 2009) and SVM (Burges 1997), which we used almost exclusively. When classifying, we want a classifier to learn the boundary between different classes and separate the feature space into different class spaces. Intuitively, a good separation is achieved by the hyperplane that has the largest distance to the nearest training data point of any class (so-called functional margin), since in general, the larger the margin the lower the generalization error of the classifier. SVM maximizes the margin and expresses it as a function of the weight vector and bias of the separating hyperplane.

(2) Semi-supervised learning (Zhu 2005)

Semi-supervised learning is a technique for training classifiers with both labeled and unlabeled data. It assumes that unlabeled data can provide distribution information to build a stronger classifier. Some popular semi-supervised learning algorithms include generative mixture models with expectation maximization, co-training, transductive SVM and graph-based approaches. We focus on label propagation (Zhu 2002), which is one of graph-based approaches.

Label propagation assumes that, while the measured samples exist in a high-dimensional space, they are distributed in a low-dimensional manifold. Based on this, a graph is constructed to analyze the distribution of both labeled and unlabeled samples. By analyzing how the labels propagate on this graph, classification can be achieved.

Multiresolution Framework

Multiresolution classification system (MRC) (Chebira 2007, Chebira 2008) is a generic classification framework. It decomposes images into localized space-frequency subbands using a wavelet packet tree (Coiffman 1991). In each subband, MRC extracts features, classifies them and gets a local classification result. A global weighting algorithm combines the local results to get a global decision. Its advantages are that (1) it extracts hidden features in localized time-frequency zones; and (2) the traditional generic classification system is only the first subband of MRC. It reaches a decision using information from all the subbands.

Summary

Version	Feature Extractor	Classifier
Cerda Thesis 2012	Top 5 Fourier discriminative features	SVM
ASCE Structures Conference 2013, Pittsburgh PA	Sparse representations	MSE
Damage Assessment of Structures 2013, Dublin Ireland.	LFDA	SVM
ASCE International Workshop on Computing in Civil Engineering 2013, Los Angeles CA	Multiresolution + PCA	SVM
IEEE International Conference on Acoustics Speech Sound and Signal Processing 2013, Vancouver, CA	Multiresolution + PCA	SVM

Comparison

1. Fourier discriminative features vs. sparse representations vs. LFDA

When the labeling ratio (the number of the labeled data/the number of all the data) is 80%, we compare Fourier discriminative features with sparse representations and LFDA under 18 scenarios.

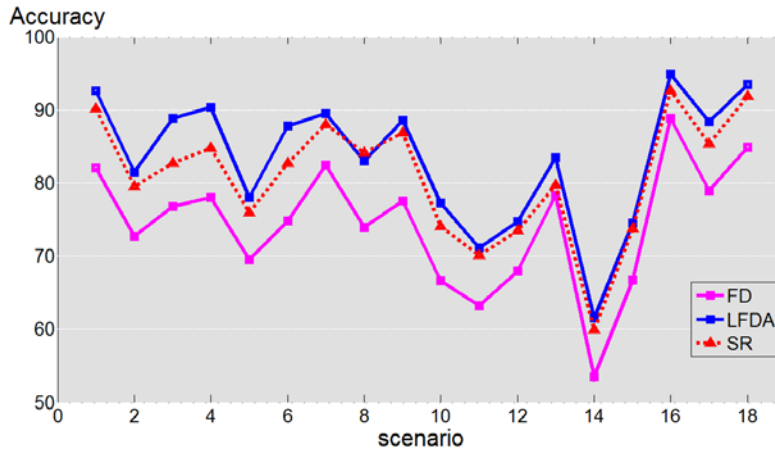


Figure 29 - Comparison of three methods, Fourier Discriminant Features, Local Discriminant Features and Sparse Representation for 18 scenarios

2. Fourier discriminative features vs. Multiresolution + PCA

When the labeling ratio is 50%, we compare Fourier discriminative features with multiresolution classification

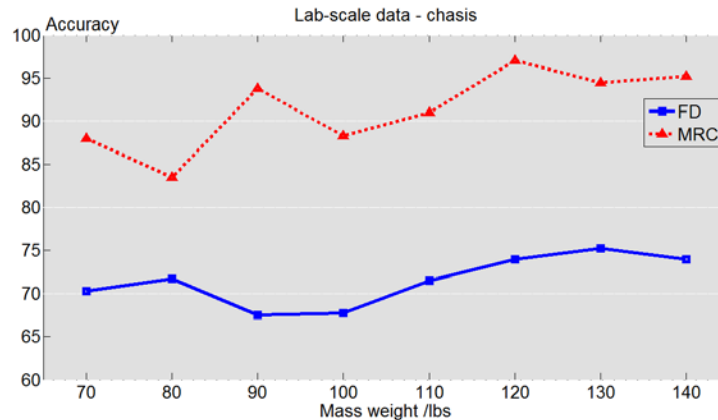


Figure 30 - Comparison of Fourier Discriminant Features and Multiresolution Classification

3. Supervised learning vs. semi-supervised learning under multiresolution framework

We compare supervised learning with semi-supervised learning by changing the labeling ratio. SMRC stands for supervised multiresolution classification while SSMRC stands for semi-supervised MRC.

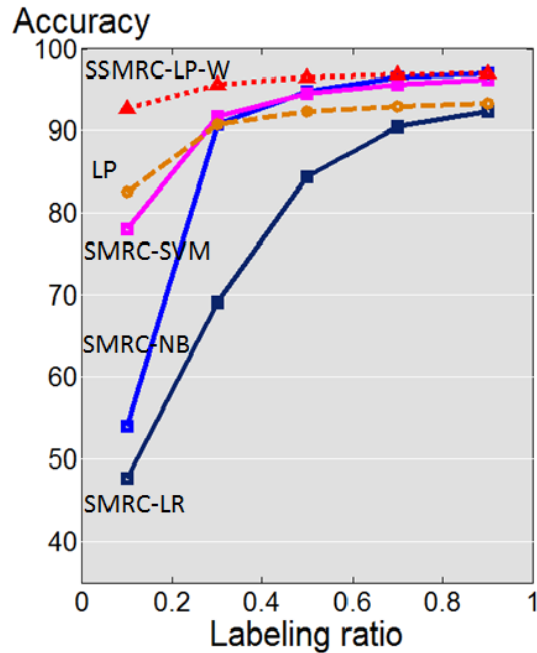


Figure 31 - Discriminant Accuracy at Various Labeling Ratios

Conclusions

Based on theoretical analysis and numerous experiments, we conclude the following:

- (1) Feature extractor: When the data is sufficiently labeled, LFDA has the best performance; when there are fewer labels, sparse representations are more effective.
- (2) Classifier: When the data is sufficiently labeled, SVM has the best performance; when there are fewer labels, a semi-supervised classifier is more effective as can be seen in Figure 31.

As a framework, multiresolution classification system provides a consistently better performance than a generic classifier.

Task 4: Garage Experiments and Light Rail Data Collection

In the first section we explain a set of experiments we conducted on a parking garage structure. We compare these results to those of the laboratory scale model.

In the second part of this section, we show some initial results from recent data collection we have begun in collaboration with the Port Authority of Allegheny County. This project is still in its early phases. We have not yet collected sufficient data to give results. However we will specify what hardware we have installed, describe the database we have setup to manage the data, and show some of the raw data.

Garage Field Experiments

Our goal was to find a long span structure where we could conduct uninterrupted experiments, while minimizing the impact on other users. We ultimately selected the 3rd level of the East Campus Parking Garage at Carnegie Mellon's Pittsburgh Campus. The lower levels of the garage fill first, so the 3rd floor was nearly empty during the early mornings when we conducted our experiments. Although there were relatively low levels of ambient vibration in the deck, we did occasionally observe some noise from cars on lower levels, and from heavy traffic on adjacent Forbes Avenue.

The deck is made of 32" x 8'6" (0.81m x 2.59m) precast prestressed concrete double tees with estimated 700lpf (1042 kg/m), each isolated from adjacent sections by an elastomer (Figure 32, 33). Due to the elastomer, each double tee section acts as a simply supported beam. The span where we ran our experiments is 51.5ft (15.7m) long with an approximate weight of 36,120lbs (16,383kg).

As our vehicle, we used an iRobot ATV-JR robot, with a weight of 50kg³, traveling at a constant speed of 2m/s. We fitted the robot with three Vibra-Metrics 5102 Piezoelectric Accelerometers, one on the front right of the vehicle, one on the rear left, and one on the rear right, as shown in Figure 34. The accelerometers on the robot were bolted down, a "direct" accelerometer was placed on the deck with a layer of surfing wax to help the accelerometer adhere to the surface. (This method of adhesion was found adequate to transfer the vibration through some free-vibration tests.) This accelerometer on the deck was placed at the midspan of the bridge and was the same model as that on the robot.

Since this is an operational garage, we could not induce real damage in the structure; instead, we simulated a change in the structure by placing mass at the midspan of the precast T-section. We used 5 gallon buckets filled with coarse aggregate which we weighed in a concrete laboratory prior to delivery to the garage. Because in the simulations we consider only a one dimensional beam, we were careful to apply the load symmetrically, so that the experiment would be similar to the simulations. As shown in Figure 32 and 33, an equal number of buckets are on each side. We varied the total mass level on the bridge from 0 to 360 lbs (163kg) in 40lbs (18.1kg) increments for a total of 10 different mass levels. For the particular experiment that we will describe in this report, we ran 5 trials at each mass level. Then we recharged the robot, and

³ This is the mass from the manufacturer's website. We did not measure the mass of the particular robot, which would be slightly different due to some modifications.

ran another 5 trials at each mass level. After some data cleansing we had a total of 9 usable trials from each mass level, which are presented in the results.

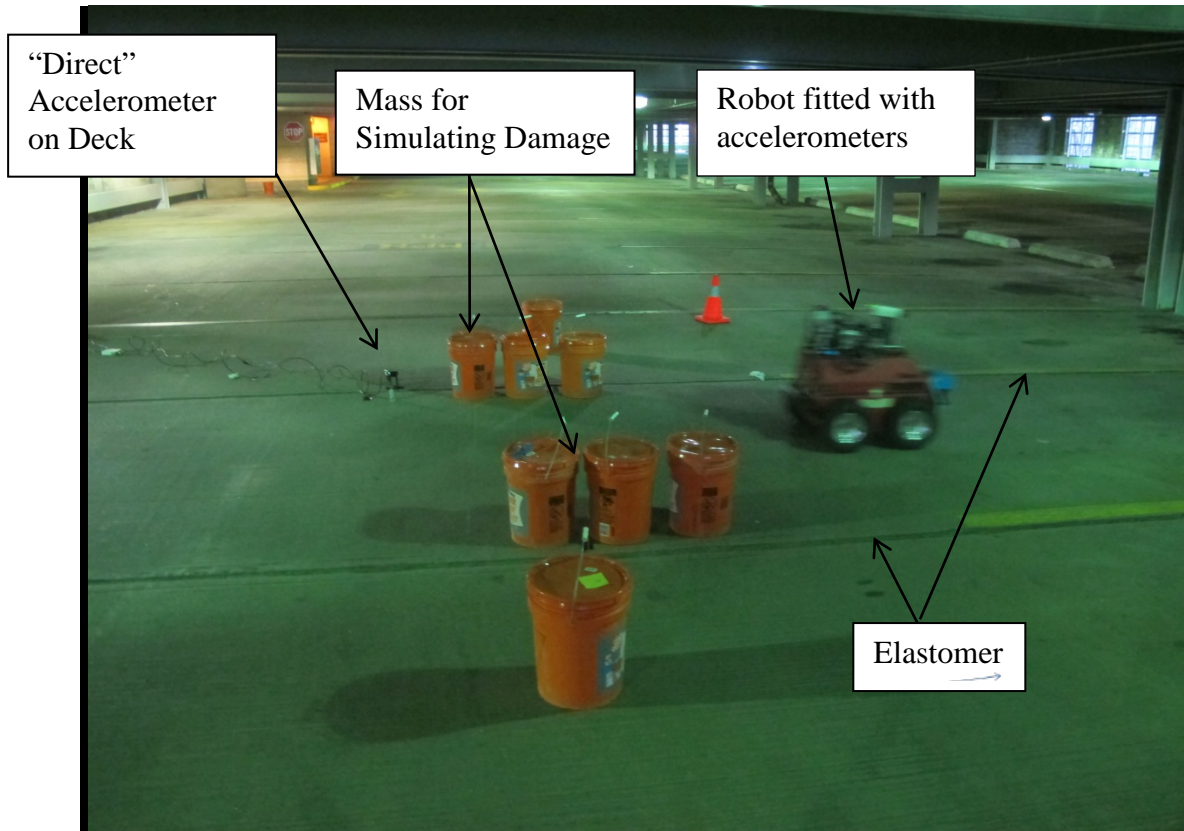


Figure 32 - Experimental Setup for Field Tests

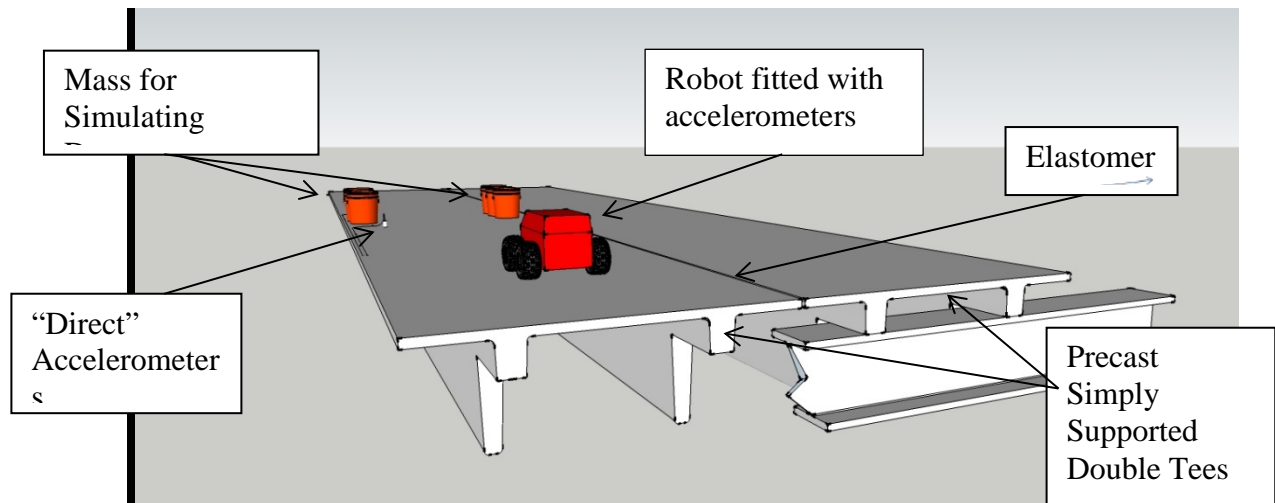
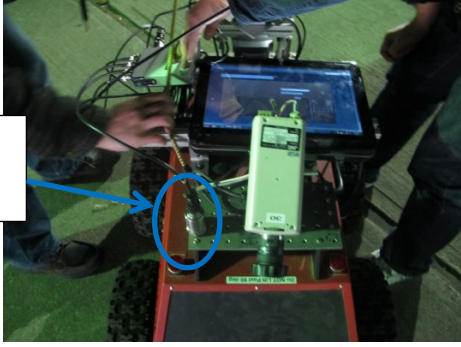
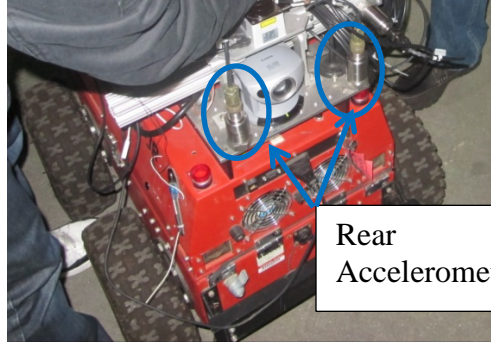


Figure 33 - Illustration Of Garage Experiments

Front Accelerometer



(a) Front View



Rear Accelerometers

(b) Rear View

Figure 34 - Detail of the Robot

Laboratory Experiments

Laboratory experiments were carried out on the scale model bridge to match the garage experiments. The ratio of added mass to the mass on the bridge deck was the same for both the garage experiment and the lab experiment. The purpose was to see if commonalities existed between the two scales (i.e. laboratory and garage deck) so that the work on the laboratory bridge could be applied more broadly.

DATA SELECTION

In the laboratory experiments, extracting the signal when the car is on the bridge is relatively easy because of a bump as the vehicle enters the main span. Extracting the signal in the garage experiments was much more difficult. Data extraction is an important process to spatially align the data so that the computer can learn feature consistently.

On the lab scale model, we selected the signal when the entire vehicle is on the bridge. The red portion of the signal shown in Figure 36 spans the time from when the back wheel enters the bridge, until the front wheel leaves the bridge. There is a noticeable spike as the front and back wheel leave the bridge due to a small gap between the track on the bridge, and the track on the deceleration ramp, as shown in Figure 35.



Figure 35 – Slight Gap between Track and Bridge Allowing for Data Selection

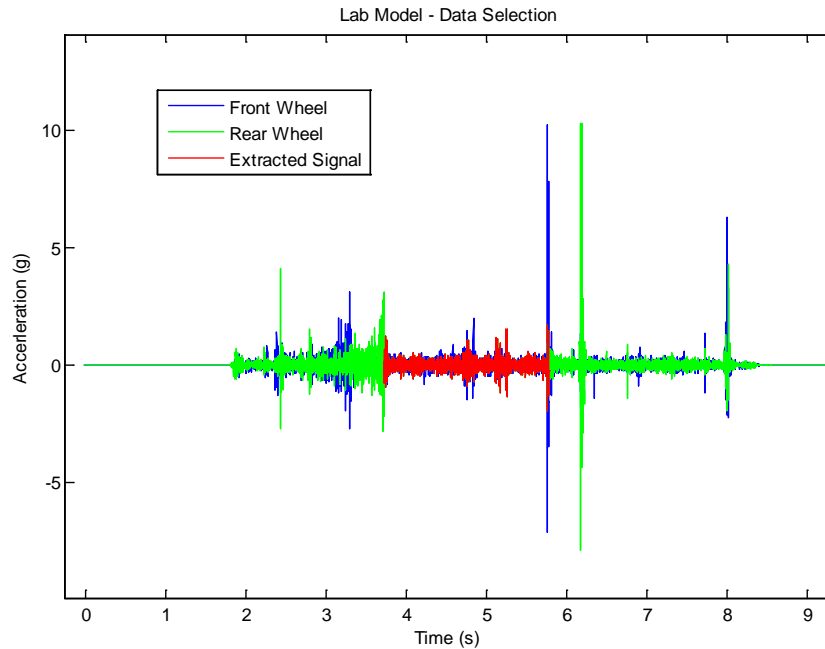


Figure 36 - Data Selection Lab Data

In the garage experiment, the vehicle is constantly on the main span and there is no sudden bump we could use to spatially align the data. In this case our goal was to select data where the vehicle was traveling at a constant speed. Given that the garage span is 15.7 meters in total, we ensured that the robot was moving at a constant speed as it traveled over the middle 7.7 meters, and only extracted that data (there was a 4m area on both sides for accelerating and decelerating.)

To facilitate data extraction we taped a broom handle to the garage deck in order that a peak would be recorded in the accelerometer signal (as shown in Figure 38). The broom handle is shown in Figure 37. The broom handle also allowed us to synchronize the data acquisition system on the garage deck with the system on the robot itself.



Figure 37 - Detail of Broom Handle

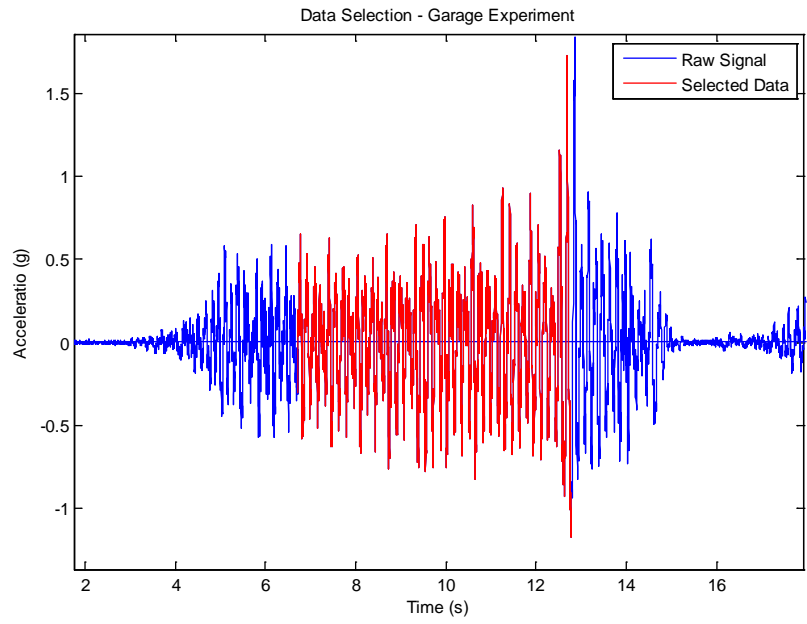


Figure 38 - Garage Experiment Data Selection

EXPERIMENTAL RESULTS

Laboratory Data

The laboratory data largely exhibits changes in the magnitude of various frequencies, as shown in the waterfall plot in Figures 39, 40 and 41. For each of these plots, the signals from the 30 trials at each mass level were averaged, and then the magnitude of the discrete Fourier transform for each mass level was plotted.

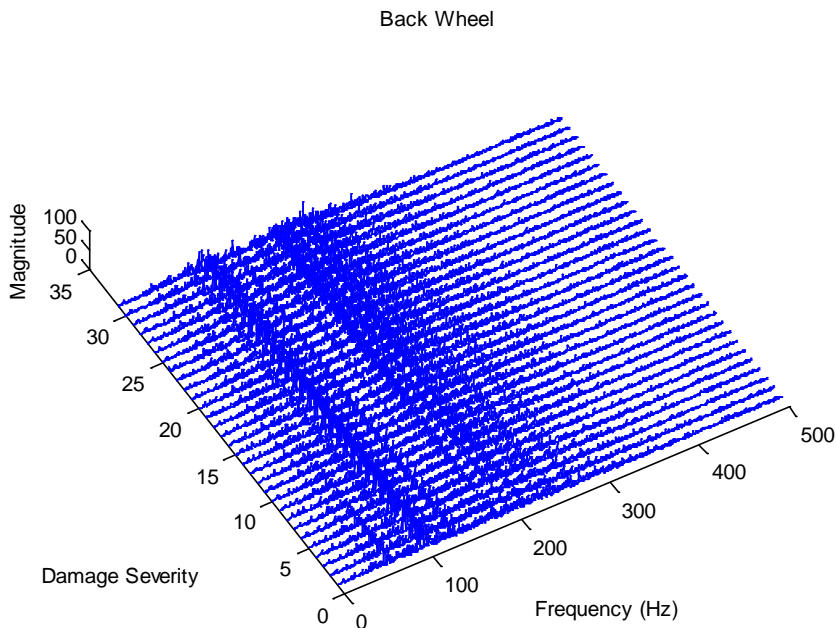


Figure 39 - Waterfall Plot, Data from Back Wheel, Laboratory Experiments (Severity Level 0 corresponds to no mass on the bridge, Level 1 correspond to 5g, up to Level 31 which corresponds to 150g)

The predominant change between damage severity levels (or more precisely, between amounts of mass placed on the structure) is changes in the magnitude of the various frequency values. Although intuitively we might expect the frequencies to shift downward as more mass is added to the structure, we do not actually observe this phenomenon in the data.

It is worth noting that the sampling rate of the accelerometer is around 1600Hz, so it only captures information up to 800 Hz. There appears to be meaningful patterns at least above 400 Hz. In fact sound recording of the vehicle crossing the bridge could also be used to classify the level of applied damage (albeit with slightly lower accuracy).

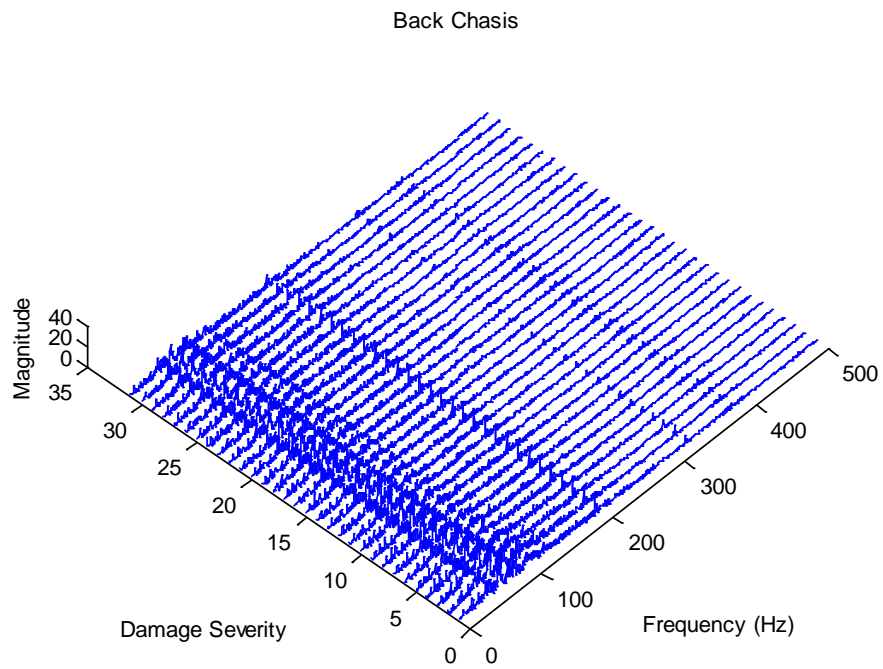


Figure 40 - Waterfall Plot, Data from Back Chasis, Laboratory Experiments (Severity Level 0 corresponds to no mass on the bridge, Level 1 corresponds to 5g... up to Level 31 which corresponds to 150g)

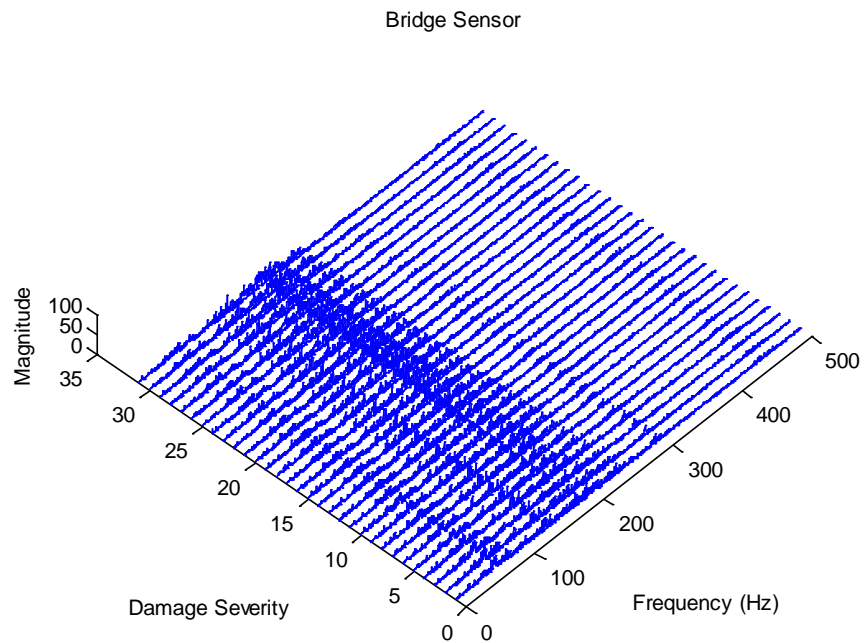


Figure 41 - Waterfall Plot, Data from Bridge Sensor, Laboratory Experiments (Severity Level 0 corresponds to no mass on the bridge, Level 1 corresponds to 5g... up to Level 31 which corresponds to 150g)

Garage Data

The signals from the robot have both a significant peak around 6Hz and a smaller peak around 400 Hz as can be seen in Figure 42. This high frequency component is particularly interesting because we do not see such high frequencies in the signal from the accelerometer on the bridge itself as seen in Figure 43. This 400Hz peak shifts downward around 3.4% as additional mass is placed on the deck, as can be seen in Figure 44. This 3.4% shift mimics the shift we see in the fundamental frequency of the bridge as seen in Figure 45, and the shift in the lower frequencies recorded by the robot as seen in Figure 46. We suspect that the shift in this high frequency component must somehow reflect the additional mass (simulated damage) placed on the bridge, although it is difficult to demonstrate causality conclusively. Because we increased the mass on the bridge in succession (rather than placing random levels of mass) it is possible this shift has something to do with the robot, for example, the battery losing charge over time, and the motor vibrating at a different frequency.

Front Robot Sensor

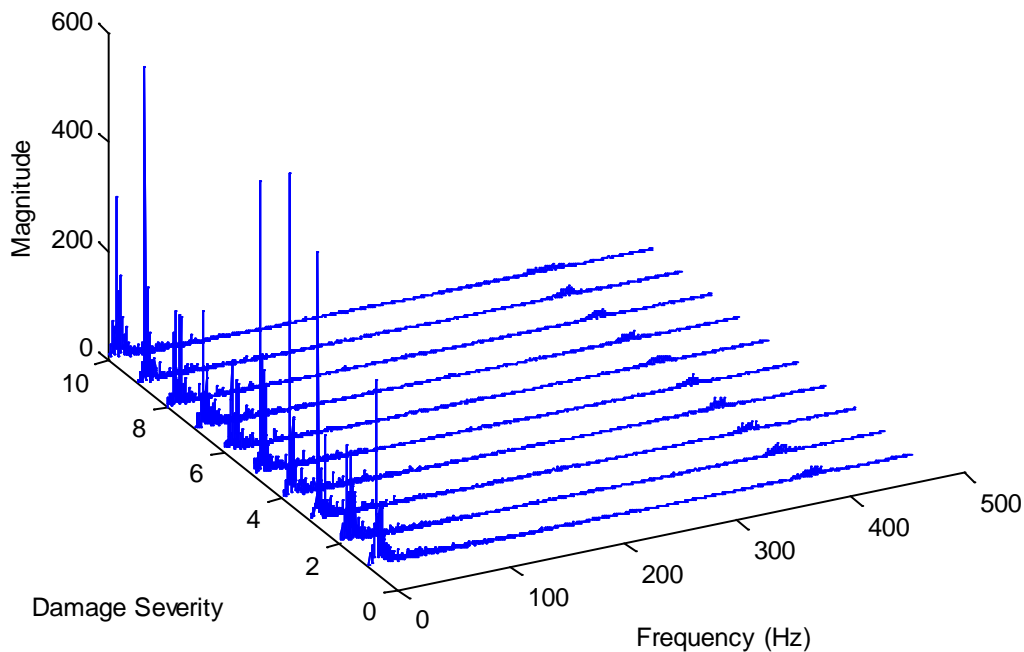


Figure 42 - Waterfall Plot, Signals from the Robot (Severity Level 0 corresponds to no mass on the bridge, Level 1 corresponds to 40lbs... up to Level 10 which corresponds to 360lbs)

Bridge Sensor

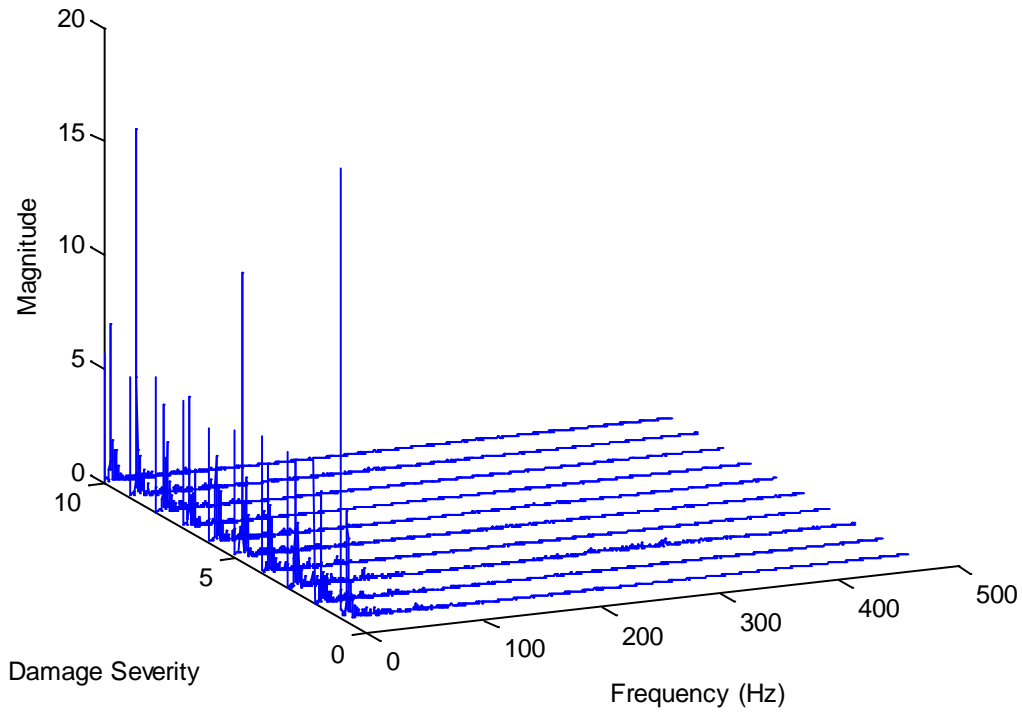


Figure 43 - Waterfall plot, signals from the bridge (Severity Level 0 corresponds to no mass on the bridge, Level 1 corresponds to 40lbs... up to Level 10 which corresponds to 360lbs)

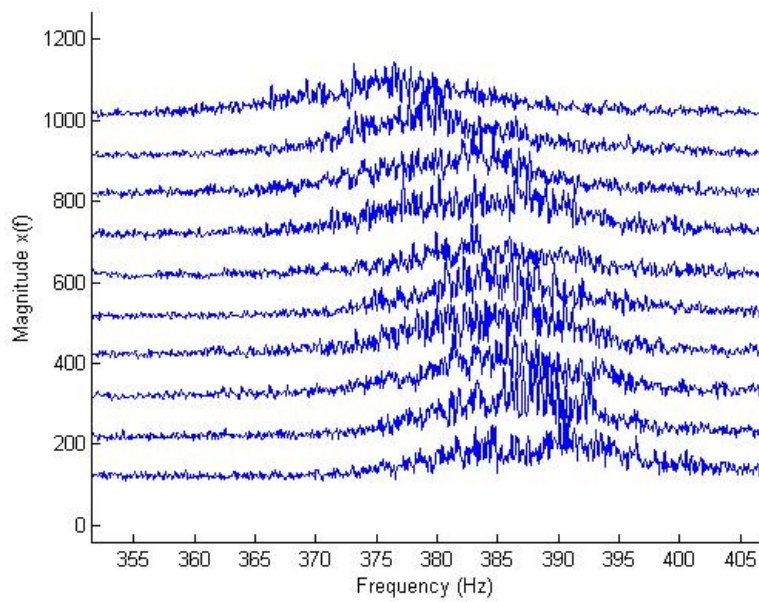


Figure 44 – Magnitude in the Frequency Domain, Each Progressive Level of Damage plotted 100 points above the previous.

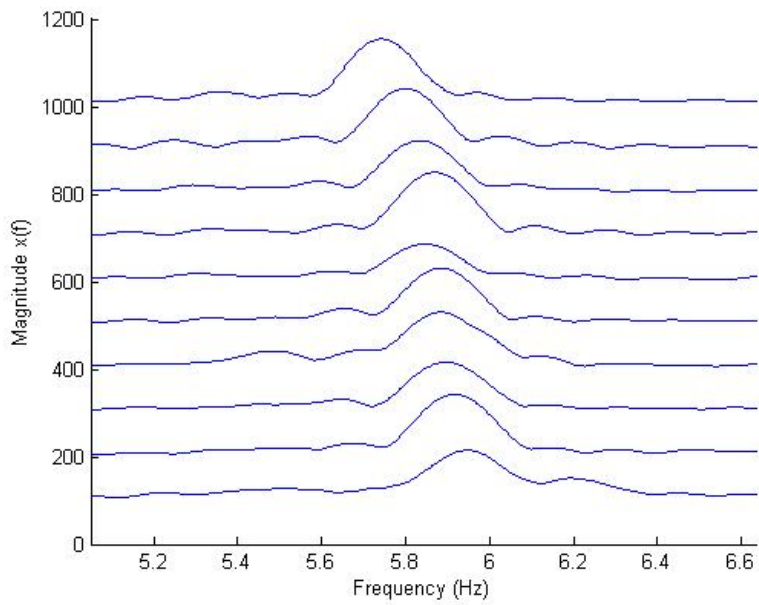


Figure 45 - Magnitude in the frequency domain of the signal directly from the bridge, with each progressive level of mass plotted 100 points above the previous. Each signal was normalized and zero padded, providing a linear interpolation of the data in the frequency domain in order to see the shift more clearly.

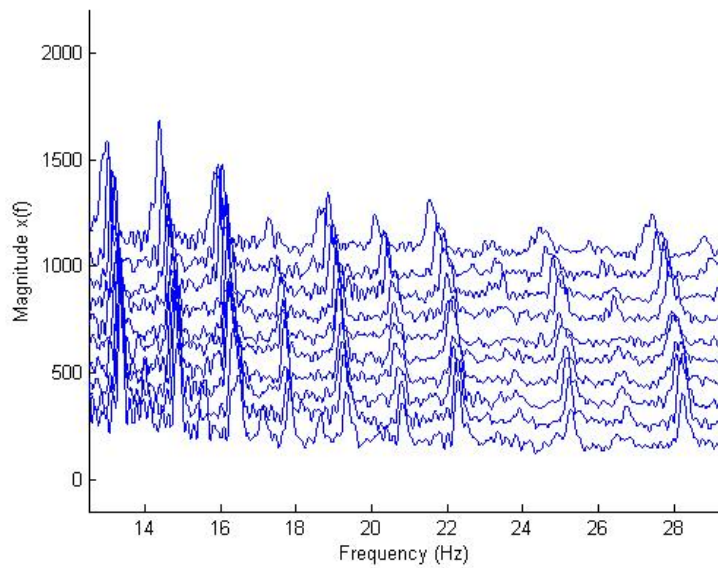


Figure 46 - Magnitude of the frequency domain from the robot, showing detail of the lower frequencies. This signal was also zero padded. A clear downward shift can be seen at many frequency levels.

Port Authority Project

With the help of the University Transportation Center (T-SET), we have begun to collect indirect data from Pittsburgh's Light Rail Line. This project has been facilitated through the connections of T-SET's staff, and by the leadership of the Port Authority, in particular Bill Miller and David Kramer.

Both the garage and the laboratory tests were simply experiments; they were an attempt to create the type of scenario we might encounter later on. The Pittsburgh Light Rail Line, known as "the T," offers an opportunity to continuously collect real data in an operational environment. While previously we had simulated temperature changes and damage scenarios, this project tries to account for natural temperature change and detect genuine damage. The downside of such a system is that we lose control over the bridges. While in the lab we can choose when to simulate damage, in this data collection process we have to wait until a bridge is damaged or until construction occurs on one of the bridges. Our data collection efforts began in September 2013. No work on this topic has been published. We will give a short summary of the work thus far and discuss the potential impact this project might have on the Structural Health Monitoring community.

Our first task was to design robust hardware capable of efficiently logging high frequency data. In September 2013 we placed our data collection system on a single train of the Light Rail System. The data acquisition system consists of an LGX AG150-V automotive computer (Figure 47a), a gps module (UsGlobalSat BU-353), and two National Instruments Dynamic Signal Acquisition Modules (Figure 47b). There are two types of accelerometers; a triaxial accelerometer (PCB 354C03) placed on the middle truck of the train and two uniaxial accelerometers (5102 Vibra-metrics) placed near the data acquisition system. A schematic of the whole system as implemented in the train car.



Figure 47 - Installed Equipment on the Train

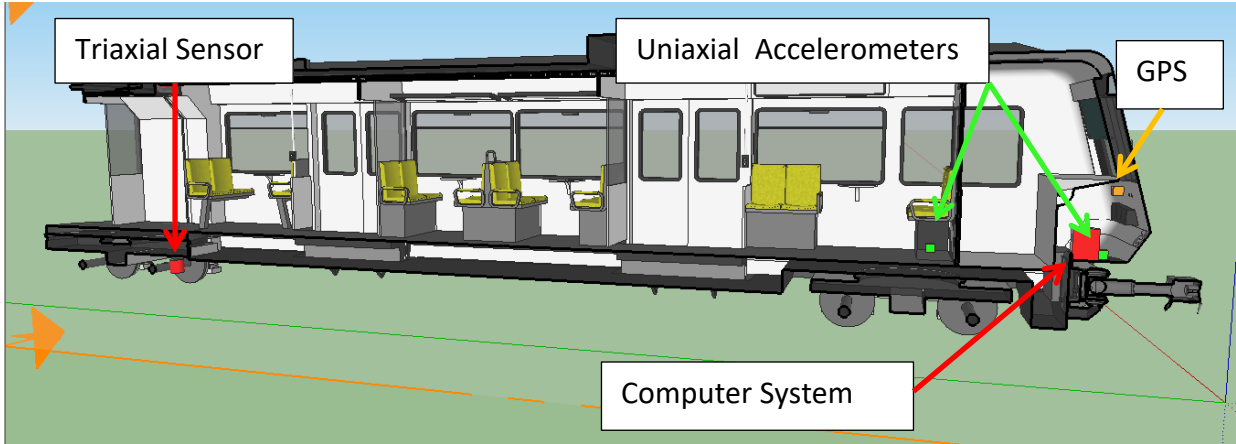


Figure 48 -Schematic of the Sensors Placed on the light rail car

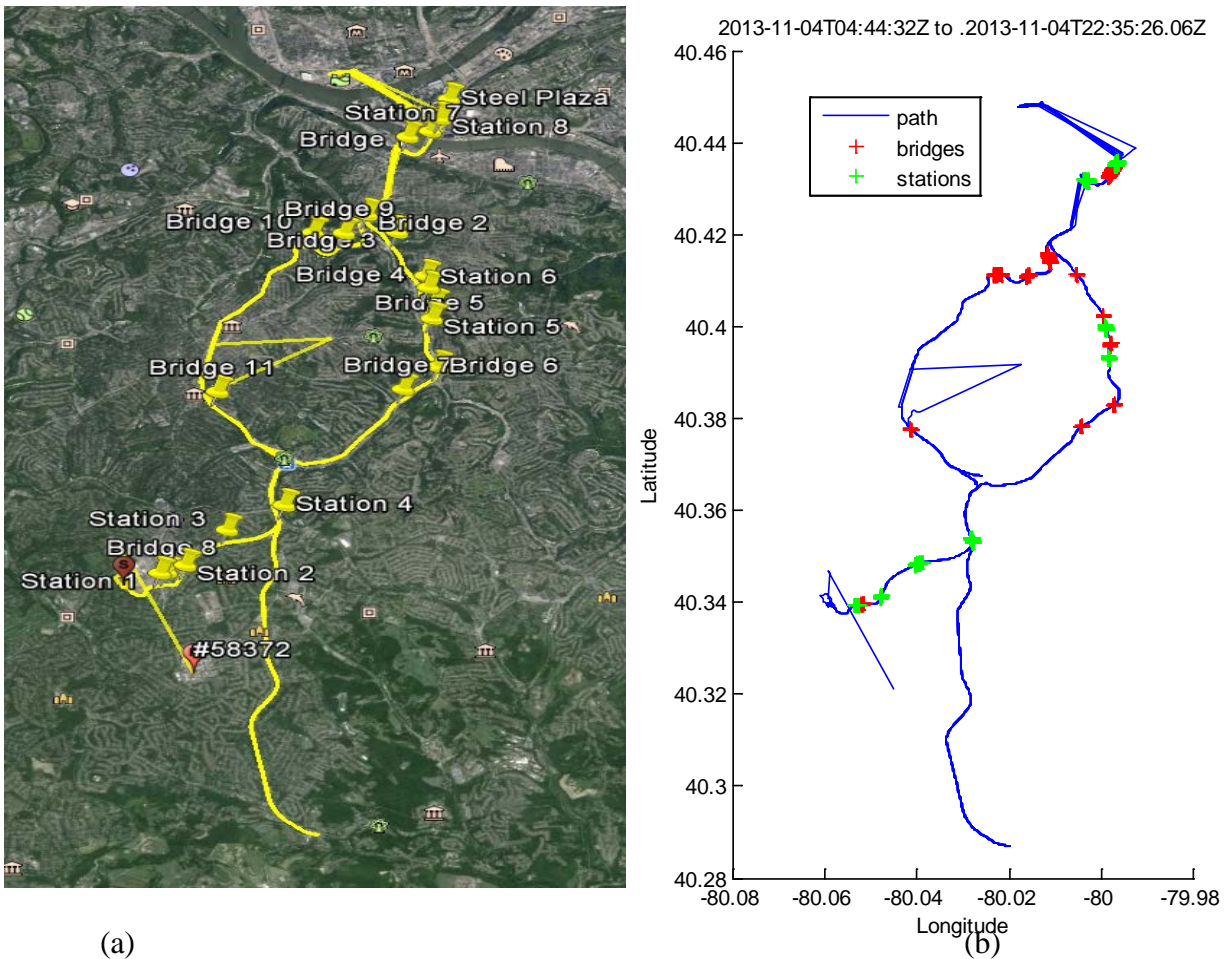


Figure 49 - (a) GPS data overlaid onto Google Maps (b)GPS plotted with bridge locations identified. When the train enters into a tunnel, the GPS accuracy deteriorates rapidly. This is why there are some straight lines veering away from the track.

We collect accelerometer signals from the train continuously at 1651Hz. This generates lots of data—in the range of 10Gb per day. We store all this raw data, but then extract the portion of the signal when the train is actually on one of the 11 bridges, and place this data into a

database which is accessible via the internet. Details of the GPS output (overlaid onto Google Maps) and the portion of the signal we extract from the bridges are shown in figure 49.

We look at the signal of the train both as it crosses the bridges and while it remains in the station. We expect to see lower accelerations while the train is stopped in the station. This serves as important verification that we are extracting the correct portion of the signals. This is shown in Figure 50.

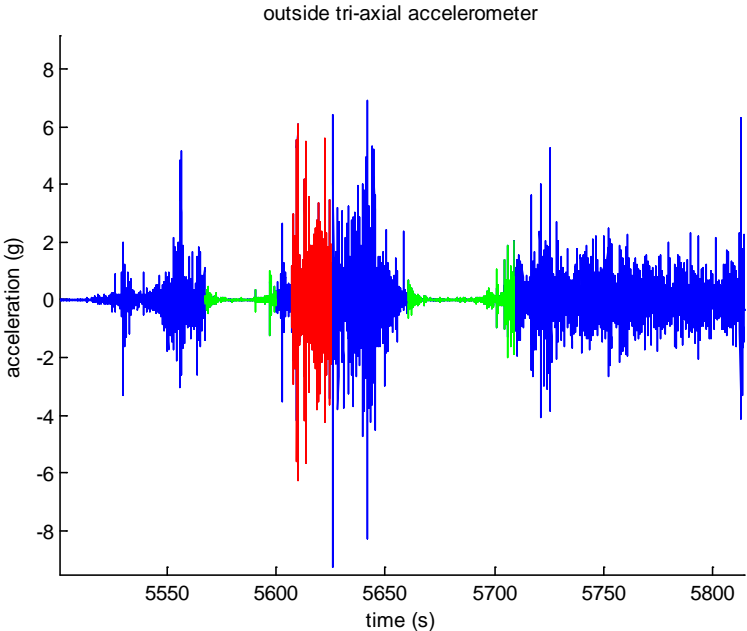


Figure 50 - This is an example of the raw signal collected from the train. Areas when the GPS shows the train to be in the station are shown in green. Areas where the GPS shows the train to be over a bridge are shown in red.

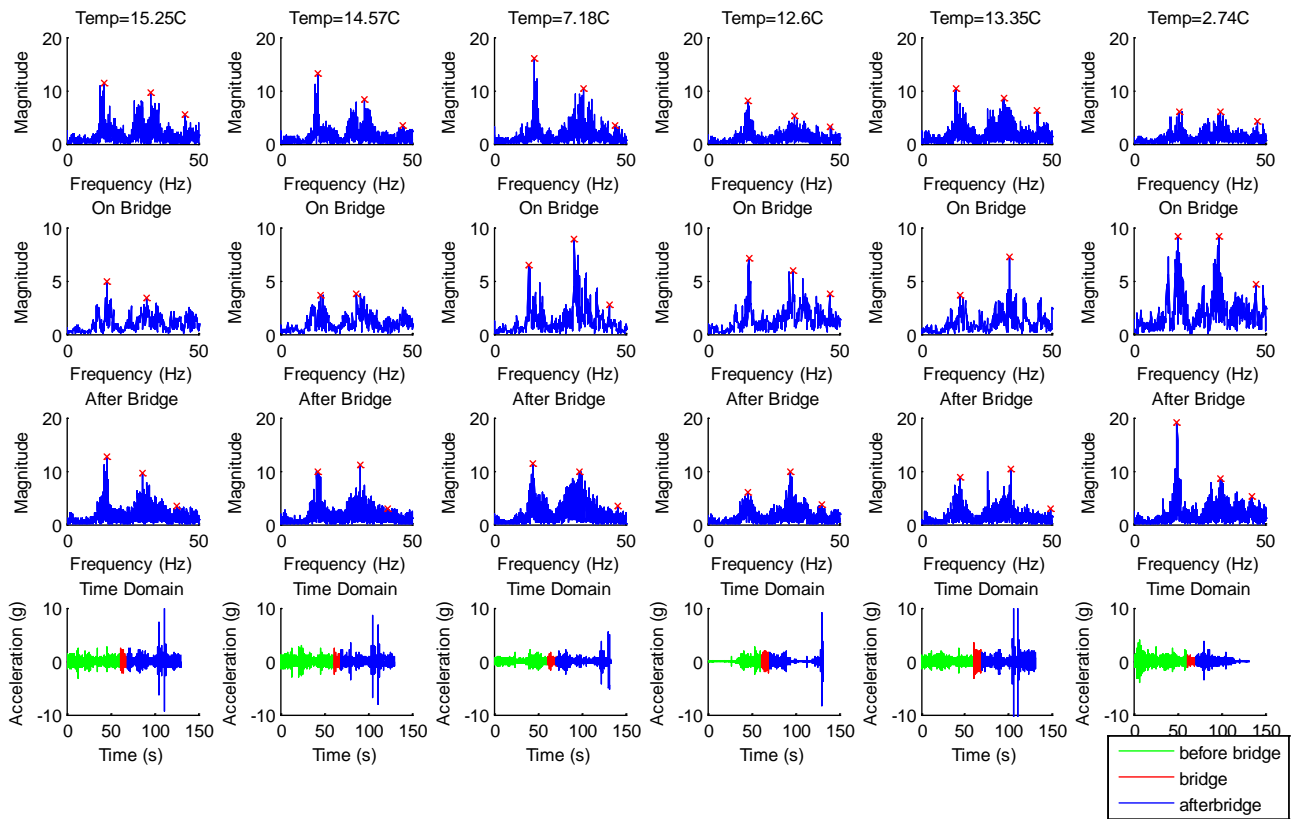


Figure 51 - Example Signals over a bridge at Different Temperatures

In addition to the accelerometer signals, we record environmental data in our database. This includes temperature, humidity, visibility and wind speed. These values are extrapolated from NOAA weather data, and triangulated to provide a “hyperlocal” forecasts. At the moment we have limited crossing for each bridge so it is difficult to know which changes are due to stochastic changes and which are due to temperature changes. Figure 51 shows six crossings over a single bridge. The frequency spectrum is shown before the train is on the bridge, while the train is on the bridge, and after the train crosses the bridge. The fourth plot at the bottom shows the time domain signal with different colors showing the different sections of the signal.

Recording the baseline dynamic response of the bridge could take a long time. As no experiments will be performed on the operational system, validation will occur when the algorithm is able to detect a fault of statistical significance that can be verified. Currently we are continuing to collect data about the bridges—to better understand how they behave at different temperatures.

In the coming months, we will apply existing signal processing and machine learning techniques to this dataset as well as try to develop new approaches.

Expected Significance: Ideally, we will find that we can use this technique to determine severity of damage, and location of damage. However, simply detecting a statistically significant change in the structure would be a huge breakthrough. This would allow the Port Authority to

prioritize when to send structural inspectors to a bridge. If nothing has changed in the bridge since the last inspection—this technique could save money. If something has happened before a scheduled inspection—this could save lives.

Conclusions

Over the course of this 23 month project we have made significant contributions in Indirect Structural Health Monitoring. This technology could be a cheap way to continuously monitor the aging infrastructure both in the United States and abroad.

We have done fundamental work on understanding the vehicle bridge interaction, and the machine learning algorithms which will best detect changes in the bridge. And we have done practical work on efficiently collecting and storing data, and how we can work with agencies like the Port of Authority of Allegheny County to help them tackle the challenge of maintaining their assets.

Tasks 1 through 3 focused on a laboratory scale model and verified that indirect monitoring is in fact a viable method. We have shown we can detect small changes in a laboratory bridge in presence of environmental variables or in cases where there is uncertainty in the data. And we explored numerous types of damage including changes in rotational restraint, changes in damping ratio, and changes in the mass of the bridge. We have explored the ways the fundamental features of the bridge change with damage so that the general trend can be understood. Without environmental variation, we can consistently achieve above 90% classification on the lab scale model. However adding some temperature variation reduces the classification accuracy down to roughly 70%. We have shown that the best algorithm thus far is a semi-supervised multiresolution classifier with label propagation and weighting. New methods using graph models may improve the accuracy while accounting for changes in temperature.

Task 4, collecting data from new sources, began only towards the end of this project, although we hope to continue this work with future support from the University Transportation Center. By applying our novel algorithms to the operational data we are collecting, we hope to be able to detect subtle structural changes, while avoiding false positives due to changes in the environmental conditions.

As many of the bridges in our national inventory approach their design life, ubiquitous computing and cheap sensors combined with novel signal processing algorithms may offer a solution. The work we have done with this funding, in particular, the papers we have published, bring us one step closer to harnessing this data to understand the state of our infrastructure. .

Perhaps the most exciting outcome of this research is the finding that algorithms developed for image processing can be applied to bridge monitoring. The semi-supervised approach described in the second half of Task 3 shows that even when only 10% of the data is label, we can still classify the state of the bridge. We hope we can continue to find such exciting connect when analyzing the data we gather from the Port Authority Trains. And we hope to develop new tools which help federal, state and local agencies maintain a safe and efficient infrastructure on tightly constrained budgets.

Bibliography

- Abdi, H., Williams, and L.J. "Principal component analysis." *Wiley Interdisciplinary Reviews: Computational Statistics*, 2: 433–459, 2010.
- Ahron, M. Elad, M. Bruckstein, A. "K-SVD: An Algorithm for Designing Overcomplete Dictionaries for Sparse Representation", *IEEE Transactions on Signal Processing*, Vol. 54, No. 11. November 2006.
- Alippi, C., and Galperti, C. 2008: "An Adaptive System for Optimal Solar Energy Harvesting in Wireless Sensor Network Nodes." *Circuits and Systems I: Regular Papers, IEEE Transactions On* 55, no. 6: 1742–1750.
- Akinci, B., Hendrickson, C., and Karaesmen, I. 2003. "Exploiting Motor Vehicle Information and Communications Technology for Transportation Engineering." *Journal of Transportation Engineering* 129, no. 5: 469–474.
- Beeby, S. P., Tudor, M. J. and White, N. M. 2006 "Energy Harvesting Vibration Sources for Microsystems Applications." *Measurement Science and Technology* 17, no. 12: R175–R195.
- Bilello, C., and Bergman L. A. 2004. Vibration of damaged beams under a moving mass: theory and experimental validation. *Journal of Sound Vibration* 274 (Jul 1): 567-582.
- Bishop, C. M. "Pattern Recognition and Machine Learning", Information Science and Statistics, Springer, 2006.
- Brownjohn, J.M.W. 2007. Structural health monitoring of civil infrastructure. *Philosophical Transactions of the Royal Society A: Mathematical, Physical and Engineering Sciences* 365, no. 1851 (February 15): 589-622.
- Bu, J. Q., Law, S. S. and Zhu, X. Q. 2006. "Innovative Bridge Condition Assessment from Dynamic Response of a Passing Vehicle." *Journal of Engineering Mechanics* 132 (12) (December): 1372–1379.
- Burges, Christopher J. C, "A Tutorial on Support Vector Machines for Pattern Recognition", *Data Mining and Knowledge Discovery* 2:121–167, 1998
- Carden, E. P., and Fanning, P. 2004. "Vibration Based Condition Monitoring: A Review." *Structural Health Monitoring* 3 (4) (December 1): 355–377.
- Casciati, F., and Giordano, M. 2010. *Structural Health Monitoring 2010: Proceedings of the Fifth European Workshop on Structural Health Monitoring Held at Sorrento, Naples, Italy, June 28-july 4, 2010*.
- Cerda, F., Garrett, J., Bielak, J., Bhagavatula, R., and Kovačević, J. 2010. "Exploring Indirect Vehicle-bridge Interaction for Bridge SHM." *Bridge Maintenance, Safety, Management and Life-Cycle Optimization - Proceedings of the 5th International Conference on Bridge Maintenance, Safety and Management: 708–715*.
- Cerda, F., Chen, S, Bielak, J, Garrett, J, Rizzo, P, Kovačević, J. 2012 "Indirect structural health monitoring of a simplified laboratory-scale bridge model". Submitted to *Smart Structures and Systems* (Special Issue).
- Chebira, A., and Kovačević, J. 2008. "Frames in Bioimaging." *Proc. CISS, Princeton, NJ, Mar. 2008*.
- Chebira, A., Barbotin, Y., Jackson, C., Merryman, T., Srinivasa, G., Murphy, R., and Kovačević, J. 2007. "A Multiresolution Approach to Automated Classification of Protein Subcellular Location Images." *BMC Bioinformatics* 8 (1): 210.

- Coifman, Y. Meyer, S. Quake, and M. V. Wickerhauser, "Signal processing and compression with wavelet packets," Tech. Rep., Yale Univ., 1991.
- Cornwell, P., Farrar, C. R. Doebling, S. W. and Sohn, H. 1999. "Environmental Variability of Modal Properties." *Experimental Techniques* 23 (6): 45–48.
- Daubechies, I. 1992. *Ten Lectures on Wavelets*. Society for Industrial and Applied Mathematics. <http://portal.acm.org/citation.cfm?id=130655>.
- Deraemaeker, A., Reynders, E., De Roeck, G., and Kullaa, J. 2008. "Vibration-based Structural Health Monitoring Using Output-only Measurements Under Changing Environment." *Mechanical Systems and Signal Processing* 22, no. 1: 34–56.
- Doebling, S. W., Farrar, C. R., and Prime, M. B. 1998. "A Summary Review of Vibration-based Damage Identification Methods." *Identification Methods, The Shock and Vibration Digest* 30: 91–105.
- Domingos, Pedro and Michael Pazzani, "On the optimality of the simple Bayesian classifier under zero-one loss", *Machine Learning*, 29:103–137, 1997
- Duda, R., Hart, P., and Stork, D. 2000. *Pattern Classification (2nd Edition)*. Wiley-Interscience.
- FHWA 2001. Reliability of Visual Inspection for Highway Bridges - FHWA-RD-01-020 <http://www.fhwa.dot.gov/publications/research/nde/01020.cfm>
- Farhey, D. 2005. "Bridge Instrumentation and Monitoring for Structural Diagnostics." *Structural Health Monitoring* 4 (4) (December 1): 301–318.
- 2007. "Quantitative Assessment and Forecast for Structurally Deficient Bridge Diagnostics." *Structural Health Monitoring* 6 (1) (March 1): 39–48.
- Farrar, C. R., and Jauregui, D.. 1998. "Comparative Study of Damage Identification Algorithms Applied to a Bridge: I. Experiment." *Smart Materials and Structures* 7 (5) (October 1): 704–719.
- Farrar, C. R., and Worden, K. 2007. "An Introduction to Structural Health Monitoring." *Philosophical Transactions of the Royal Society A: Mathematical, Physical and Engineering Sciences* 365 (1851) (February 15): 303–315.
- Frangopol, D. M., Strauss, A., and Kim, S. 2008. "Bridge Reliability Assessment Based on Monitoring." *Journal of Bridge Engineering* 13 (3) (May): 258–270.
- Frangopol, D.M., Sause, R., and Kusko, C. eds. 2010. *Bridge Maintenance, Safety and Management - IABMAS'10: Proceedings of the Fifth International IABMAS Conference, Philadelphia, USA, 11-15 July 2010*. 1st ed. CRC Press.
- Friswell, M. I. 2007. Damage identification using inverse methods. *Philosophical Transactions of the Royal Society A: Mathematical, Physical and Engineering Sciences* 365, no. 1851 (February 15): 393-410.
- Fugate, M. L., Sohn H., & Farrar C. R. 2000. Unsupervised learning methods for vibration-based damage detection. Presented at IMAC, San Antonio, Texas. February 7-10.
- Haralick, R.M, Shanmugan, K., and Dinstein, I. (1973). "Textural Features for Image Classification." *IEEE Trans. on Systems, Man, and Cybernetics* 3 (6): 610–621.
- Hilbe, Joseph M, "Logistic Regression Models", Chapman & Hall/CRC Press, ISBN 978-1-4200-7575-5, 2009
- Ikenaga, S., Lewis, F.L., Campos, J., and Davis, L. 2000. "Active Suspension Control of Ground Vehicle Based on a Full-vehicle Model." *Proceedings American Control Conference, 2000. Proceedings of the 2000*. Vol 6:4019–4024 vol.6.

- Isemoto, R., Kim, C.W., and Sugiura, K. 2010. "Abnormal Diagnosis of Bridges Using Traffic-induced Vibration Measurements." *The Twenty-Third KKCNN Symposium on Civil Engineering*, Taipei, Taiwan: 189-192.
- Kellogg, R.A., Chebira, A., Goyal, A., Cuadra, P.A., Zappe, S.F., Minden, J.S., and Kovačević, J. 2007. "Towards an Image Analysis Toolbox for High-throughput Drosophila Embryo RNAi Screens." *Proc. IEEE Intl. Symp. Biomed. Imaging, Arlington, VA*,: 288-291.
- Kim, C.W., and Kawatani, M. 2008. "Pseudo-static Approach for Damage Identification of Bridges Based on Coupling Vibration with a Moving Vehicle." *Structure and Infrastructure Engineering* 4 (5): 371-379.
- Kim, C.W., Kawatani, M., and Fujimoto, T. 2010. "Identifying Bending Stiffness Change of a Beam Under a Moving Vehicle." *Bridge Maintenance, Safety, Management and Life-Cycle Optimization - Proceedings of the 5th International Conference on Bridge Maintenance, Safety and Management*, 180-180.
- Kullback, S., and Leibler, R.A. 1951. "On Information and Sufficiency." *Ann. Math. Statist* 22: 79-86.
- Law, S. S., and Zhu X. Q. 2004. Dynamic behavior of damaged concrete bridge structures under moving vehicular loads. *Engineering Structures* 26, no. 9 (July): 1279-1293.
- Law, S. S., and Zhu. X. Q. 2005. Nonlinear characteristics of damaged concrete structures under vehicular load. *Journal of Structural Engineering-ASCE* 131, no. 8 (August): 1277-1285.
- Li, H., Wekezer, J. and Kwasniewski, L. 2008. "Dynamic Response of a Highway Bridge Subjected to Moving Vehicles." *Journal of Bridge Engineering* 13 (5): 439-448.
- Lin, C.W., and Yang, Y.B. 2005. "Use of a Passing Vehicle to Scan the Fundamental Bridge Frequencies: An Experimental Verification." *Engineering Structures* 27 (13) (November): 1865-1878.
- Lynch, J. P. 2007. An overview of wireless structural health monitoring for civil structures. *Philosophical Transactions of the Royal Society A: Mathematical, Physical and Engineering Sciences* 365, no. 1851 (February 15): 345-372.
- Mahmoud, M. A., and Abou Zaid, M. A.. 2002. Dynamic response of a beam with a crack subject to a moving mass. *Journal of Sound and Vibration* 256, no. 4 (September 26): 591-603.
- Mal, A., Ricci, F., Banerjee, S., and Shih, F. 2005. "A Conceptual Structural Health Monitoring System Based on Vibration and Wave Propagation." *Structural Health Monitoring* 4, no. 3: 283-293.
- Mallat, S. 1999. *A Wavelet Tour of Signal Processing*. 2nd ed. Academic Press.
- McGetrick, P.J., González, A., and O'Brien, E.J. 2009. "Theoretical Investigation of the Use of a Moving Vehicle to Identify Bridge Dynamic Parameters." *Insight: Non-Destructive Testing and Condition Monitoring* 51 (8): 433-438.
- McGetrick, P.J., Kim, C.W., and O'Brien, E.J. 2010. "Experimental Investigation of the Detection of Bridge Dynamic Parameters Using a Moving Vehicle." *The Twenty-Third KKCNN Symposium on Civil Engineering*, Taipei, Taiwan: 177-180.
- Melhem, H., and Kim, H. 2003. "Damage Detection in Concrete by Fourier and Wavelet Analyses." *Journal of Engineering Mechanics* 129 (5) (May): 571-577.
- Meruane, V., and Heylen, W. 2012. "Structural damage assessment under varying temperature conditions." *Structural Health Monitoring-an International Journal* 11 (3) (May): 345-357.

- Peeters, B., and De Roeck, G. 2000 . “One Year Monitoring of the Z24-bridge : Environmental Influences Versus Damage Events.” In *SPIE Proceedings Series*, 1570–1576. Society of Photo-Optical Instrumentation Engineers.
- Miyamoto, A., and Yabe, A. 2011. “Bridge Condition Assessment Based on Vibration Responses of Passenger Vehicle.” *Journal of Physics: Conference Series* 305 (July 19): 012103.
- Reda Taha, M. M., Noureldin, A., Lucero, J. L. and Baca, T. J. 2006. “Wavelet Transform for Structural Health Monitoring: A Compendium of Uses and Features.” *Structural Health Monitoring* 5 (3) (September 1): 267–295.
- Rytter, A. (1993). “Vibration Based Inspection of Civil Engineering Structures”. Denmark: Department of Building Technology and Structural engineering, Aalborg University.
- Serker Kamrujjaman, N. H. M., Wu, Z. and Li, S. 2010. “A Nonphysics-based Approach for Vibration-based Structural Health Monitoring Under Changing Environmental Conditions.” *Structural Health Monitoring* 9 (2) (March 1): 145–158.
- Siringoringo, D.M., and Fujino, Y. 2012. “Estimating Bridge Fundamental Frequency from Vibration Response of Instrumented Passing Vehicle: Analytical and Experimental Study.” *Advances in Structural Engineering* 15 (3): 417–433.
- Sohn, H. 2007. “Effects of Environmental and Operational Variability on Structural Health Monitoring.” *Philosophical Transactions of the Royal Society A: Mathematical, Physical and Engineering Sciences* 365 (1851) (February 15): 539–560.
- Sugiyama, M. “Dimensionality reduction of multimodal labeled data by local Fisher discriminant analysis”, *Journal of Machine Learning Research*, vol.8 (May), pp.1027-1061, 2007.
- Toshinami, T., Kawatani, M. and Kim, C.W. 2010. “Feasibility Investigation for Identifying Bridge’s Fundamental Frequencies from Vehicle Vibrations.” In *Bridge Maintenance, Safety, Management and Life-Cycle Optimization - Proceedings of the 5th International Conference on Bridge Maintenance, Safety and Management*, 329–334.
- Van der Auweraer, H., and Peeters B. 2003. International Research Projects on Structural Health Monitoring: An Overview. *Structural Health Monitoring* 2, no. 4 (December 1): 341-358.
- Vetterli, M and Kovačević, J. 1995. *Wavelets and Subband Coding*. Signal Processing. Prentice Hall PTR. <http://waveletsandsubbandcoding.org>.
- Worden, K., & Dulieu-Barton J. M. 2004. An Overview of Intelligent Fault Detection in Systems and Structures. *Structural Health Monitoring* 3, no. 1 (March 1): 85-98.
- Worden, K., & Manson G. 2007. The application of machine learning to structural health monitoring. *Philosophical Transactions of the Royal Society A: Mathematical, Physical and Engineering Sciences* 365, no. 1851 (Feb. 15): 515-537.
- Wright, J. Yang, A. Ganesh, A. Sastry, S. and Ma, Y. “Robust Face Recognition via Sparse Representation” *IEEE Transactions on Pattern Analysis and Machine intelligence*, February 2009.

- Wright, J., Yi Ma, Mairal, J., Sapiro, G., Huang, T.S., and Shuicheng Yan. "Sparse Representation for Computer Vision and Pattern Recognition." *Proceedings of the IEEE* 98, no. 6 (June 2010): 1031–1044.
- Yan, A.-M., G. Kerschen, P. de Boe, and J.-C. Golinval. 2005a "Structural Damage Diagnosis Under Varying Environmental conditions---Part I: A Linear Analysis." *Mechanical Systems and Signal Processing* 19: 847–864.
- 2005b. "Structural Damage Diagnosis Under Varying Environmental Conditions--part II: Local PCA for Non-linear Cases." *Mechanical Systems and Signal Processing* 19: 865–880.
- Yabe, A and Miyamoto, A. 2010. "Development of a bridge condition assessment system by using city bus." *Bridge Maintenance, Safety, Management and Life-Cycle Optimization - Proceedings of the 5th International Conference on Bridge Maintenance, Safety and Management*: 2056–2063.
- Yang, Y.B., and Chang, K.C. 2009. "Extraction of Bridge Frequencies from the Dynamic Response of a Passing Vehicle Enhanced by the EMD Technique." *Journal of Sound and Vibration* 322 (4-5): 718–739.
- Yang, Y. B., Lin, C.W., and Yau, J. D. 2004. "Extracting Bridge Frequencies from the Dynamic Response of a Passing Vehicle." *Journal of Sound and Vibration* 272 (3-5) (May 6): 471–493.
- Yang, Y.B., and Lin, C.W. 2005. "Vehicle-bridge Interaction Dynamics and Potential Applications." *Journal of Sound and Vibration* 284 (1-2) (June 7): 205–226.
- Yin, S.H., and Tang, C.Y. 2011. "Identifying Cable Tension Loss and Deck Damage in a Cable-Stayed Bridge Using a Moving Vehicle." *Journal of Vibration and Acoustics* 133 (2): 021007.
- Zhu, X.Q., and Law, S.S. (2006). "Wavelet-based Crack Identification of Bridge Beam from Operational Deflection Time History." *International Journal of Solids and Structures* 43 (7-8) (April): 2299–2317.
- Zhu, X., and Rizzo, P. (2011). "Guided Waves for the Health Monitoring of Sign Support Structures Under Varying Environmental Conditions," *Structural Control and Health Monitoring*, Available online: 21 AUG 2011
- Zhu, X. "Semi-supervised learning literature survey", Tech. Rep. 1530, Univ. Wisconsin-Madison, 2005.
- Zhu, X. and Ghahramani, Z. "Learning from labeled and unlabeled data with label propagation," Tech. Rep., Carnegie Mellon Univ., 2002.